NTNU
Norwegian University of
Science and Technology

Numerical Modeling and Analysis of the Combined Wind and Wave Energy Concept SFC
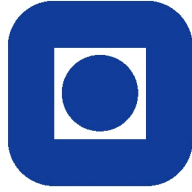
Md. Rafiur Rahman

Numerical Modeling and Analysis of the Combined Wind and Wave Energy Concept SFC

Md Rafiur Rahman

Spring 2016

Master's Thesis

Department of Marine Technology

Norwegian University of Science and Technology

Supervisor 1: Professor Zhen Gao

Supervisor 2: Chenyu Luan

MSC THESIS IN MARINE TECHNOLOGY

SPRING 2016

FOR

STUD.TECHN. Rafiur Rahman

Numerical Modeling and Analysis of the Combined Wind and Wave Energy Concept SFC

Background: Offshore wind energy is widely recognized as a useful renewable energy capable to satisfy the increasing energy need and to increase globally the security of energy supplies. Floating wind turbine concepts have also been proposed and tested at sea. Significant opportunities and benefits have been identified in the area of ocean wave energy and many different types of Wave Energy Converters (WECs) have been proposed. It might be beneficial to combine these energy systems of different technology in a farm configuration or even into one platform and to investigate possible combined systems for simultaneous extraction of wind and wave energy.

The Semi-submersible with rotating Flaps Combination (SFC) concept has been proposed by NTNU in the EU project MARINA Platform. SFC consists of a braceless semi-submersible floating platform with four columns and three fully submerged pontoons, a 5 MW wind turbine, three rotating fully submerged flap type WECs and a mooring lines system. However, one of the challenges for combined systems is the numerical evaluation of internal loads of semi-submersible's pontoons and the comparison of numerical analysis results against experimental data.

The purpose of this thesis is to develop a numerical model to predict dynamic responses of the combined concept under wind and wave actions and to validate the numerical results against the experimental data. The focus should be given to the prediction of the motion responses and the internal loads in the semi-submersible's pontoons of the SFC.

The MSc candidate will be provided with geometry details of the different parts of SFC as well as the Response Amplitude Operators (RAOs) of motions and internal loads in one position of semi-submersible's pontoon obtained by experiments for regular wave conditions.

Assignment: The following tasks should be addressed in the thesis work:

1. Literature review on coupled dynamic analysis of combined wind and wave energy concepts and estimation of internal loads for offshore structures, with focus on hydrodynamic load and response analysis. Literature review on the frequency-domain and time-domain methods for motion and internal load analysis. Understand the basic principle to

obtain internal loads based on the motion analysis.

2. Based on the work carried out in the project, finalize the frequency-domain HydroD analysis and obtain the frequency-domain results of the platform motions and the cross-sectional loads of the SFC concept.

3. Compare the frequency-domain numerical and experimental results of the motions and the cross-sectional loads for static and regular wave conditions. Discuss the possible reasons for discrepancy and investigate the difference between the numerical model of the flap-type WECs and the physical model in the experiment.

4. Establish a numerical model of the SFC model in Simo-Riflex-Aerodyn, using one-body formulation for the floater. Compare the time-domain numerical and experimental results with focus on motion responses.

5. If time allows, develop a multi-body model in Simo-Riflex-Aerodyn so that the calculation of the internal loads at a certain cross-section of the semi-submersible pontoon is made possible and then compare the time-domain numerical results against the experimental data for regular wave conditions, as well as the frequency-domain numerical results.

6. Report and conclude on the investigation.

In the thesis the candidate shall present his personal contribution to the resolution of problem within the scope of the thesis work.

Theories and conclusions should be based on mathematical derivations and/or logic reasoning identifying the various steps in the deduction.

The candidate should utilize the existing possibilities for obtaining relevant literature.

The thesis should be organized in a rational manner to give a clear exposition of results, assessments, and conclusions. The text should be brief and to the point, with a clear language. Telegraphic language should be avoided.

The thesis shall contain the following elements: A text defining the scope, preface, list of contents, summary, main body of thesis, conclusions with recommendations for further work, list of symbols and acronyms, reference and (optional) appendices. All figures, tables and equations shall be numerated.

The supervisor may require that the candidate, in an early stage of the work, present a written plan for the completion of the work. The plan should include a budget for the use of computer and laboratory resources that will be charged to the department. Overruns shall be reported to the supervisor.

The original contribution of the candidate and material taken from other sources shall be clearly defined. Work from other sources shall be properly referenced using an acknowledged referencing system.

The thesis shall be submitted electronically in DAIM:

- Signed by the candidate

- The text defining the scope included

- Codes, drawings and/or computer prints which cannot be bound should be organized in a separate folder.

Zhen Gao Supervisors

Deadline: 4.7.2016

Preface

This document is a Master's thesis along with the conclusive work of the autor's Master's Degree. This is carried out in department of Marine Technology at the Norwegian University of Science and Engineering (NTNU). This thesis work is pursued in the Spring of 2016 at Marinteknisk senter in Tyhold, Trondheim.

This topic is proposed by Prof. Zhen Gao and I found this topic quite interesting as it deals with the numerical analysis of combined wind and wave energy concept. I have been gathered a great deal of understanding and experience throughout the semester from my supervisor and co-supervisor.

I would really like to thank Professor Zhen Gao & Chenyu Luan for their utmost guidance throughout my whole theis work.

Trondheim, 04-07-2016

(Your signature)

Md Rafiur Rahman

Abstract

This thesis work primarily aims to achieve a good understanding of the basic principle of the frequency domain and time domain analysis methods for response analysis of combined wind and wave energy concept SFC. SFC is a semi-submersible floating wind turbine concept with 3 wave energy converter units on each pontoon. However, this work is intended to investigate the motion RAOs of the whole platform and internal load RAOs in the floater's pontoon of the SFC at a particular position for the aligned condition. Besides, the comparison between numerical and experimental results are also performed for motion RAOs. Finally, the response analysis of the SFC in the irregular sea is performed. In time domain analysis, the motion responses of surge, heave and pitch are carried out. Besides, the response analysis of tower base bending moment at the base of the tower is also carried out.

When performing a comparative study it is important to ascertain that the numerical model is as much close as the physical model. But, it is important to mention that there are some differences between the experimental model and the numerical model. In frequency domain analysis the basic difference is the absence of mooring lines and the assumption of the WECs to be rigidly connected to the pontoons. So it is to be kept in mind while comparing the numerical motion RAOs of the numerical model and the experimental model. The numerical frequency domain analysis is performed in HydroD which uses the 1st order potential theory along with the Morison's drag for viscous forces. The differences could be the reason for discrepancies in surge and pitch motion RAOs specially. However, the physical model is modelled as 1:50 using Froude's scaling law for performing the experimental analysis. But, all of the results are provided in full scale. Besides the sectional load analysis is performed for two wave directions (0^0 and 120^0) for investigating the dominating criteria.

Finally, the fully coupled time domain numerical analysis is performed in SRA (SIMO-RIFLEX-Aerodyn). Here, both of the wind and wave conditions are considered. The first step is to build the model with the import of hydrodynamic coefficients from HydroD into SIMO. This is an important step, as this may affect the accuracy of the result if there is any mistake. However, the main focus in this section is to perform the decay test of the SFC for verification. Again, there was some discrepancy specially for pitch natural period. The final task intends to perform numerical analysis in extreme and operational environmental conditions. The aligned condition is considered in TD analysis in terms of both wind and wave direction.

Contents

List of Figures

List of Tables

Chapter 1

Introduction

1.1 Background

The declination of the available typical energy resources i.e. oil, coal and gas is creating the crucial economic crisis in terms of energy balance and distribution. Therefore, it is imperative to look for new source of energy. Renewable energy resources can be the best solution to fulfil the present energy requirements along with providing a green environment to the future generation. The 'Europe 2020' target (a strategy that intends for a 20% reduction of green house gases along with 20% increase of renewable energy in total power production within 2020) is becoming the reality from a dream. As spaces are abundant in the sea compared to the limited space onshore, offshore wind and wave sector have greater potential to materialise the dream even faster.

The arena from shallow to deep water in the sea has not become very much popular yet for the deployment of floating wind turbine platform commercially. For utilising the great potential & opportunity of this unexplored arena immense amount of research works have been carried out for decades for the substantial increase of floating offshore wind turbine. Simultaneously, the integration of wave energy conversion units into the floating platform has become an efficient solution with respect to economy and power production capacity.

This thesis work is an attempt to investigate and compare the motion response of the combined concept named SFC (Semi-submersible flap type concept) both in regular and irregular waves with the experimental results. The regular wave analysis has been performed in the frequency domain through the use of HydroD. The irregular wave analysis is performed in time domain through the extensive use of SIMO-RIFLEX-Aerodyn. Moreover, sev-

eral constant wind tests are performed for visualising the operational scenario of this SFC. The final task is to investigate the internal loads at a particular section close to the central column of the SFC while the platform is subjected to regular waves. The explanation of the trend of internal loads for different wave frequencies is elaborately briefed in this thesis work as well.

This thesis work would be a guideline which indicates and explains some fundamental steps to build the numerical model of the SFC for performing the regular & irregular wave analysis.

The combined concept of the WT, where the WECs with elliptical cylinders and supporting arms are mounted on a semi-submersible wind turbine is the SFC (semi-submersible flap type concept) which is a modified version of the 5MW CSC (Luan et al., 2014a), where only one single WEC is installed.

1.2   Chapter outlines

In the present chapter, some background information about this thesis topic is drawn out along with a short brief of the thesis work. Later, some previous works on this related topic are discussed and how it has motivated the author to deal with the topic is enlightened.

In chapter 2, some basic theoretical formulations are discussed in short such as the regular wave theory, frequency domain response analysis, irregular wave theory, time domain response analysis, retardation function etc. moreover, some additional theory is given so that reader can understand some explanation in the result section.

In chapter 3, the numerical modelling for the frequency domain analysis in HydroD is discussed in brief. Simultaneously, the important decisions are pointed out while building the model in Genie.

In chapter 4, the results extracted from the frequency domain hydrodynamic analysis for the global motion and wave induced internal loads in the SFC platform are presented as plots, tables and effort are made to explain as much as possible.

In chapter 5, the procedure for numerical modelling of the SFC in SIMO-RIFLEX are described step by step. Some examples of the important input files are illustrated as well. The important parameters and some important steps are described which can control the accuracy of the results.

In chapter 6, the irregular wave analysis results both for survival and operational conditions are presented in terms of global motion analysis of the platform.

In chapter 7, discussion along with the conclusion are made to enlighten the key findings from this thesis work.

1.3   Previous work on similar topics

Along with the wind resource available onshore, the offshore wind has immense potential for long-term sustainable energy supply as well. Day by day, the installed capacity of wind turbine is increasing and the consequence is the scarcity of the sites in shallow water. Consequently, the exploration of deeper waters is becoming an important issue but comes with several challenges regarding the design, installation, operation and maintenance, grid connection etc. Simultaneously, offshore wind energy cost is increased as well and to reduce the cost the integration of offshore wind with wave energy could be a good solution. The EU project- MARINA Platform is contributing to investigate the potential for integration of offshore wind and wave energy devices.(Martínez and Pavn, 2011).

Different types of combined concepts of WT(wind turbines) and WECs(wave energy converters) have been proposed in the EU FP7 MARINA platform Project. The important criteria to be assessed are cost of energy, constructability, installability, operation & maintenance and survivability.(Gao et al., 2014). Three combined concepts named spar torus combination(STC), semi-submersible flap combination(SFC) & oscillating water column (OWC) array plus wind turbine are selected for further scrutinization through numerical & experimental methods. During these recent years, many research works have been performed regrading these concepts for investigation of the motion characteristics and the coupling effect of mooring lines.

Both frequency domain and time domain global analysis model of SFC is the focus in this thesis work. The first task encompasses the responses (i.e. motion RAOs of the floater and the internal loads RAOs at a particular section) while the platform is only subjected to the floater hydrodynamic loads. The second task covers the investigation of the global motion responses of the floater while the platform is subjected to external environmental loads(where both hydrodynamic loads and aerodynamic loads are included) for the time domain model. Hence, some previous works related to the chosen SFC concept are discussed

here. Moreover, the motion characteristics of a general semi-submersible platform is not a new rather a developed sector for oil and gas industry. The new idea here is to utilise the same platform concept with some modification so that it becomes compatible to support the wind turbine along with the WECs. The wind turbine replaces the deck and superstructure of a typical semisubmersible platform. Generally, semisubmersible comprises of several structural components such as pontoons, columns, bracing or truss members, mooring lines etc. The SFC is without bracing and unlike the concept WindFloat which makes this structurally less complex.

Some works have been performed to investigate the synergy along with the motion performance and the effect of WECs on the platform for SFC and STC by (Gao et al., 2014). It has been found that the synergy is greater for STC compared to SFC by almost 2-3% for additional wave power production. But the effects of WECs on the floater motions for the SFC in operational conditions are quite insignificant. In comparison to the STC, SFC shows better motion performance in extreme conditions.(Gao et al., 2014).

The response analysis of the SFC in harsh environmental conditions was performed for three wave directions ($0^0, 45^0$ & 90^0) using several seeds for every short-term sea states through 1-hour simulation. The comparison between numerical & experimental models has been made as well. The wind turbine was kept parked and the WECs are kept free to rotate during the harsh environmental condition simulation. The change of wave and wind seed numbers have affected mostly the heave and pitch motion of the platform. The choice of 10 seeds is found to be sufficient for the investigation of the dynamic response of the combined SFC concept in extreme environmental conditions.(Michailides et al., 2015). But, in this paper only short term sea states are investigated.

The simplification of the structural parts of the numerical model along with the modelling of external loads on different parts of the SFC & STC are discussed briefly in (Gao et al., 2015). The structural model in short: floater and the WECs are designed as a rigid body in SIMO while tower, blades and mooring lines are designed as beam element in RIFLEX. The external load model in short: hydrodynamic forces[(1st and 2nd order), Morison(drag) are accounted for the floater(Semi-sub) and the WECs. Turbulent wind(BEM or GDW sectional forces) including the tower shadow effects are considered for blades. No wind loads are accounted for hub and nacelle. Drag forces due to turbulent wind or mean wind are accounted for the tower. Morison's equation along with wave kinematics at an instantaneous position

are used for the evaluation of hydrodynamic forces acting on the mooring line. However, after the investigation of the dynamic behaviour of the SFC in both survival and functional conditions, it was found that the SFC behaves well with less dynamic motions compared to the STC. To reduce the uncertainty while comparing the numerical and experimental results the measured wave elevation and wind speeds were utilised. The whole global dynamic response analysis is performed in coupled SIMO-RIFLEX-Aerodyn (SRA). The comparison of experimental and numerical results for SFC showed quite good agreement to predict all of the response parameters accurately. Based on the preliminary comparison it has been found that combined wind and wave energy concept is not as economy efficient as pure wind turbine because of the immaturity of wave energy technology.(Gao et al., 2015). So, further research work is required to make the combined concept more economy efficient to produce the lower cost of energy.

Floating wind turbine platforms are a current research and development area because offshore wind industry is moving towards deeper water. This implies a wide range of the wind, wave and electrical conditions during their operational and survival lifetime. This must be taken into account to establish the structural integrity for both fatigue and ultimate load states (FLS and ULS respectively).(Commission et al., 2005) and (Quarton, 2005). To establish the structural integrity of the platform it is important to perform the global motion analysis as well as to investigate the wave induced internal loads specially at several particular crucial sections of the platform. Moreover, for the purpose of the classification and structural design of these floating platforms, it is paramount to evaluate the internal loads (sectional loads) along with the platform motions.

Fewer works have been found for the investigation of internal loads of the moored floating semi-submersible platforms in regular and irregular waves. The motions and the wave induced internal loads in a moored semisubmersible had been studied both experimentally and numerically in regular waves by (Wu et al., 1997). The moored semi-submersible platform was modelled as an externally constrained floating platform in waves and thus the linear equations of motion were derived. The hydrodynamic computations were performed using surface panel methods assuming potential wave theory. Besides, the body was subdivided in the derivation of linear equation of motion due to the sack of systematic formulation of internal loads. The exerted loads (force & moment) as well as the wave induced internal loads were decomposed into two parts i.e a constant and a linearized motion de-

pendent component. Here, the total rigid body motions are evaluated first and then for the evaluation of internal forces, one part is isolated. The effect of another part on that isolated part was replaced by an unknown force and moment vector. Later on, these unknown load vectors were calculated by solving the static equilibrium equation and the linear equation of motion for the isolated part. This is how the internal splitting loads are calculated at a specific cross-section where the body was subdivided. However, as maximum design loads at mid-deck elevation happened in beam seas(90^0 wave direction) as expected by Murray et al. (1993) the comparisons were done for beam seas only. So, the internal splitting forces at the mid-deck level were evaluated in regular waves. It was found that the mooring effect on the platform motions and internal loads were insignificant in the wave-frequency range. But, the overall task was done in the frequency domain. As the platform is symmetric with respect to xz and yz planes, in beam seas, the pitch moment (MY) and the yaw moment (MZ) of the internal splitting force vector were found to be practically zero. The other internal splitting forces and moments calculated numerically were found to be in good agreement with the experimental results with little discrepancies. (Murray et al., 1993).

In another paper by (de Bruijn et al., 2011), an investigation of wave loads on semi-submersible along with the internal loads for this moving semi-submersible is performed for regular waves. The CFD simulations were performed by ComFLOW. Comflow is based on incompressible Navier-Stokes equations and improved Volume of Fluid method. The results obtained by ComFLOW were compared with linear diffraction theory by and experimental results. The linear calculations were performed in WAMIT and the GustoMSC internal load calculation program DYNLOAD. Here, only sectional loads FX (surge splitting force) an MY (pitch overturning moment) at the aft section are measured because the motion was restricted to surge, heave and pitch. The hydromechanical coefficients were derived from WAMIT and the motions were achieved from the solution of FD (frequency domain) analysis in WAMIT. Viscous effects were linearized using Morison elements. The internal loads were calculated by DYNLOAD which is a finite element program and this is a shell around the WAMIT. DYNLOAD combines hydromechanical, gravity and internal loads on the floating platform. The loads are evaluated on the nodes of a structural model. The dynamic internal loads on a specific section of the semi-submersible were calculated by integrating all dynamic loads on that specific section. The dynamic loads include inertia loads, gravity induced loads, wave loads and hydromechanical loads (adddded mass, damping and restor-

ing loads). Overall the results were seemed to be quite reasonable. It is to be noted that, for calculation of the distribution of inertial loads a mass model was used.

The investigation of the internal loads for this particular floating wind turbine platform has become interesting to me. That is why I have chosen this thesis topic to learn how to build a numerical model for both frequency and time domain analysis. Throughout this thesis work, I have learned how to make a numerical model in SIMO-RIFLEX-Aerodyn. I have obtained deeper insight about the coupling effect of mooring line as well as the wind turbine(the rotor blades and tower) on the floater. Besides, I have acquired a great deal of understanding of floating wind turbine dynamics concept.

Chapter 2

Theoretical Background

This chapter covers the development of regular wave theory in brief. Moreover, the discussion of FD (frequency domain) equation of motion and the TD (time domain) equation of motion are also provided here. A short overview of internal loads is also given. Additionally, some theories are provided as well which are related to the performed task during modelling and analysis of the SFC platform.

2.1   Linear wave theory

There are two practical options available for evaluating the hydrodynamic loads in a global analysis. Potential wave theory and Morison's equation are these two options. The first order potential wave theory or airy wave theory which is implemented here considers the solution for linearized boundary value problem including three main assumptions:***inviscid, incompressible and irrotational flow***.

This potential wave theory using a panel method solution accounts for Froud-Krylov forces and diffraction effects for large volume structures. The yielding solution is frequency dependent as well as linearly proportional to wave amplitude.

According to Faltinsen (1993) the linear theory means that the velocity potential is proportional to the wave amplitude and this is valid if the wave amplitude is small relative to the characteristic wavelength and body dimension.

Linear wave theory is the foundation for the calculation of wave loads on structures. This theory is derived by assuming horizontal sea bottom and a free surface of infinite horizontal extent. Some basic assumptions are needed to establish for the simplification of the linear

wave theory as mentioned earlier. Sea water is assumed as incompressible and inviscid along with the motion of fluid as irrotational. Even though, these are not the case for real sea.

- Incompressible fluid

  Incompressibility is an approximation. If the density remains nearly constant, the approximation is correct. That means, the volume possessed by every portion remains unchanged through the course of its motion when the flow is assumed as incompressible. Density is no longer a function of time or spae in this case.

- Inviscid flow

  In reality there is no fluid without viscosity and all fluids have some viscosity to some extent. The regions where the net viscous forces are negligible compare to pressure and/or inertial forces is referred as an inviscid regions of flow.(simply referred as inviscid flow). Sometimes, neglecting the viscosity simplifies the analysis without much loss in accuracy in such inviscid regions. (When two layers of fluid move to each other, the friction force developed between them which results in slower and faster layer. Slower layer tries to slow down the faster layer. This internal resistance of flow is referred as fluid viscosity.)

- Irrotational flow

  This simply states that rates of rotation of a fluid particle about the x, y and z-axes are zero. So, no vorticity and no circulation as well. Vorticity is a phenomenon of fluid which is not of importance as per the context of this thesis work, so not described here.

2.1.1   Governing Equations

The continuity equation can be derived by the application of conservation of mass on a control volume. The conservation of mass simply implies

$$\int_{CV} \frac{\partial \rho}{\partial t} \partial V = \sum_{in} \dot{m} - \sum_{out} \dot{m} \tag{2.1}$$

In words, the net rate of change of mass in a control volumeis equal to the inflow of mass rate minus outflow of mass rate. (The mass flow rate through a surface is equal to $\rho V_n A$). Derivation of continuity equation using an infinitesimal control volume can be obtained

and expressed as follows:

$$\frac{\partial \rho}{\partial t} + \frac{\partial (\rho u)}{\partial x} + \frac{\partial (\rho v)}{\partial y} + \frac{\partial (\rho w)}{\partial z} = 0 \tag{2.2}$$

If the equation derived by Divergence theorem, is expanded using the chain or product rule, it implies

$$\frac{\partial \rho}{\partial t} + \vec{\nabla}.(\rho \vec{V}) = \frac{\partial \rho}{\partial t} + \vec{V}.\vec{\nabla}\rho + \rho \vec{\nabla}.\vec{V} \tag{2.3}$$

In this equation 2.3, the first two terms together is calle dthe *material derivative* of ρ. Here, $\vec{\nabla} = \frac{\partial}{\partial x}\hat{i} + \frac{\partial}{\partial x}\hat{j} + \frac{\partial}{\partial x}\hat{k}$, is an operator. The alternative form can be written as:

$$\frac{1}{\rho}\frac{D\rho}{Dt} + \vec{\nabla}.\vec{V} = 0 \tag{2.4}$$

So, finally if the changes in the density of material element are very small compared to the magnitudes of the velocity gradients in $\vec{\nabla}.\vec{V}$ as the element moves around , then it can be approximated as incompressible and $\frac{1}{\rho}\frac{D\rho}{Dt} = 0$. The equation of continuity for incompressible flow yields into the following equation

$$\vec{\nabla}.\vec{V} = \frac{\partial u}{\partial x} + \frac{\partial v}{\partial y} + \frac{\partial w}{\partial z} = 0 \tag{2.5}$$

In which u, v, w represents the velocity in x, y, z directions repectively. Now, vector identity concerning the curl of gradient of any scalar function ϕ and the curl of any vector $\vec{V}$, are expressed as follows

$$\vec{\nabla} \times \vec{\nabla}\phi = 0 \quad \& \text{ if } \quad \vec{\nabla} \times \vec{V} = 0, \quad \text{then} \quad \vec{V} = \vec{\nabla}\phi \tag{2.6}$$

To be noted, the vector identity can be easily proven in Cartesian coordinates, but it can be implemented to any orthogonal system as long as ϕ is a smooth function. The divergence

($\vec{\nabla}.\vec{V}$) of any vector (i.e velocity) simply indicates the rate of changes of magnitudes with respect to the space. The curl $\vec{\nabla} \times \vec{V}$ of any vector (i.e $\vec{V}$) demonstrates the rotation of the field or if any object is placed on that field, how much it will affect to rotate the object. In equation 2.6, the last expression ϕ presents the potential function. In fluid mechanics, ϕ is called the ***velocity potential function***, which is a continuous, differentiable, scalar function $\phi = \phi(x, y, z, t)$ so that its gradients satisfy automatically.This implies it can be used to describe the velocity vector at time t and position $\bar{x} = (x, y, z)$.

As stated above, the irrotationality of flow region states that the vorticity vector which is the curl of the velocity vector is equal to zero. So, in an irrotational region of flow, it is possible to express the velocity vector as the gradient of a scalar function which is referred as velocity potential function. That's why regions of irrotational flow are referred as regions of potential flow. The usefulness of $\vec{V} = \vec{\nabla}\phi$ becomes apparent when it is substituted into equation 2.5(the incompressible continuity equation) and can be expressed as follows

$$\nabla^2 \phi = \frac{\partial^2 \phi}{\partial x^2} + \frac{\partial^2 \phi}{\partial y^2} + \frac{\partial^2 \phi}{\partial z^2} = 0 \tag{2.7}$$

Where the ***Laplacian operator*** ∇^2 is a scalar opertaor($\vec{\nabla}.\vec{\nabla}$). The equation 2.7 is referred as ***Laplace equation***. The beauty of this equation is, it only depends on one variable instead of three variables. once, the solution of ϕ is obtained, the evaluation of all the three components of the velocity field gets easy.

To be noted, the solution is even valid spontaneously for an unsteady flow as well. In other words, at any instant of time, the incompressible flow field instantly adjusts itself in such a manner so that it satisfies the Laplace equation & the existing boundary conditions at that time instant.

Hence, the velocity potential function can easily be obtained from continuity & irrotationality whereas the pressure in the fluid field is to be obtained from the renowned ***Bernoulli equation***. it can be derived very easily applying Newton's second law(linear momentum equation in fluid mechanics) in the direction of stream where a particle is moving on. For steady and incompressible flow it can be written as:

$$p + \rho g z + \frac{\rho}{2}\left|\nabla\phi\right|^2 = Constant \quad \text{along a streamline} \tag{2.8}$$

In words, the sum of the kinetic energy, potential energy & flow energies of a fluid particle is constant along a streamline. It can be viewed as the *conservation of mechanical energy principle*. So, there is no dissipation of mechanical energy during such flows as this is assumed as frictionless(conversion of mechanical energy to thermal energy is negligible). For unsteady and incompressible flow in inviscid region of flow, the equation of Bernoulli can be expressed as

$$p + \rho g z + \rho\frac{\partial\phi}{\partial t} + \frac{\rho}{2}\left|\nabla\phi\right|^2 = Constant \tag{2.9}$$

The last important step to obtain the solution of ϕ requires boundary conditions around the control volume or fluid domain of interest. The necessary boundary conditions are enlightened here in brief.

2.1.2 Kinematic boundary conditions

Kinematic boundary condition comprises of three conditions i.e. impermeability condition on the sea bottom, impermeability condition on the body surface and the free surface condition.

$$\frac{\partial\phi}{\partial n} = 0 \qquad on \quad S_{SB} \tag{2.10}$$

Here, $\frac{\partial}{\partial n}$ denotes the differentiation along the normal to the sea surface, that implies no fluid enters or leaves the sea bottom. Similarly, this same logic holds for the fixed body which implies no fluid enters or leaves the body. When the body is moving with velocity U(for a rigid body U includes translatory and rotational motion), equation 2.10 can be written as

$$\frac{\partial\phi}{\partial n} = \mathbf{U.n} \qquad on \quad S_B \tag{2.11}$$
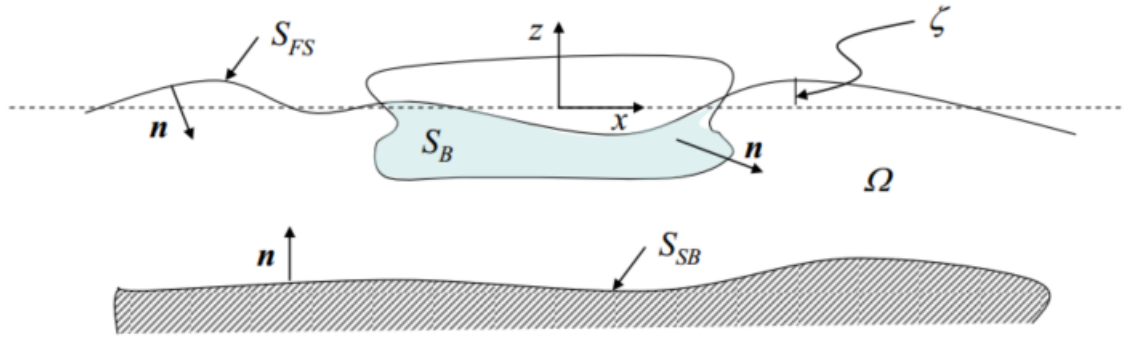
Figure 2.1: Boundary condition for floating body for potential theory

The equation 2.12 represents the substantial derivative of any function F(x,y,z,t). This can be found by simple mathematical derivation. This is expressing the rate of change of F with time if a fluid particle is followed in space. **V** is the fluid velocity at a point (x,y,z) and time t.

$$\frac{DF}{Dt} = \frac{\partial F}{\partial t} + \mathbf{V}.\nabla F \tag{2.12}$$

Now, the free surface can be defined as $z = \zeta(x, y, t)$ where ζ is the wave elevation. So, the function can be defined as $F(x, y, z, t) = z - \zeta(x, y, t) = 0$. Simply, this implies a fluid particle is assumed to be on the free surface. That means equation 2.12 yields into $\frac{DF}{Dt} = 0$. Hence the kinematic boundary condition on free surface can be written as follows:

$$\frac{\partial}{\partial t}(z - \zeta(x, y, t)) + \nabla\phi.\nabla(z - \zeta(x, y, t)) = 0 \quad i.e. \quad \frac{\partial\zeta}{\partial t} + \frac{\partial\phi}{\partial x}\frac{\partial\zeta}{\partial x} + \frac{\partial\phi}{\partial y}\frac{\partial\zeta}{\partial y} - \frac{\partial\phi}{\partial z} = 0 \tag{2.13}$$

To be noted, $\mathbf{V} = \nabla\phi$ has been used in the above equation what is described in the previous section. If the linear terms are only kept and by Taylor expansion the free surface conditions are transferred from free surface position to mean surface position, the above equation yields into equation 2.14. That can be said in other words ϕ is assumed constant from z=0 to the instantaneous free surface elevation.

$$\frac{\partial\zeta}{\partial t} = \frac{\partial\phi}{\partial z} \quad on \quad z = \zeta(x, y, t) \tag{2.14}$$

2.1.3 Dynamic free-surface conditions

The dynamic surface conditions simply state that the water pressure is identical to the constant atmospheric pressure on the free surface. If the constant in Bernoulli equation is chosen as $\frac{P_0}{\rho}$ so that this equation represents no fluid motion, then

$$g\zeta + \frac{\partial \phi}{\partial t} + \frac{1}{2}[(\frac{\partial \phi}{\partial x})^2 + (\frac{\partial \phi}{\partial y})^2 + (\frac{\partial \phi}{\partial z})^2] = 0 \quad z = \zeta(x, y, t) \tag{2.15}$$

The same logic can be used as used for the kinematic free surface condition and this equation 2.15 after keeping only the linear terms, can be written as

$$g\zeta + \frac{\partial \phi}{\partial t} = 0 \tag{2.16}$$

By combining equation 2.14 and equation 2.16, the following equation can be obtained

$$\frac{\partial^2 \phi}{\partial t^2} + g\frac{\partial \phi}{\partial z} = 0 \tag{2.17}$$

2.2 Regular wave theory

The linear wave theory or Airy theory for propagating waves can be derived by assuming a horizontal sea bottom & a free-surface of infinite horizontal extent. The theory can be found in many Fluid Dynamics books (i.e. chapter 6 in (Newman, 1977).)

When the velocity potential ϕ is oscillating harmonically in time with the circuar frequency ω the equation 2.17 can be written as

$$-\omega^2\phi + g\frac{\partial \phi}{\partial z} = 0 \quad z = 0 \tag{2.18}$$

The above combined kinematic & dynamic free surface condition along with the boundary condition at sea bottom are used together to obtain the solution by the method of 'separation of variables' which satisfies the Laplace equation and written as follows:

$$\phi = e^{kz}(A\cos kx + B\sin kx)\cos(\omega t + \alpha) \tag{2.19}$$

Here, A,B & α are arbitrary constants. From the free surface condition, the dispersion relation between the wave number(k) and circular frequency(ω) can be established as $\omega^2 = kg$. Nevertheless, in general, the equation 2.19 is not representing the travelling or propagating wave. Propagating wave means that, the wavefronts move with a certain speed. The combination of the solution in equation 2.19, can be performed so that x and t dependence is like $\cos(\omega t \pm kx + \gamma)$, in which γ is a constant phase angle.

The above equation is only representing the wave propagation along the x-axis in positive(the + sign in the expression) or negative(the - sign in the expression) direction. The expression can be generalised to any wave travelling direction. The figure below is illustrating the transformation of two co-ordinate system which has an angle β between x-axis and X-axis. For instance, wave propagating along X-direction which is aligned β^0 with x-axis can be transformed into (x,y,z) system and written as follows:

$$\phi = e^{kz}\cos(\omega t - kx\cos\beta - ky\sin\beta + \gamma) \tag{2.20}$$

One important physical phenomenon results from the expression are used frequently for fluid motion in deep water waves. That is, the fluid motion is negligible from half a wavelength down in the fluid. For instance, if $z = -.5\lambda$, exp(kz)=.043 and if $z = -\lambda$, exp(kz)=.002. Another important phenomenon is a fluid particle moves in a circle for deep water and in ellipse for infinite depth. The figure below illustrates the horizontal velocity distribution under a wave trough and crest. This can also explain the cancellation effect in motion RAOs for different types of platform(i.e. semi-submersible).

2.3   Response in regular waves

In this section the evaluation of response in regular waves (the solution of the wave-body interaction problem in terms of ϕ) is discussed. The assumptions encompass deep water(infinite water depth), regular incoming waves, steady state conditions(no transient effects due to initial condition), zero forward speed, no current etc. So, simply this implies that the excitation due to the wave loads induces linear dynamic motions and loads in the structure which are oscillating harmonically with the same circular frequency of the wave loads. This hydrodynamic problem in regular waves can be divided into two sub-problems

and superposition principle is valid due to the linearity. That means the loads achieved in subproblem A & B can be added to obtain the total hydrodynamic loads.

- **Subproblem A**: Diffraction Problems

- **Subproblem B**: Radiation Problems

The following figure 2.2 illustrates the superposition principle and the total hydrodynamic problem.

Excitation loads

Added mass
Damping & restoring
forces and moments
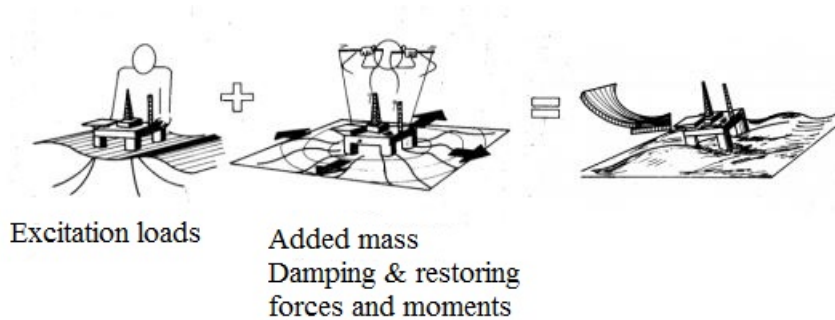
Figure 2.2: Superposition of wave excitation and hydrodynamic loads.(Faltinsen, 1993)

To obtain the solution of the problems, the velocity potential (for infinite water depth) which is going to be used can be obtained from equation 2.19. This was explained in the previous chapter that ϕ can be written as $Ce^{kz}\cos(\omega t \pm kx + \gamma)$. Now, inserting the dynamic free-surface condition as stated below:

$$\zeta = -\frac{1}{g}\frac{\partial \phi}{\partial t} = \frac{C\omega}{g}\sin(\omega t - kx + \gamma) \tag{2.21}$$

Hence, $\frac{C\omega}{g} = \zeta_a$ implies $C = \frac{g\zeta_a}{\omega}$. So, the expression for ϕ can be written as follows:

$$\phi = \frac{g\zeta_a}{\omega}exp(kz)\cos(\omega t - \overline{k}.\overline{r}) \tag{2.22}$$

The above equation has been written for any arbitrary direction of wave propagation(i.e. β^0 w.r.t x) where $\overline{k} = (k\cos\beta, k\sin\beta \, and \, \overline{r} = (x, y))$. For, simplification the phase angle γ is set

equal to zero. The equation of the wave profile can be written as:

$$\zeta = \zeta_a \sin(\omega t - \overline{k}.\overline{r})$$ (2.23)

Now, the equation 2.22 for the incoming wave velocity potential can be written as

$$\phi_0 = \frac{g\zeta_a}{\omega} exp(kz)\cos(\omega t - \overline{k}.\overline{r}) = \Re[\phi_0(x,y,z)exp(i\omega t)]$$ (2.24)

Where, $exp(i\omega t) = \cos\omega t + i\sin\omega t$ and $\Re$ means the real part of the expression. The assumption of linearity combined with the steady state condition implies:

$$\phi(x,y,z,t) = \Re[\phi_0(x,y,z)exp(i\omega t)]$$ (2.25)

So, the overall problem can be solved for ϕ by the frequency domain analysis which is discussed later.

2.3.1   Subproblem A

In this case, the body is restrained from oscillation (fixed) and interacting with incident waves. The hydrodynamic loads are called *wave excitation loads*. These excitation loads are composed of two loads such as:

- **Froud-Krillof loads**(sometimes called incident loads) refers to such hydrodynamic loads which get created due to the absence of the body(as it is assumed that the body wasn't there) when the flow for ϕ_0 penetrates the body with normal velocity $\frac{\partial \phi_0}{\partial n}$. Hence, the pressure field is undisturbed in this case.

- **Diffraction loads**(sometimes called scattering loads) takes into account the recovery of body impermeability. So, the presence of the body or structure changes the pressure field. The diffraction potential(ϕ_D) can be found from the Laplace equation by using the boundary condition on the body. To ensure the total component of normal velocity of the disturbed pressure or wave field equal to zero, the normal derivative of the diffraction potential should be equal and opposite to the normal derivative of the incident or FK(Froude-Kryloff) wave potential. This implies that the impermeability condition,$\frac{\partial(\phi_0+\phi_D)}{\partial n} = 0 \quad on \quad S_{0B}$, is satisfied for the spatial potential $\phi = \phi_0 + \phi_D$.

This is the boundary condition which is applied for obtaining the diffraction potential. Additionally, the combined free surface condition along with the far-field radiation condition is required.
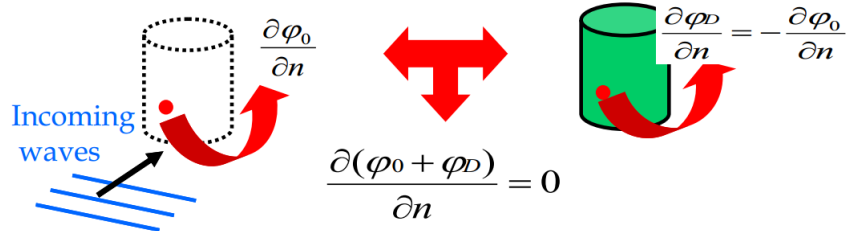
Figure 2.3: Boundary condition on the body for diffraction problem

The velocity potential for the *subproblem A* can be written as the sum of two velocity potentials as follows:

$$\phi(x, y,, z, t) = \phi_0(x, y, z, t) + \phi_D(x, y, z, t) \tag{2.26}$$

Now, the excitation loads can be obtained by simply integrating the incident wave dynamic pressure and the diffraction dynamic pressure along the mean wetted surface. The expression for the generalized excitation load can be stated as follows:

$$\overline{F}_{exc,k}(t) = -\int_{S_{0B}} \rho \frac{\partial \phi_0}{\partial t} n_k dS - \int_{S_{0B}} \rho \frac{\partial \phi_D}{\partial t} n_k dS \tag{2.27}$$

The convention of sign used here is, positive for the direction from body to fluid and negative for the opposite. According to that condition, the pressure gets negative here.For, k=1,2,3 the excitation loads in x,y and z directions are represented and for k=4,5,6 the moment w.r.t x,y and z- directions are represented as well. n_k is the generalized normal vector i.e.

$$n_k = \begin{cases} n_k & for \quad k = 1, 2, 3 \\ (\mathbf{r} \times \mathbf{n})_{k-3} & for \quad k = 4, 5, 6 \end{cases} \tag{2.28}$$

$$\overline{F}_{exc,k}(t) = \Re[\int_{S_{0B}} -i\omega \, exp(i\omega t)\rho(\phi_0 + \phi_D)n_k dS] = \zeta_a \Re[exp(i\omega t)\overline{X}_k(\omega,\beta)] \quad k = 1,2,...,6$$

(2.29)

In the above equation 2.29, $\overline{X}_k(\omega,\beta) =| \overline{X}_k(\omega,\beta)exp(i\alpha)$ is the transfer function for the excitation loads. Here, ω is the circular frquency and β is the wave direction. This transfer function is the loads amplitude per unit wave amplitude and α is the phase of excitation loads. If the transfer function is known, the excitation loads can be obtained for any wave amplitude for different wave frequencies but within linear wave theory. the transfer function is written as follows:

$$| \overline{X}_k(\omega,\beta) |= \frac{| \overline{F}_{exc,k} |}{\zeta_a}$$

(2.30)

2.3.2 Subproblem B

In this case, the body is no more restrained to oscillation. Now, the body is forced to oscillate in its six degrees of freedom with frequency ω, but with no incoming waves as it is considered in the *subproblem A*. The rigid body motions can be written as follows:

$$\eta_j(t) = \eta_j a\cos(\omega t) = \Re[\eta_{ja}exp(i\omega t)]$$

(2.31)

Where, j=1,2,..,6. j=1,2,3 implies three translatory motions named as surge, sway & heave respectively in x,y & z directions. Similarly, j=4,5,6 represents three rotational motions named as roll, pitch & yaw with respect to x,y & z directions respectively. The coordinate system and the translatory and rotational displacement conventions are shown in the following figure.

Now, the velocity potential for solving this problem is denoted as $\phi(x, y, z, t) = \phi_R(x, y, z, t)$. This can be splitted into six subproblems for 6 d.o.f(degrees of freedom) and can be written as:
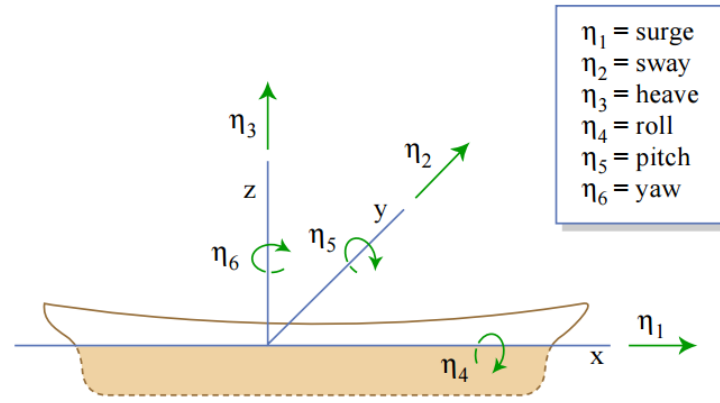
Sign convention for translatory & angular displacements

Figure 2.4: Right hand coordinate system

$$\phi_R(x, y, z, t) = \Re[\sum_{j=1}^{6} \dot{\eta}_j \phi_j] \tag{2.32}$$

Here,$\dot{\eta}_j$ is the velocity and ϕ_j is the velocity potential per unit velocity in j-th mode. Like the procedure of obtaining the solution of velocity potential discussed previously, the solution for this radiation velocity potential has to satisfy the Laplace equation as well. Along with the necessary boundary conditions such as the combined free surface condition & the body boundary condition, radiation condition for far-field is also required. So, in this case, the body bondary condition can be written as:

$$\frac{\partial \phi_j}{\partial n} = n_j \quad on \quad S_{0B} \quad j = 1, 2, ..., 6 \tag{2.33}$$

Here, n_j is the j-th comoponent of generalized normal vector. For instance, in a 2-D problem in x-z plane n_3(i.e. heave motion) will be equal to $-\cos\theta$ when $n = \hat{i}\sin\theta + \hat{k}\cos\theta$(i.e.$\hat{i}\&\hat{k}$ are the unit vector in x & z direction) as per the sign convention of the normal vector. As, the body is oscillating or moving, the forced motion of the body generates waves which is referred as radiated waves(yet, there is no incident wave in this case). This corresponds to the radiation velocity potential and is subjected to the steady-state hydrodynamic loads which are identified as ***added mass & damping loads***. The restoring loads are connected with the hydrostatic and mass consideration which is discussed later. The added mass and damping terms are connected with the dynamic pressure (from Bernoulli equation) on the body sur-

face created by the forced motion of the body itself. The integration of this dynamic pressure of radiation velocity potential results into the added mass and damping loads which is stated below as:

$$\overline{F}_{rad,k}(t) = -\int_{S_{0B}} \rho \frac{\partial \phi_R}{\partial t} n_k dS \quad k = 1,2,...,6 \tag{2.34}$$

By the integration of pressure and energy relations it can be easily shown that

$$\overline{F}_{rad,k}(t) = \sum_{j=1}^{6} [-A_{kj}\ddot{\eta}_j - B_{kj}\dot{\eta}_j] \quad k = 1,2,...,6 \tag{2.35}$$

Where,

$$A_{kj}(\omega) = \mathbf{R}[\rho \int_{S_{0B}} \phi_j n_k dS] \quad \& \quad B_{kj}(\omega) = -\omega \Im[\rho \int_{S_{0B}} \phi_j n_k dS] \tag{2.36}$$

Here, A_{kj} is the added mass coefficient and B_{kj} is the damping coefficient. $\ddot{\eta}_j$ is the rigid body acceleration(j-th mode) and $\dot{\eta}_j$ is the body velocity as well. As ϕ is the complex spacial velocity potential for the oscillating body, the integration of the radiation problem gives the hydrodynamic coeficients. Some significances about these coefficients are discussed later.

2.3.2.1 Added mass & damping coefficient

The added mass (A_{kj}) and damping (B_{kj}) coefficients are important hydrodynamic coefficients and for that reason the significance and the dependence are shortly discussed here. How these coefficients can be obtained are explained in many popular hydrodynamics books i.e. (Faltinsen, 1993). Generally, numerical methods are to be used to evaluate these quantities.

The concept of added mass coefficient can be understood very easily. For instance, in fluid like water, the larger density has an effect on the moving or oscillating body. Because, the body is moving along with the fluid as the fluid can not penetrate the body. The fluid around the body which is also moving with the body is to be calculated and results into added mass. But, it's important to know that, added mass does not represent a finite accelerated mass added to the body mass. Even sometimes the dimensions are not like the mass.

This can be clearer if the mass matrix is observed. So, the body oscillations result into a perturbation everywhere in the fluid with varying intensity and the disturbance always decay going far away from the body.

The damping coefficients (linear) are connected with the wave energy radiated from the structure. This implies it is directly proportional to the square of the amplitudes because the energy is as well(i.e. wave energy $=0.5\rho g\zeta^2; \zeta = waveamplitude$). This implies, without any generated waves the damping coefficients become zero for some cases.

However, A_{kj} and B_{kj} may be strongly dependent on the frequency and body shapes. As the oscillation causes disturbance ϕ_j everywhere in the water and from the solution of fluid velocity potential, it is a function of circular frequency, so these coefficients (A_{kj} and B_{kj}) are dependent on the frequency as well. Some plots are given in the appendix where the effects are illustrated.

Moreover, the vicinity of the free surface, water depth, forward speed, water confinement may also be influencing parameters on the behaviour of those coefficients.

2.3.2.2 Restoring loads

The restoring loads follow the hydrostatic and mass considerations for a freely floating body. The force and moment components can be written as:

$$F_k = -C_{kj}\eta_j \tag{2.37}$$

Here,C_{kj} is the restoring coefficients. For instance, the heave restoring coefficient comes only from the hydrostatic consideration(static part of the Bernoulli equation) and can be written as:

$$C_{33} = \rho g A_{wp} \tag{2.38}$$

But, the roll and pitch restoring coefficients comprise both hydrostatic and mass consideration. The 2nd term of the expression is from the mass consideration.

$$C_{44} = \rho g V (z_B - z_G) + \rho g \iint_{A_{wp}} y^2 \, ds = \rho g V G M_T \qquad (2.39)$$

$$C_{55} = \rho g V (z_B - z_G) + \rho g \iint_{A_{wp}} x^2 \, ds = \rho g V G M_L \qquad (2.40)$$

A_{wp} is the water plane area, V is the displaced volume of water, $z_B \& z_G$ are the centre of buoyancy and centre of gravity z-coordinates respectively. So, the body with a x-z plane symmetry only have the non-zero components which are $C_{33}, C_{35}, C_{53}, C_{44} and C_{55}$. But, when there is mooring system available additional restoring terms are to be considered for surge, sway and yaw motions as well. But, the effect of the spread mooring system on the linear wave system is quite insignificant in wave frequency range. For long wave periods, the case is not the same and has significant influence.

2.3.3 Haskind Relations

Sometimes for the convenience, the linear wave exciting force and the second order potential force (which is not discussed here) are not evaluated from the diffraction solution rather evaluated from the radiation solution(This 1st order wave is referred as Haskind exciting force). This method simply states that, instead of wave generation the body is moving with the same velocity and acceleration of the wave and thus the solution for diffraction potential can be achieved from the radiation potential. This method is easier and safer to use when the strip theory can not be used for the diffraction problem. Some discussions about the strip theory and the applicability are discussed in the appendix. The Haskind relations can be used when the detailed pressure distribution is not of interest but the evaluation of wave excitation loads only. Moreover, this relation is an independent test to evaluate the accuracy of numerical calculation of wave excitation loads. The Haskind relation can be written as from Newman (1977)

$$\iint_{S_{0B}} \phi_j \frac{\partial \phi_D}{\partial n} \, dS - \iint_{S_{0B}} \phi_D \frac{\partial \phi_j}{\partial n} \, dS = 0 \qquad (2.41)$$

So, the excitation loads(subproblem A) in the equation 2.33 can be written in terms of

ϕ_0&ϕ_k and written below:

$$\overline{F}_{exc,k}(t) = \Re[\iint_{S_{0B}} -i\omega exp(i\omega t)\rho](\phi_0 + \phi_D)n_k\,dS \tag{2.42}$$

$$\overline{F}_{exc,k}(t) = \Re[\iint_{S_{0B}} -i\omega\rho(n_k\phi_0 - \frac{\partial\phi_0}{\partial n}\phi_k)\,dS] \tag{2.43}$$

2.3.4   Equation of Motion

The evaluation of hydrodynamic loads can be found analytically as discussed earlier. Once these loads are found, the equation for the rigid body motions can be established in a straightforward way using equation lof linear and angular momentum. This states as below:

$$\sum_{j=1}^{6} M_{kj}\ddot{\eta}_j(t) = F_k(t) \tag{2.44}$$

Here, the loads F_k are the hydrodynamic loads(subproblem A + subproblem B) resulted from wave-body interactions. M_{kj} are the components of the genaralized mass matrix for the body or structure. So, now, the radiation loads of F_k is transferred from the right side of the equation to the left side and diffraction loads of F_k referred as F_k^e is on the right side. Where $F_k = F_R + F_k^e$ and the expression for both of these loads are discussed earlier.

$$\sum_{j=1}^{6}(M_{kj} + A_{kj}(\omega))\ddot{\eta}_j(t) + B_{kj}(\omega)\dot{\eta}_j(t) + C_{kj}\eta_j(t) = F_k^e(t) \quad k = 1, 2, ..., 6 \tag{2.45}$$

The lateral symmetry(symmetry about x-z plane) implies two sets of algebraic equations. One set with surge, heave and pitch and another set with sway, roll an yaw motions. So, there is no coupling with the first set and second set but only among their own set, for instance, coupling between heave and pitch or surge and pitch etc. Some discussions are made in the appendix regarding the mass matrix and other hydrodynamic coefficient matrices in the appendix for this particular situation.

It is important to remember this equation of motion is only valid for steady-state sinusoidal motions in general. Because, in the transient free surface problem, due to the memory ef-

fect of hydrodynamic loads it can not be based on the instantaneous values of velocity and
acceleration of body.
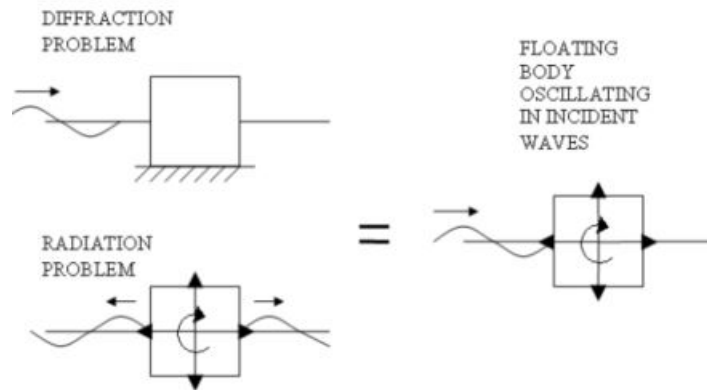
Figure 2.5: Superposition of floating body subproblem

2.4   Frequency Domain(FD) method for solving the equation

The frequency response method is developed for a single degree of freedom(SDOF) system
and later the expression for six degree of freedom will be given. The dynamics of the whole
floating structure can be thought of being constructed by several numbers of coupled mass-
spring-damper systems. However, the SDOF is the simplest case. This method is a way to
describe the dynamic characteristics of a linear system in which the response is determined
to a sine wave input. For convenience, the linear system is considered with the constants
with same notations which are used before. So, this system is considered with mass, M ,
spring or stiffness constant C and linear damping constant B which is subjected to an ex-
ternal horizontal time varying force F(t) with frequency ω. So, the equilibrium equation of
motion can be written as

$$M\ddot{\eta}_3 + B\dot{\eta}_3 + C\eta_3 = F_3(t) = F_{3a}\sin\omega t \tag{2.46}$$

Now, the complete solution of this differential equation is consisted of free oscillation
known as homogeneous solution and forced oscillation known as particular solution. How-
ever, the homogeneous solution dies out after a while following the beginning of the motion,
only the steady state oscillation (particular solution) remains and is discussed here. The
steady state solution of the response is a harmonic function with the same frequency of ex-

ternal load and written as follows:

$$\eta_3 = \eta_{3a}\sin(\omega t - \beta) \tag{2.47}$$

Where η_{3a}= response amplitude β= phase angle between external force or input and the response. Differentiating η_3 with respect to time and substituting in the equation 2.45 yields into

$$\{-M\omega^2\sin(\omega t - \beta) + B\omega\cos(\omega t - \beta) + C\cos(\omega t - \beta)\}\eta_{3a} = F_{3a}\sin\omega t \tag{2.48}$$

Since, this equation has to satisfy for all t, if the coefficients of $\sin\omega t$ and $\cos\omega t$ are equated to zero (as they are orthogonal to each other)two equations can be obtained and written as below:

$$\{-M\omega^2\cos\beta + B\omega\sin\beta + C\cos\beta\}\eta_{3a} = F_{3a} \tag{2.49}$$

$$\{M\omega^2\sin\beta + B\omega\cos\beta + C\sin\beta\}\eta_{3a} = 0 \tag{2.50}$$

Hence, $\eta_{3a} and \beta$ can be solved from these two equations and written as follows:

$$\eta_{3a} = \frac{F_{3a}}{[(C - M\omega^2) + (B\omega)^2]^{0.5}} \quad \& \quad \tan\beta = \frac{B\omega}{C - M\omega^2} \tag{2.51}$$

Here, the ratio between η_{3a}(response) and F_{3a}(input or external loads) is defined as the transfer function and written as:

$$RAO = \frac{\eta_{3a}}{F_{3a}} = \frac{1}{[(C - M\omega^2) + (B\omega)^2]^{0.5}} \tag{2.52}$$

The applicability of this system to the analysis of offshore structure problem can be done quite easily. The example given here would make clear the concept behind the equation of motion for a floating body. For instance, if a barge is now subjected to an incident wave(external

load), there are two distinct effects of this wave i.e as it strikes the barge it gets diffracted and scattered in all directions. At the same time, as the barge is free to move in surge direction it also starts to oscillate in that direction. The motion of the body starts to generate the waves in water as well and these waves are radiated in all directions. As discussed earlier, for first order case linear superposition is possible to apply meaning these two subproblems can be dealt separately and then added together. Then by knowing all the coefficients on the left side along with the excitation force on the right side the solution for surge can be obtained easily.

Utilising the complex expression by avoiding the dependence on time as written below the body motion system in equation 2.44 can be obtained. As here the problem deals with the linear system, so the response oscillates with the frequency of the excitation but with different phase. The response is harmonic because the load is harmonic. So it can be assumed that the excitation loads F_k^e is also proportional to the incident wave amplitude. Hence, the excitation loads can be written as $F_k^e = \zeta_a X_k(\omega, \beta)$

$$\eta_j = \Re[\eta_{ja} exp(i\omega t)] \quad \& \quad F_k^e = \zeta_a X_k(\omega, \beta) \tag{2.53}$$

Where, $\eta_{ja} = |\eta_{ja}| exp(i\alpha_j)$ and $X_k = |X_k| exp(i\delta_j)$ are complex quantities denoting the amplitude and phase of the platform motions and the excitation loads respectively.

Now, for the floating structure which is not restricted to any single direction but free to oscillate in every directions (in all 6 directions) while subjected to waves are discussed here. The equation of motion is already discussed in the previous section. In this situation as the body is free to oscillate in all directions there will be coupling effects as discussed in the earlier section. So, now the equation of motions from the equation 2.44 can be written in frequency domain as follows:

$$\sum_{j=1}^{6} \left[[C_{kj} - \omega^2(M_{kj} + A_{kj}(\omega))] - i\omega B_{kj}(\omega) \right] \eta_{ja} = \zeta_a X_k(\omega, \beta) \quad k = 1, 2, ..., 6 \tag{2.54}$$

So, now this equation leads to six coupled algebraic equations for real and imaginary part of the complex amplitude of the first set means (surge, heave and pitch) and a similar sets of equation for the second set(roll, pitch and yaw) in case of lateral symmetry of the

body or platform. Once, the motions are known the wave loads can be obtained as discussed previously.

2.4.1   Motion RAOs

The elaboration of RAO is Response amplitude operator. Often, this is also referred as mechanical transfer function. The reason is, this transfers the exciting waves into the response of the structure. The response of the structure subjected to a regular wave can be found from the theoretical method described above. This RAO is referred as unique because it is invariant with the wave amplitude at a certain wave frequency for a linear system when the response is normalised with respect to the wave amplitude. The normal practice is to define the RAO per unit wave amplitude. In the computation of RAO the waves are regarded as regular and a sufficient number of frequencies are chosen to cover the whole range of frequency covered by the frequency domain wave spectrum.

The motion RAO can be expressed as:

$$\mathbf{H}(\omega, \beta) = \frac{\eta_a}{\zeta_a} \tag{2.55}$$

$$\mathbf{H}(\omega, \beta) = \left[\mathbf{C} - \omega^2 (\mathbf{M} + \mathbf{A}(\omega)) + i\omega \mathbf{B}(\omega) \right]^{-1} \mathbf{X}(\omega, \beta) \tag{2.56}$$

2.5   Viscous effect

The viscous damping term comes from the viscous effects or the flow separation effect. This is not to be confused with the 2nd order wave drift damping or another damping term. For example, in case of a ship with bilge keel, there will be extra damping term due to the bilge keel as well.

Previously discussed equation of motion does not take into account viscous effect and now this effect is discussed here and later on the equation of motion is established considering viscous effect. The viscous effect gets important within the resonance frequency range specially. Due to the viscous effect, the additional viscous damping is not very significant

outside the resonance region as the potential damping is quite large compared to the viscous damping. But, in case of resonance frequency region the viscous damping term gets important and can be understood easily from the expression written below:

Moreover, the following figure is demonstrating the importance of viscous force in different regions. The regions are classified according to some parameters such as the body characteristic dimension(D), wave height(H), wavelength(λ) etc. In the area of 'inertia forces' as the viscous phenomena are not very important so it may be quite okay to use the empirical formulation proposed by Morison. Moreover, in HydroD(discussed later) it is not possible to evaluate the effect of flow separation exactly. In the equation of motion only potential damping is considered but for long waves(large time period) the damping related to the wave generation is small, then large amplification is expected according to the equation of DLF, consequently, viscous damping gets important to take into account. The decision can be taken from the Figure 2.6 from Chakrabarti (2005) Drag force which is neglected by the airy theory
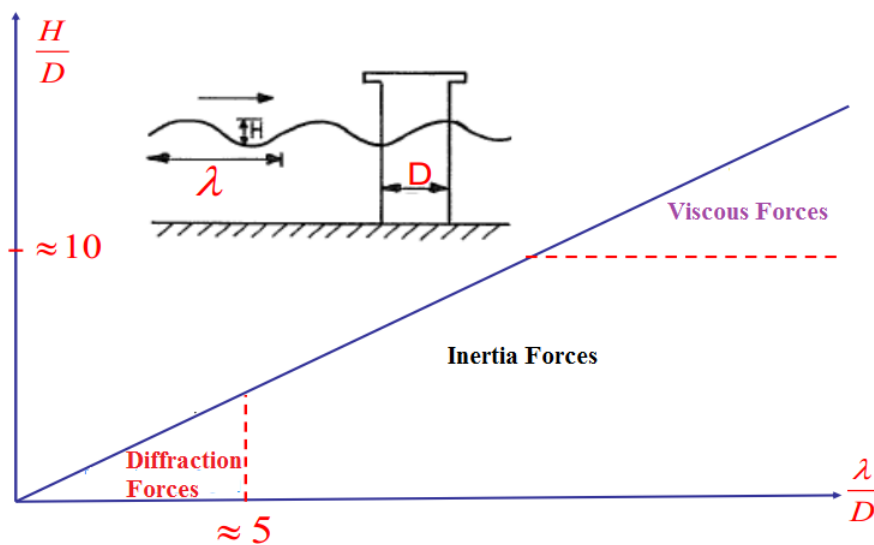
Figure 2.6: Classification of Wave forces

can be the main source of viscous damping and can be taken into account by Morison equation.The derivation of mass force proportional to the undisturbed fluid acceleration is based on the linear potential theory.So, the horizontal force per unit length on the strip of the fixed pile can be written according to Morison et al. (1950) as

$$dF = \rho\pi\frac{D^2}{4}C_M\ddot{u} + \frac{\rho}{2}C_D D|\dot{u}|\dot{u} \tag{2.57}$$

These mass and drag coefficients change for each and every half cycle in case of irregular
wave, but constant value depending on the shape of the structure can be used for linear
wave theory.The hydrodynamic coefficients(Cm & Cd) for submerged member of structure
are evaluated by experiments. It is important that, this is only valid for a circular cylinder
standing on the sea floor and penetrating the free surface.

Where, D is the pile diameter, $\dot{u}$ and $\ddot{u}$ are horizontal wave particle velocity and acceler-
ation of undisturbed fluid, dF is the horizontal force per unit length.
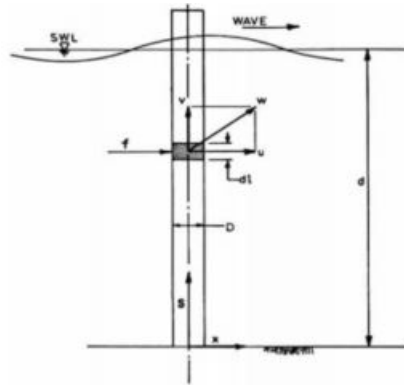
Figure 2.7: Morison force on a vertical pile

Different parameters like Reynolds number, Keulegan-Carpenter number, relative cur-
rent number and surface roughness ratio affect the value of C_m & C_d while empirically de-
termined.

The equation 2.57 gets modified when the structure oscillates due to environmental loads
and results into as follows

$$dF = m\ddot{u} + \rho\pi\frac{D^2}{4}C_A\ddot{u} + \frac{\rho}{2}C_D D |\dot{u}| \dot{u} \tag{2.58}$$

Here the first term on the right side is for the inertia of the body and C_A is the added mass
coefficient.

Limitations and the correspondence with the existing task: The sectional force RAOs are
mainly observed within the wave frequency range and it is quite away from the resonance
frequency range so the viscous effect may not very significant regarding the evaluation of
sectional force within the wave frequency range. But, for the observation of motion RAOs
over a wide frequency range(i.e. 3- 40 sec) the viscous effect is to be included to obtain the
exact information.

2.6   Numerical method for linear wave-induced motion

The detail theory of numerical method is not discussed here but it can be found in many popular Hydrodynamics books i.e. (Faltinsen, 1993). Here, a short overview is given so that the choice of some parameters(i.e. mesh size, mesh type etc.) regarding numerical analysis using panel method can be understood clearly. Besides, the theory for the evaluation of linear wave induced motions are discussed earlier which can give analytical results for some specific body shapes but not for general body shapes. For solving these types of problems, there are several established numerical techniques for the prediction of linear wave induced motions and loads on large volume structures. However, panel methods are based on the potential theory which means the oscillation amplitudes are small compared to the cross-sectional dimensions of the structure.

However, in panel method the problem (i.e 3-D case) is generally discretized by dividing the body surface into sufficient numbers of elements. For instance, for a 2-D circular section it is discretized into several straight lines and is shown in the figure. That is why, there is a little difference between the analytical solution and the numerical solution.

As, due to the limitation of computational time and cost, the choice of panel numbers is to be optimum. Generally, around 100 elements are sufficient for this type of large volume structure problem.((Faltinsen, 1993)). HydroD(a short overview about this is given in the next chapter) has limitation on maximum panel numbers. Hence, Symmetry advantage as well as reduced equation system advantage can be utilised if the structure symmetrical. For instance, for N elements the reduced equation system becomes $N/2 \times N/2$ or $N/4 \times N/4$ for one or two symmetry planes respectively.

Besides, the size of panel is an important issue as well. It is important to know that, the source density and the fluid potential remain constant over each element. So, the smaller size of the panel secures more accuracy in the result. But, the choice of panel size and the computational time required for this are mutually antagonistic. However, a characteristic length of an element is to be at most 1/8th of the wavelength as stated in (Faltinsen, 1993). Another important factor is that, the element must not be so small as the midpoint gets close to the edges of other elements around it. However, the optimum or a sufficient number of panels can be found by doing the convergence test of the results.

This is important to know the limitations of this method for analysing the accuracy of the results and hence some limitations are discussed here. One important thing is, this does not

account for the flow separation effect. This effect is very important for riser , jacket or tether problems. Sometimes, this is important for large volume structures as well. For instance, the hydrodynamic forces at the interaction of pontoon and column are counteracted by the hydrodynamic forces on the pontoon and due to the small forces because of the potential flow effects other physical effects become significant and in these type of cases viscous effects matter.

2.7 Numerical modelling in SRA

2.7.1 Time domain equation of motion

The equation of motion of a submerged rigid floating body with 6 degrees of freedom subjecte to external loads can be written from equation 2.54 in **frequency domain** as follows

$$\left[-\omega^2 \Big(\mathbf{M} + \mathbf{A}(\omega) \Big) + i\omega \mathbf{B}(\omega) + \mathbf{C} \right] \overrightarrow{X}(\omega) = \overrightarrow{F^{ex}}(\omega) \tag{2.59}$$

Here, $\mathbf{M}$ and $\mathbf{A}(\omega)$ is the body mass matrix and the frequency dependent added mass matrix with 6 degrees of freedomrespectively. Similarly, $\mathbf{B}(\omega)$ is frequency dependent damping matrix and $\mathbf{C}$ is restoring matrix with 6 degrees of freedom. $\vec{F}^{ex}$ can be wave forces, mooring forces, current forces or any other external forces. Viscous drag can be included on the left side of the equation by introducing the linearized term for getting rid of non-linearity which is dicussed earlier. It is to be noted that previously, the rigid body motion was denoted as η and here it is replaced with X for convenience. In the above equation the second order terms are not included, but these terms are important in case of moored structure since these forces may excite the natural modes of horizontal motions such as surge, sway or yaw. As, second order wave loads are not considered in this thesis topic it is not included but can be added very easily. However, $\mathbf{A}(\omega)$ and $\mathbf{B}(\omega)$are frequency dependent and a short discussions are provided earlier. These can be written as $\mathbf{A}(\omega) = \mathbf{a}(\omega) + \mathbf{A}_{\infty}$ and $\mathbf{B}(\omega) + \mathbf{B}_{\infty} = \mathbf{b}(\omega)$ as $\mathbf{B}_{\infty}$ is equal to zero.

However, the solution of the equation of motion (for instance from Wadam) is to be performed in the time domain by iteration specially for non-linear systems. By the way, this equation can be converted a non-linear time domain equation system by utilising the Cummins equation which is described in short as follows. Rewriting the equation 2.59 the follow-

ing expression is obtained,

$$-\omega^2\Big(\mathbf{M}+\mathbf{A}_\infty\Big)\vec{X}(\omega)+\Big(i\omega\mathbf{a}(\omega)+\mathbf{b}(\omega)\Big)i\omega\vec{X}(\omega)+\mathbf{C}\vec{X}(\omega)=\vec{F}^{exc}(\omega) \qquad (2.60)$$

The inverse Fourier Transform can be written as

$$\vec{x}(\omega)=\frac{1}{2\pi}\int_{-\infty}^{+\infty}\vec{X}(\omega)exp(-i\omega t)d\omega=\mathscr{F}\Big[\vec{X}(\omega)\Big] \qquad (2.61)$$

By utilizing the Inverse Fourier transform, the following expression can be obtained as

$$\Big(\mathbf{M}+\mathbf{A}_\infty\Big)\ddot{\vec{x}}(t)+\int_{-\infty}^{+\infty}\Big(i\omega\mathbf{a}(\omega)+\mathbf{b}(\omega)\Big)i\omega\vec{X}(\omega)exp(i\omega t)d\omega+\mathbf{C}\vec{x}(t)=\vec{f}^{exc}(t) \qquad (2.62)$$

In the above equation for the second term, it can be said that the Fourier or Inverse Fourier transform of multiplication is a convolution of the Fourier transforms. The derivation of convolution using the Parseval's theorem is given in the appendix. Ultimately, the equation of motion can be written in the time domain as follows

$$\Big(\mathbf{M}+\mathbf{A}_\infty\Big)\ddot{\vec{x}}(t)+\int_{-\infty}^{+\infty}\mathbf{k}(t-\tau)\dot{\vec{x}}(\tau)d\tau+\mathbf{C}\vec{x}(t)=\vec{f}^{exc}(t) \qquad (2.63)$$

From the above equation it is seen that there is an impulse-response function, this is called the retardation function and is denoted by $k(\tau)$. Frequency dependent added mass and linear radiation damping are taken into account by this function in the time domain. Physically the limit of the integral is from 0 to t. However, this equation can be implemented to body motion in irregular seas as well.(Gao, 2016).

2.7.2   Nonlinear method in FEM

A numerical method referred as finite element analysis (FEM) approximates solution of differential equations for displacement of the structure while this method is applied for structural analysis. Here, the structure is generally divided into smaller elements. This method considers the effect of large displacements along with nonlinear material behaviour. Since

this method introduces a memory effect , typical structural mechanics principles are becoming invalid. Non-linearities are not discussed here.

Geometric non-linearites, for instance effect of large displacements, quadratic loads due to thrust and drag forces are relevant nonlinearities for floating wind turbine modelling. The geometric nonlinearity and the method of solution in FEM solver RIFLEX are mainly paid attention in this section.

The nonlinear equation for dynamic equilibrium of a spatial discretized finite element system model can be expressed as follows:

$$\vec{R}^I \ddot{\vec{r}}(t) + \vec{R}^D \dot{\vec{r}}(t) + \vec{R}^S \vec{r}(t) = \vec{R}^{Ext}\left(\vec{r}(t), \dot{\vec{r}}(t)\right) \tag{2.64}$$

Where, $\mathbf{R}^I$ - Inertia force vector, $\vec{R}^D$ - damping force vector, $\vec{R}^S$ - internal structure reaction force vector and $\vec{R}^E$ - external force vector. $\vec{r}$, $\dot{\vec{r}}$, $\ddot{\vec{r}}$ are the structural displacement, velocity and acceleration respectively. The external force vector accounts for weight & buoyancy, viscous drag and wave excitation terms, forced displacements due to support vessel motions etc.

The above equation can be expressed as

$$\left(\mathbf{M}^S + \mathbf{M}^H\right)\ddot{\vec{r}}(t) + \mathbf{C}^S \dot{\vec{r}}(t) + \mathbf{K}^S \vec{r}(t) = \vec{R}^{Ext}\left(\vec{r}, \dot{\vec{r}}, t\right) \tag{2.65}$$

Where, $\mathbf{M}^S$ and $\mathbf{M}^H$ are structural mass matrix and displacement dependent hydrodynamic mass matrix respectively. The second one is accounting for structural acceleration terms in Morison's equation as added mass contributions in local directions. $\mathbf{C}^S$ is internal structural damping matrix and $\mathbf{K}^S$ is the structural stiffness matrix.

Geometric non-linearities may be specifically paramount for wind turbines with large deflection of the rotor blades and also in mooring lines. The Newmark-β method is used for finding the dynamic equilibrium at every time step. The following parameters can be defined during simulation (RIFLEX theory manual).

These parameters are used to control the accuracy, numerical damping of integration method and numerical stability.

METHOD	γ	β	θ
Central difference method	1/2	0	1
Fox-Goodwins method	1/2	1/12	1
Linear acceleration method	1/2	1/6	1
Constant average acceleration method	1/2	1/4	1
Wilson θ-method	1/2	1/6	>1

Figure 2.8: Integration method covered by Newmark-β family including Wilson θ method

2.7.3 Coupled analysis

To consider the important coupling effects among substructures coupling analysis is important and provides a great deal of flexibility for estimating accurate responses. Specially for floating wind turbine the coupling effects become more important. In this context, the coupling effects are as follows:

- Platform motions which influence the wind force

- Aerodynamic damping from the rotor blades on the floater

- Mean position of platform influences wind force and mooring force

- Mooring line dynamics influences platform motions

The rigid body and the flexible slender elements are connected at common nodes in a coupled analysis. The equation of motion in equilibrium is solved for both the flexible element system as well as the rigid body system individually but simultaneously in TD (time domain) by exchanging external forces and displacements at every time step. A number of iteration is required to obtain accuracy at every time step. The iteration number can be specified by the user.

In a coupled model, the force vector $\vec{f}(t)$ in equation 2.66 for a rigid structure including catenary mooring lines and a wind turbine comprises of wave loads, nonlinear inertia, restoring & damping from mooring lines, aerodynamic loads (wind loads) and inertia and damping forces from the turbine and can be expresses as

$$\vec{f}(t) = \vec{f}_{wave}(t) + \vec{f}_{mooring}(t) + \vec{f}_{wind}(t) + \vec{f}_{turbine}(t) \tag{2.66}$$

In the above equation, all the forces are functions of platform motions, velocities and accelerations along with the time. it is to be noted that, for 1st order wave excitation , wave loads are function of time. in the previous section it is already mentioned that $\vec{R}^{Ext}$ contains the forced displacements, velocities and accelerations from the rigid structure in the coupled analysis. Some short details of fully coupled tool SIMO-RIFLEX-Aerodyn can be found in chapter 5.

2.8   Internal Loads

If the load does not change intensity, direction or location with time, it is referred as static load whereas dynamic load is the opposite. Sometimes the changes in dynamic load are so small that it can be regarded as static load. The dynamic load can be of different types such as: moving load, repeated load, impact load etc.
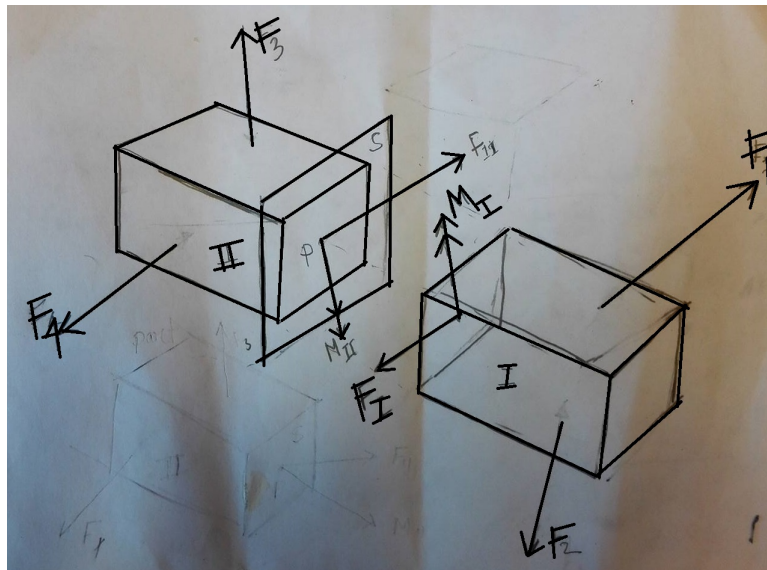
Figure 2.9: Sectional loads

If the sum of all forces acting on a particle is zero, as follows

$$\sum F = 0 \qquad (2.67)$$

then the particle is in equilibrium. As a body is comprised of many particles, so if all of the particles in that body are in equilibrium, then the whole body is in equilibrium. Equilibrium

of a rigid body is defined by the following two equations

$$\sum F = 0 \quad \& \quad \sum M = 0 \tag{2.68}$$

Here, $\sum F$ represents the vector sum of all external forces acting on the body and $\sum M$ represents the vector sum of all external moments acting on the body.

If the particle is accelerating, the so-called inertia force can be defined as

$$\sum F' = -ma \tag{2.69}$$

Hence,

$$\sum F + \sum F' = 0 \tag{2.70}$$

In any study of deformable bodies, it's paramount to investigate the forces that act between the adjacent parts of the body. Though here the study considers the body as a rigid body but in reality the hull structure can not be considered as rigid body. Hence, the investigation of the global load which is found from the analysis can be used for further investigation related to the section scantling, fatigue analysis etc. for local analysis. Suppose, several forces are acting on a body or a system.For instance, if the body is split at any position there are two portions I and II now with a common surface S. If the free-body diagram of portion II is investigated, excluding the force F_3 and F_4 there are other forces that the material of portion I exert on the material of portion II. These forces are internal forces for the body as a whole but are external forces to portion II. The vector sum of the forces F_3 and F_4 is denoted by F_{II} and the vector sum of the moments is denoted by M_{II} about a point P in S. The force system consisting of F_{II} and $M_I I$ is statically equivalent to the system of distributed forces on the surface. These, F_{II} and M_{II} are referred as the ***net internal force system*** on S.

Since portion II is in equilibrium, the net internal force systems on S is

$$F_{II} = -[F_3 + F_4] \quad \& \quad M_{II} = -[M_3 + M_4] \tag{2.71}$$

Here, M_3 and M_4 are the moments of the forces F_3 and F_4 about the point P. So, point P plays passive but important role. If the free body diagram of the portion I was to use instead of portion II, the net internal force system on S would be F_I and M_I. As a direct result of

Newton's third law(each and every force on a system has its equal and opposite reaction on that),

$$F_I = -F_{II} \quad \& \quad M_I = -M_{II} \tag{2.72}$$

2.8.1 Approach in Wadam

The sectional load at any specific cross-section are evaluated by the integration of distributed forces on specified sides of given planes which intersect the hydro model. The forces include the frequency dependent excitation forces and inertia forces. To be more precise, it can be stated that the sectional loads at a section are obtained from the integration of (F-Ma) over the portion of the structure. For the calculation of moment a point is generally specified for each plane. For instance, in the following figure, the cross-section is specified in input co-ordinate system and the limitation is that it has to be normal to one of the main axes of the global coordinate system.
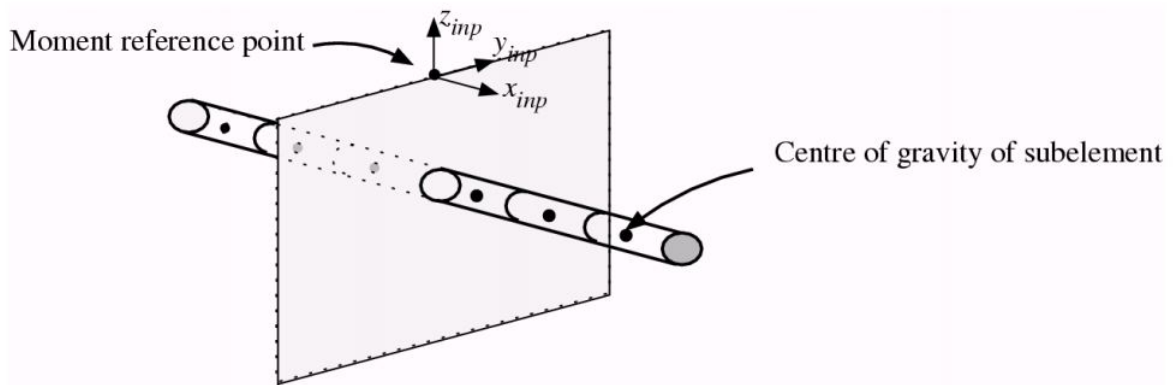
Figure 2.10: Sectional loads at a plane through x=0

It is to be kept in mind that the sectional loads are evaluated corresponding to a body-fixed coordinate system. One other important thing to remember, in the panel model excitation forces are evaluated at the centroid of every panel. The inertia forces are included corresponding to a COG evaluated for the part of the model which is on the specified side of the cross-sectional plane.

2.9   Specified Force

For oil and gas industry, the numerical models of floating platform are to be considered as neutrally buoyant. It means, the gravity force and the buoyancy force of the submerged body are identical. But, for floating wind turbine, the case is not simple like the previous one. In SIMO-RIFLEX coupled analysis, the entire structure including the hull (supporting platform), mooring lines, tower, hub, RNA (rotor and nacelle) are not considered as one single rigid body. That means, only the hull, hub and nacelle are considered as rigid body.In SIMO, these bodies are balanced with their weight by default. But, in RIFLEX, the tower, rotor and mooring lines are considered as beam elements and the gravity forces are regarded as nodal forces. Hence, there is net resultant gravity force from the tower, rotor, mooring lines which result in a different situation. Hence, for the bodies in SIMO, gravity forces are included . Now, these are not balanced by default. So, to establish the equilibrium at the mean water line so that the draught remains the same according to the real case, total buoyant force equal to the gravity force of the whole platform including wind turbine is required to be specified at the COB (0,0,-20.76) in the upward direction. Now the entire force equation for the system stands for

$$
\begin{aligned}
TotalBuoyantforce = {}&[Gravityforce(Floater) + Gravityforce(Hub\&nacelle)]_{SIMO} \\
&+ [Gravityforce(mooring) + Gravityforce(tower) + Gravityforce(Rotor)]_{RIFLEX}
\end{aligned}
$$
$$(2.73)$$

This implies, now the whole structural model becomes neutrally buoyant regarding the platform keeps floating at the same mean position. No force is exerted on the structure, so no movement in the upward or downward direction unless there is any external force.

Due to this modification, it becomes necessary to update the restoring coefficient matrix imported from the WADAM. The restoring forces follow from hydrostatic and mass considerations when a body is freely floating. Hence, the first part of the following equations which are related to the mass considerations are to be modified only. Otherwise, the restoring coefficients are going to be over estimated.

Here, one thing is to be kept in mind that, for this semi-submersible type structure the modification is not as significant as for spar case. Because the distance between the CoB and CoG is not big. Moreover, the second term which comes from the Bernoulli(hydrostatics) is

dominant here. Even though, to get an accurate result, the modification is necessary.

$$C_{44} = \rho g V(z_B - z_G) + \rho g \iint_{A_{wp}} y^2 ds \qquad (2.74)$$

$$C_{55} = \rho g V(z_B - z_G) + \rho g \iint_{A_{wp}} x^2 ds \qquad (2.75)$$

Modified Restoring matrix elements are as follows:

$$C_{44}^{Modified} = C_{44}^{WADAM} - [\rho g B_{Total} z_B - \rho g G_{Total} z_G)] \qquad (2.76)$$

$$C_{55}^{Modified} = C_{55}^{WADAM} - [\rho g B_{Total} z_B - \rho g G_{Total} z_G)] \qquad (2.77)$$

It is important to be noted that, G_{Total} does not include the mass of the mooring system as it was not included in Genie mass model. But the B_{Total} is the total buoyancy obtained from the platform at mean water line.

2.10   Fourier Transform

In case of Simo-Riflex-Aerodyn, the regular and irregular wave analysis, the output results (i.e motion response, hydrodynamic force response, other force responses etc.) are obtained in terms of time series for a given length of time. Time series is referred either to a sequence of discrete numbers (as this discrete series is derived from the continuous time function) or to refer the original continuous time sample x(t).The figure above illustrates a sample of time series at regular intervals. It is important to analyse the time series to obtain the statistical characteristics of the original function x(t). The intention behind the time series analysis is to obtain the statistical characteristics of the original function x(t). A short overview of FFT(Fast Fourier Transform) is given here as it is used frequently for postprocessing the result found from the irregular analysis.
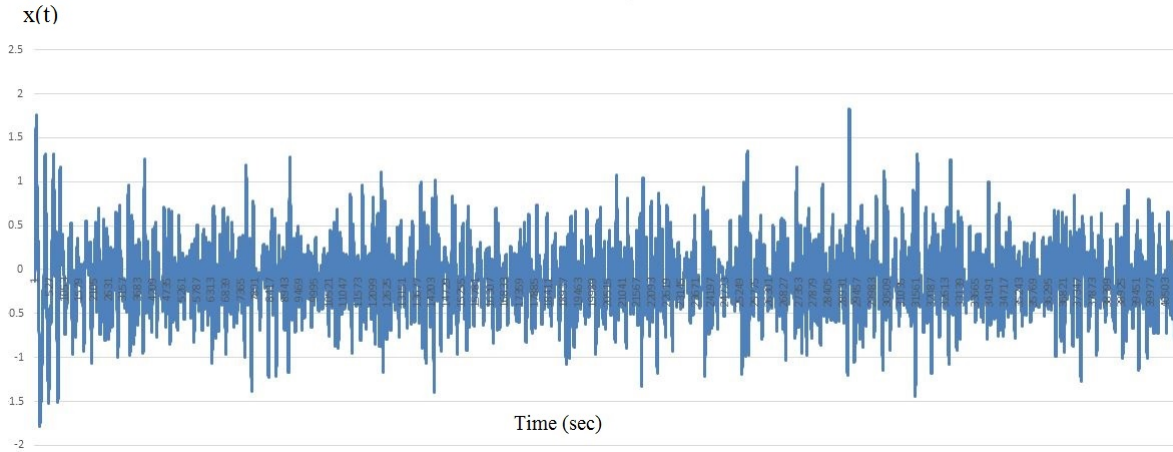
Figure 2.11: Time series of a random function x(t)

If xt is any random profile(.i.e wave or response etc.) as a function of time, the energy spectrum can be written as follows:

$$\S(\omega) = \frac{1}{T_s}\Big[\sum_{n=1}^{N} x(n\delta t)exp(i2\pi f(n\delta t))\delta t\Big]^2 \tag{2.78}$$

Here, the derivation of this formulation is not going to be discussed here as it can be found in many popular books for instance (Newland, 2012). The important parameters and how these influence the shape of the spectrum are discussed here. T_s is the total length of simulation, T_s is divided into many smaller segments, M. Each M is consisted of an equal number of data points, N at a constant time increment, δt . Here, N is chosen as a power of 2 as it makes the system more time efficient. The final result is averaged over M sections as it can be observed from the equation given above. The length of the record is dependent on M,N and δt which implies $T_s = MN\delta t$. When the results are obtained, the record or simulation length and the time increment are already fixed. So, during the FFT for obtaining the spectrum the choice of M and N are only left. Other two important parameters are frequency resolution δf and the frequency range or Nyquist frequency, f_N.

Using these expressions $\delta f = 1/N\delta t$ and $f_N = 1/2\delta t$ it is easy to find out the last two parameters if the above-mentioned parameters are known.

During plotting the power spectrum from the time series results, the choice of M and frequency resolution are to make carefully to obtain the shape of power spectrum properly. To attain the confidence M is required to be as large as possible. But, there is a mutually

antagonistic relation between the choice of M and the degree of frequency resolution. If M gets too large it causes to decrease N as well as frequency resolution get decreased as well (because the value of δt gets increased). While M gets large it produces high degree of confidence regarding the reality of such spectrum and the peaks get blunter and spectrum becomes more smooth. On the other hand, if frequency resolution is high(δt) then spectrum becomes peakier and details of such energy spectrum are more clear and precise but with a great amount of risk of having very low degree of confidence. So, an optimum value of frequency resolution is required to choose so that M becomes large enough to give a high confidence. Generally, M is taken as $M \geq 8$ and N is normally between 512 to 2048.

It is important to keep in mind that, the form or shape of a spectrum (i.e wave spectrum or response spectrum etc.) is not unique. If the number of data points is changed, the relative distribution of energy gets changed as well. Hence the comparison can be made between two spectrums while the length and parameters are almost same. But, the total energy content under the curve of the spectrum in different spectral shape remains nearly same. Chakrabarti (1987).

2.11   Decay Method and evaluation of damping coefficient

The free decay test is a way to evaluate the natural period of the platform as well as the damping coefficients as it is a common engineering practice. The motion can be written as from (Faltinsen, 1993).

$$\ddot{x} + p_1 \dot{x} + p_2 |\dot{x}|\dot{x} + p_3 x = 0 \tag{2.79}$$

Here, p_1 is linear damping and p_2 is quadratic damping coefficient. It's to be noted that, the damping is constant with respect to the amplitude of oscillation is assumed here. The coefficients can be evaluated from the following expression.

$$\frac{2}{T_m} \log(\frac{X_{n-1}}{X_{n+1}}) = p_1 + \frac{16}{3} \frac{X_n}{T_m} p_2 \tag{2.80}$$

Here, in the above equation, X_n is denoted das the amplitude of the nth oscillation. For

any n, $T_m/2$ is one half period between X_n and X_{n+1}. So, now the above equation can be compared with y= mx+c, where $y = \frac{2}{T_m}\log(\frac{X_{n-1}}{X_{n+1}})$, $m = \frac{16}{3}\frac{X_n}{T_m}p_2$ and $c = p_1$. So from the plot the slope, m will give the value of non-linear damping coefficient and the intercept, c will give the value of linear damping coefficient. It is to be noted that sometimes it is not easy to obtain a straight line from experimental results. However, more than 10 oscillation periods may be required to obtain a precise estimate of the damping.

2.12 Retardation Function

In the first section linear wave induced response was discussed in the frequency domain. But, now the behaviour of the platform is taken into account in an irregular sea where it is composed of regular waves of different wave frequencies . This implies it would cause many different excitation frequencies. In time domain analysis it is not possible to use the frequency dependent added mass or damping coefficients anymore.

However, if the steady state response is of importance then it is still correct to add up the response to each and every regular wave components. But, when the transient (temporary, lasting only for a short time) response is of importance, it gets essential to evaluate the retardation function which can be used in the equation system given in 2.50 in time domain.

The motion of equation is formulated in different manner which is discussed in **?**. It is to be kept in mind that, the response calculated by this reformulated equation system is influenced by the high-frequency behaviour of added mass(A_{kj}) and damping (B_{kj}) coefficients.

Moreover, it is also important to keep in mind that equation system may get ill-conditioned at high frequencies due to the presence of irregular frequencies. Beside, there is a limit reduce panel size(which is necessary to be small at high frequency because of the computation time. $\lambda = 2\pi g/\omega^2$) implies the inversely proportional relationship between frequency and wavelength. So, higher frequency means smaller wavelength as well as smaller panel size.

Either, frequency dependent added mass or damping coefficients and one value of the added mass are needed to know to calculate the retardation function. In SIMO, frequency dependent damping coefficients and added mass infinity(as one value) are used for the calculation of retardation function. However, when the sys file is generated using the SIMO-RIFLEX coupled software, the program automatically generates the retardation function from the frequency dependent damping coefficients. It is important to have the information of damp-

ing coefficients at all frequencies which are already calculated in hydrodynamic analysis in HydroD. The theory used here can be found in the SIMO theory manual(Chapter 4).

2.13 Linear Response Spectra

There is a way to verify response spectra of the platform which can be obtained from the time domain analysis. In a linear system the response spectrum S_R of a structure can be written as the multiplication of wave spectrum S_W and the square of response $RAO(\omega)$ and as follows:

$$S_R(\omega) = [RAO(\omega)]^2 . S_W(\omega) \tag{2.81}$$

2.14 Irregular Wave theory

Generally, the simulation of irregular sea and gathering information of statistical estimates are based on linear theory. The following expression is used to generate a long-crested irregular sea traversing along X-axis. Long-crested sea implies wave propagation in one direction only.

$$\zeta = \sum_{j=1}^{N} A_j \sin(\omega_j t - k_j x + \epsilon_j) \tag{2.82}$$

Here, A_j is the wave amplitude, ω is the circular frequency , k_j is the wave number and ϵ_j is the phase angle for j-th mode. The following figure demonstrates the expression clearly and hence the irregular sea simulation in time domain from several numbers (i.e j=1 to j=N) of regular waves are understood easily.

For getting a clear idea about the parameters used to define irregular wave, a short overview is given here. But detailed theory can be found in (Chakrabarti, 1987) (for instance). However, the wave amplitude can be expressed by a wave spectrum $S(\omega)$ as follows

$$\frac{1}{2} A_j^2 = S(\omega_j)\delta\omega \tag{2.83}$$
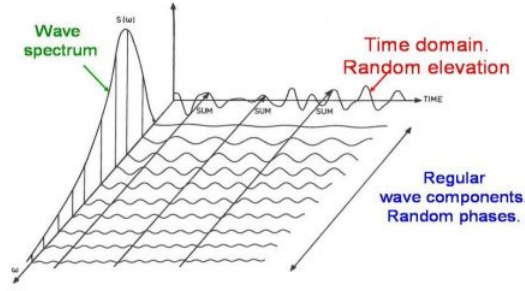
Figure 2.12: Connection between a frequency domain and time domain representation of waves in a long crested short term sea state((Faltinsen, 1993))

In the above equation $\delta\omega$ is the difference between successive frequencies. Here, the wave elevation is Gaussian distributed with zero mean and this implies the variance is equal to the integration of the wave spectrum from 0 to ∞. Since the sea can be described as a stationary random process and in practice it is for a limited time period in a range of 0.5 to 10 hours. Generally, this is referred to as short-term description of the sea.

However, the JONSWAP spectrum given in SIMO theory manual is written here

$$S_\zeta(\omega) = \frac{\alpha g^2}{\omega^5} exp\left(-\beta\left(\frac{\omega_p^4}{\omega}\right)\right) \times \gamma^{exp\left(-\frac{\left(\omega/\omega_p - 1\right)^2}{2\sigma^2}\right)} \tag{2.84}$$

Where, α spectral parameter which can be defined by Hs as follows

$$\alpha = \left(\frac{H_s \omega_p^2}{4g}\right)^2 \frac{1}{0.065\gamma^{0.803} + 0.135} \tag{2.85}$$

ω_p is the paek frequency, γ is the peakedness factor, β is the form factor, default value is 1.25 and σ is another spectral parameter with default values. [σ_a=0.07 for $\omega < \omega_p$ & $\sigma_b = 0.09$ for $\omega > \omega_p$].

For short crested sea(i.e a short-crested sea is referred to a two-dimensional wave spectrum) the equation 2.82 can be written as

$$\zeta(\omega,\theta) = \sum_{j=1}^{N}\sum_{k=1}^{N}(2S(\omega_j,\theta_k)\Delta\omega_j\Delta\theta_k)^{0.5} \times \sin(\omega_j t - k_j x\cos\theta_k - k_j y\sin\theta_k + \epsilon_{jk}) \tag{2.86}$$

H_s is the significant wave height which is defined as the mean of the one-third highest

waves and ω_p is the peak frequency where the spectrum has its peak value. $[\omega_p = \frac{2\pi}{T_p}]$

Chapter 3

Numerical Modeling

The basis for handling the diffraction & radiation problem of large volume structure is linear wave theory. Morison equation is generally used for slender structures. to include the viscous effect this is also used along with the panel model by taking the mass coefficient equal to zero otherwise the mass matrix would get over estimated.

Once the wave induced loads are estimated from the hydrodynamic analysis as mentioned in the theory part, using the principle of load for hydrodynamic equilibrium internal loads are found. Similarly internal loads can be obtained by establishing the hydrostatic equilibrium. As, here the first task is to perform hydrodynamic analysis and analyze the rigid body motions along with the hydrodynamic coefficients, the first prerequisite is to make a panel model.

3.1   SFC parameters

The parameters and the detail geometry of this SFC concept is already provided and taken from (Luan et al., 2014b) , (Michailides et al., 2015) & (Gao et al., 2014). The description of the structure is already given in the end of literature review. Here the main properties are shown in the Table 3.1

While modeling the panel model the detail geometry is taken from the schematic diagram is as shown in the Figure 3.1b .

Table 3.1: Main properties of SFC concept in mass model(Genie)

Platform	SFC
Width(m)	83.3
Height(m)	50
Draft(m)	30
Total Displaced volume(m^3)	11470
Mass(ton)	11626
WEC	SFC
Rated Power(kW)	350
No. of WECs	3
Width of WEc	20
Displaced volume of WEC(m^3)	384(each WEC)
Mass(ton)	100(each)
Wind turbine	NREL 5MW
Rated power(kW)	5000
Rotor diameter(m)	126
Total mass of tower, RNA & hub (ton)	697
Nacelle height(m)	90 m above SWL

(a)   (b)
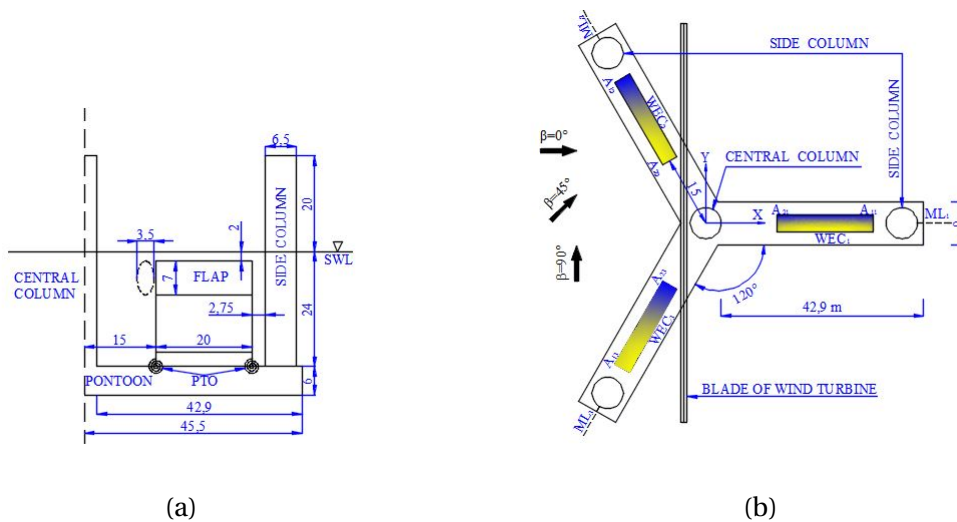
Figure 3.1: Schematic diagram of the SFC(side view on left and top view on right)

3.2 Response analysis software

In this section a general description of software used are mentioned. The detail link and how these softwares are used are disussed in the next section.

3.2.1 Genie

Genie provides an integrated design environment for modeling, analysis(Wajac, Sestra & Splice in the background), simple result presentation(Xtract for advanced purpose) and code checking. Concept modeling can be performed by either whole beam(i.e. several beams) or whole plate/curved surface or combination of both with respect to the application. Moreover equipments, loads, mass, FE model creation(FE mesh) can also be performed in this package. Panel model, structure model or mass model can be modeled here which are generally the input files for HydroD. Panel model includes the geometry as well as generate the panel mesh and assigning the hydro pressure. Whereas the structure model in principle is same, but includes tank walls. Genie can also perform static and dynamic linear analysis for fixed structures. It also provides the feasibility for importing models from SACS, StaadPro, StruCAD and Ansys.

To obtain the panel and mass model Genie is used here.

3.2.2 HydroD

HydroD is for modeling the environment and preparing the input data for stability(hydrstatic) and hydrodynamic analysis. In hydrosatic analysis, it includes the free surface effect, calculates still water force and bending moments, GZ curve, allowable VCG(vertical center of gravity) etc. While in hydrodynamic analysis on fixed and floating rigid bodies, it calculates (with (WASIM)and without forward speed(WADAM)) the hydrodynamic coefficients, excitation forces, displacement, acceleration, sectional forces etc. Moreover it it provides the feasibility to transfer the hydrostatic and hydrodynamic loads to structural analysis.

Wadam(Wave Analysis by Diffarction And Morison theory) provides different features such as: 3D radiation /diffraction theory, Combination of large and small volume structure, multi body, zero speed, finite/infinite water depth, frequency domain(1st / 2nd order), motion and loads, pressure and wave elevations, viscous effect from eddy viscosity, skin friction, bilge keels, automatic load transfer. This program uses potential wave theory and sink-

source technique(described in previous section for 1st order wave). Wasim also provides some other features with some common features which are not discussed here as not used. Here, the stability analysis, hydrodynamic analysis including the sectional loads are obtained using HydroD.

3.2.3 Postresp

Postresp is a graphical postprocessor for statistical processing and presentation of response in both frequency and time domain. The features in postresp in the frequency domain are as follows:

- Transfer function-wave loads and global response from hydrodynamic analysis, loads from structural analysis

- Response variable can be combined

- Forward speed/doppler shift can be handled

Postresp is used here to obtain the results in .xml file and then processed using Matlab.

3.3 Panel model

The panel model is modeled in the genie which is sufficient for the hydrostatic and hydro-dynamic analysis. A typical maximum size of elements used for global model of a semi-submersible is around 2×2 meter.Element type is usually 8-node shell element and 3-node beam element. Here, *sesam quad mesher* is used which provide both the option for 4 & 8 node element. As here the model is used for hydrodynamic analysis, element length of 1 m is chosen as mesh density to save the computational time.It also satisfies the requirement of $\delta x < \lambda/8$. Sometimes the java script is also used to modify the model which is really feasi-ble and saves a lot of time. The model is built using the advantage of symmetry(half of the model is built) as this software has a maximum limitation of elements of 15000, moreover it also reduce the size of matrix during computation and thus time effective. one more impor-tant thing is to assign the wet surface. This case is handled by the load case *Dummy Hydro pressure* and then is assigned as required and shown in the Figure 3.2.
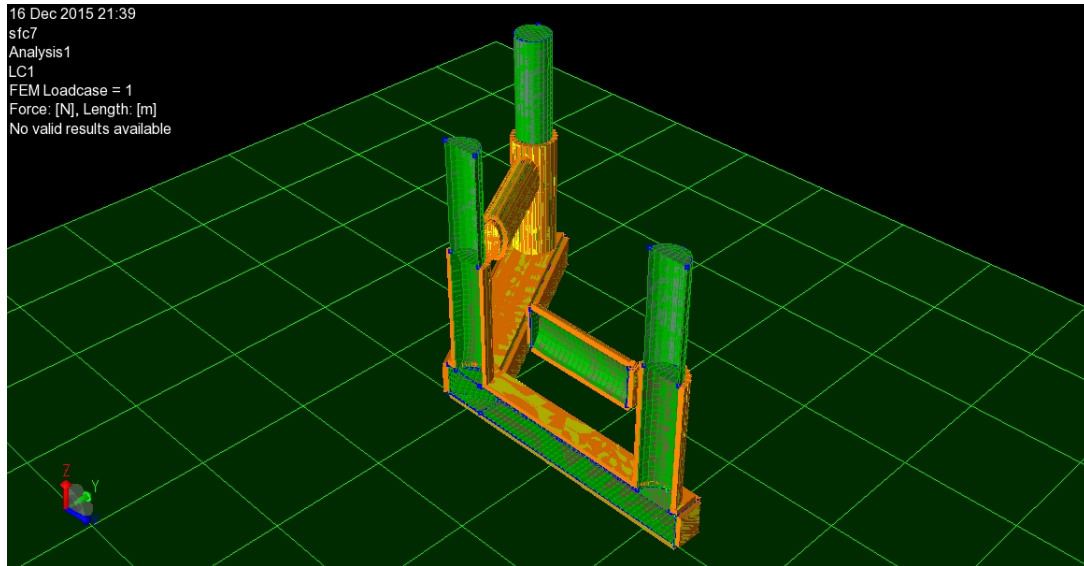
Figure 3.2: 3D view of panel model in Genie

3.4   Mass model

The main purpose to build the mass model is to calculate the internal load at the particular position near the center column on the pontoon which is described later. As, HydroD gives the flexibility to consider the mass from *fill from buoyancy* or *homogeneous density panel model* when the mass is distributed uniformly, this facility can be used for hydrodynamic analysis. But, for the calculation of sectional loads it is important to take the mass information from the mass model. During the modeling of mass model, 2 node beam element is used without considering any stiffness or other properties related to the structural analysis, but just the density and section. As the pontoon is ballasted fully and the side columns are partially ballasted till 16m from the bottom of the column, equivalent density is calculated to model the mass model properly. So, the mass is taken as consistent mass for the whole submerged part and the tower as well. The tower, blade, hub and nacelle are modeled according to the guideline from the NREL 5MW wind turbine. But the hub, nacelle and the blade are modeled as concentrated mass at the center of gravity using artificial beam of negligible density and section property. The detail of the mass model is shown in the Figure 3.3.

Under the modeling of the mass model this simplification is considered which can be sometimes non-conservative in terms of free surface effect or the local moment of inertia of the blades etc. The effect of free surface effect is handled by assuming that the top of the side column at 16m is covered with steel plate, so provide negligible free surface effect and

secures the conservatism of stability analysis. The local moment of inertia of the blades are quite negligible compared to the global inertia. So, it is important for the analysis of stress at the root of the blade, but in this case to evaluate the sectional load it is okay.

ballast water is upto 16 meter.
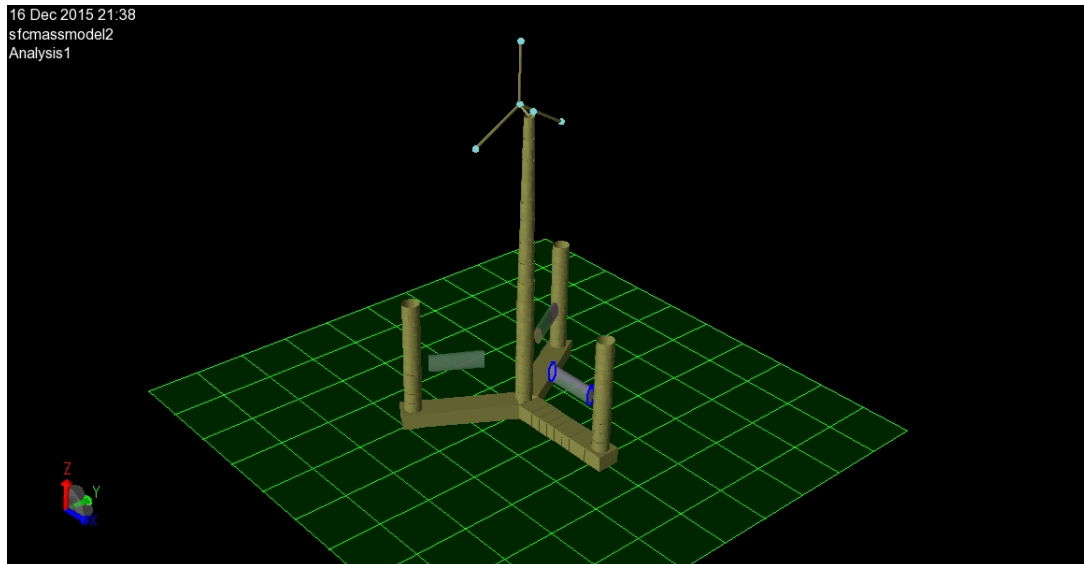
Figure 3.3: 3D view of mass model in Genie

3.5   Morison model

The morison model is not modeled separately. But during the hydrodynamic analysis for wave load and sectional loads calculation, to consider the viscous force contribution to the damping this morison model is defined and as well as the mass and drag coefficients. In the morison model, artificial sections of negligible diameter and equivalent diameter for rectangular section are modeled as shown in the Figure 3.4. The reason is if artificial diameter is not considered then the buoyancy get overestimated as this is recalculated again. Moreover, while the coefficients are assigned mass coefficients are taken zero as it is already considered by means of panel model. The upper part above the SWL is assigned as *dry section.* The detail about these coefficients are described later in this chapter.
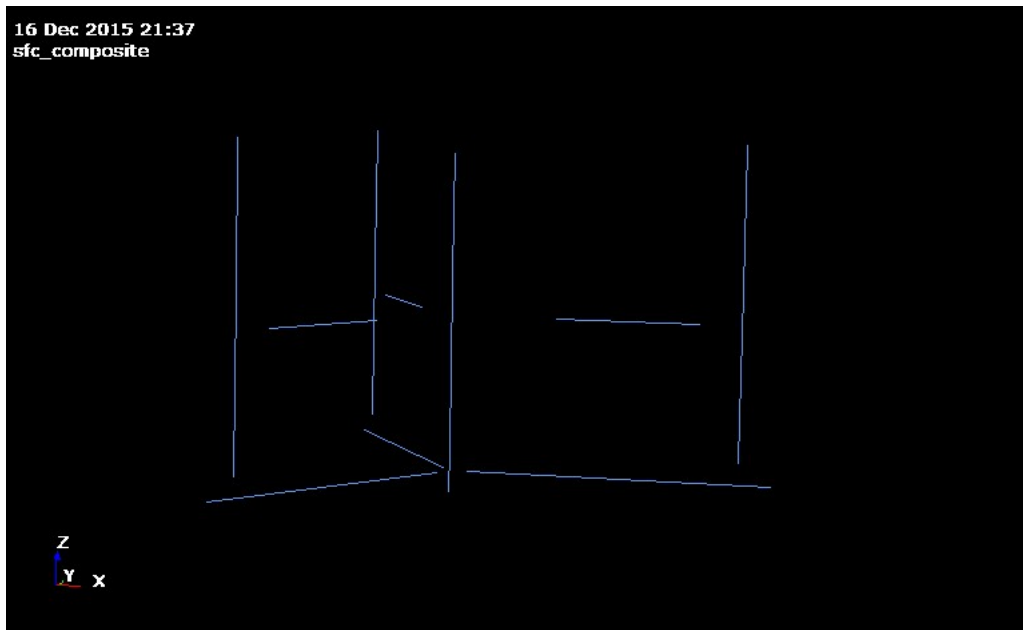
Figure 3.4: 3D view of morison model in HydroD

3.6 Environmental condition

Wave & wind heading interval

The hydrostatic analysis is performed for 0^0 of wind heading angle. The description of wind force model is given later. Whereas the hydrodynamic analysis is carried out for $0^0 \& 120^0$ wave direction.

Frequency interval

The response due to single linear wave is evaluated at 60 frequencies in the interval of $\omega = 0.209 - 6.1416 \text{rad/s}(\text{T=2-40s})$ with random stepping.

Water and location properties

Table 3.2: Water environment

Water density	$1025 \ kg/m^3$
Water kinematic viscosity	$1.19 \times 10^{-6} m^2/s$
Water depth	200m

3.7 Hydrostatic analysis

Hydrostatic analysis is performed to achieve the righting moment curve and to check from the GZ curve whether the structure is stable or not. Moreover the mean sectional force for different wind heading angle is also of interest. The results are discussed in the next chapter. As input, the panel model is taken but this time the wet surface is defined till 20m above the SWL(sea water level) as shown in the Figure 3.5. This is done as when the model is going to be heeled at 180^0 then the top of the side as well as center columns are getting submerged. So, to take into account the buoyancy effect from the top of the columns above the mean water level, this is to be taken into account.

The wind force is not modeled as wind profile, the drag coefficient and the blockages are also not considered. So, the wind force which gives the thrust force as well as the heeling moment of 82755000 Nm using the thrust around 750 KN at rated speed (as shown in the Figure 3.6) and the arm length as 110.34 m (from the CG of nacelle to the CB of the whole structure).
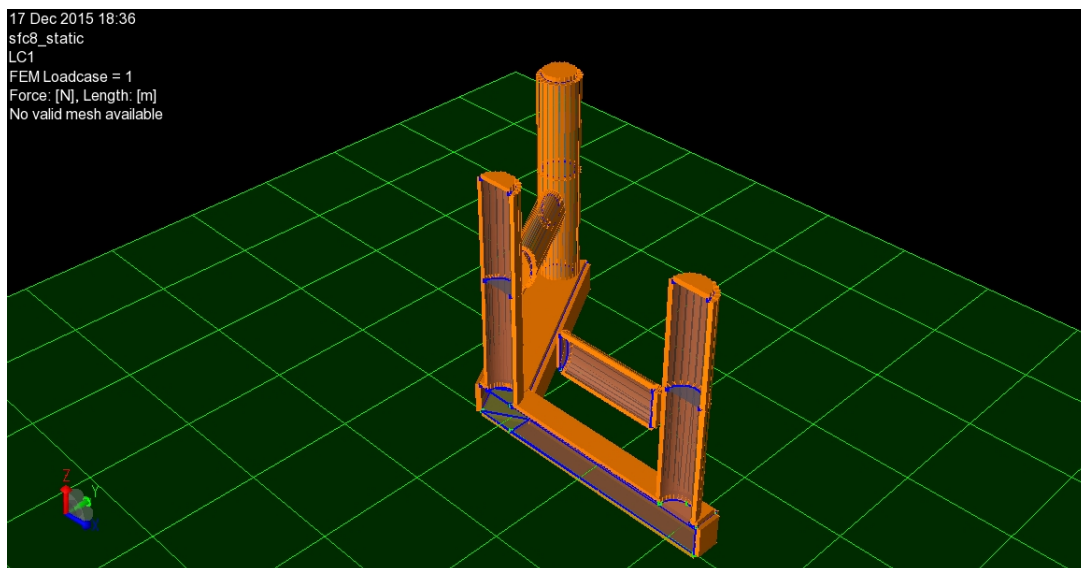
Figure 3.5: 3D view of panel model for stability analysis

3.8 Hydrodynamic analysis

For large-volume structures, radiation-diffraction theory is employed since it gives a satisfactory prediction of mass forces at deep draft, which are generally dominating. For slender structures the Morison equation is used in linearized form due to the large importance of
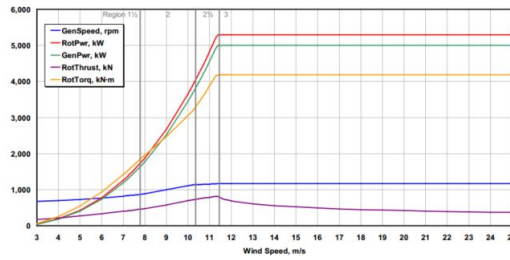
Figure 3.6: Performance curve for NREL 5MW WT

viscous terms. These two methods can be combined in a dual model or composite model where Wadam selects the most appropriate method depending on the body dimension (diameter) compared to the wavelength. As here this section focuses on uncoupled analysis, it does not considers about the current force around the mooring system or any other dynamics which is really important. For this analysis viscous terms are taken into account by using composite model.Composite model is also suitable as here no mapping or transfer of loads are not considered from the HydroD to the structure model. Using the equation of motion as discussed in the chapter 2 in frequency domain HydroD solves the *transfer function or RAO* of rigid body motions.

So, the panel model and mass models are given as input. In addition, the morison model is also added, to take into account the viscus effect coming from the drag. Environment condition is defined as mentioned earlier.

Mass and drag coefficient

From *DNV RP C205* the drag coefficient is taken as 1.0 for rectangular pontoon section and for other cylindrical sections 0.65 is taken. The mass coefficient is taken as zero to avoid over calculation. Parts above the water is taken as dry section.The ellipse is taken as cylindrical section of negligible diameter. And then the equivalent coefficients are assigned. A simple example is given below and drag coefficient becomes 42250.

$$D_{column} \times C_D = D_{dummy} \times C_{equivalent}(6.5 \times 0.65 = .0001 \times C_{equivalent}) \tag{3.1}$$

Table 3.3: My caption

Parameters	Description
Platform model	Rigid body
Mass model	Floater and tower (uniformly distributed)
	RNA (concentrated mass)
Force model	1st order potential theory and
	Morison's equation for viscous drag
Aerodynamic load	Not considered
Current	Not considered
Mooring	Not considered
Cross section location w.r.t global coordinates	(3.3 m, 0 m, -27 m)

Drag linearization by waveheight

There are several methods for applying drag linearization such as stochastic method or wave-height. Among those methods wave height matrix for different wave period along with wave heading is chosen for drag linearization. As, here linear wave theory is used, so the limit for breaking wave is considered. because, breaking waves do not follow linear theory. The maximum wave height is taken less than $\lambda/7$ where λ is the wave length. and for higher time periods when it exceeds 20 m, it is taken as limit.

3.9   Internal loads

Hydrodynamic analysis handles this section to obtain the sectional load in hydrodynamic equilibrium. The main task is to define the cross-section of interest. the section is cut at (3.3m, 0m, -27m) parallel to the YZ plane as shown in the Figure 3.7. During hydrostatic analysis same cut is also taken to obtain the sectional load in static equilibrium.

3.10   Short overview of experimental set-up

In this section a short overview of experimental set-up which is given so that it can be easy to highlight the difference between the numerical and experimental results later on. *is to be noted that, the experiment is not performed as a part of this thesis topic..* That is why detail discussion is not drawn here rather some important parameters like the scaling law, scale factor, load model, structural model etc. are mentioned here.
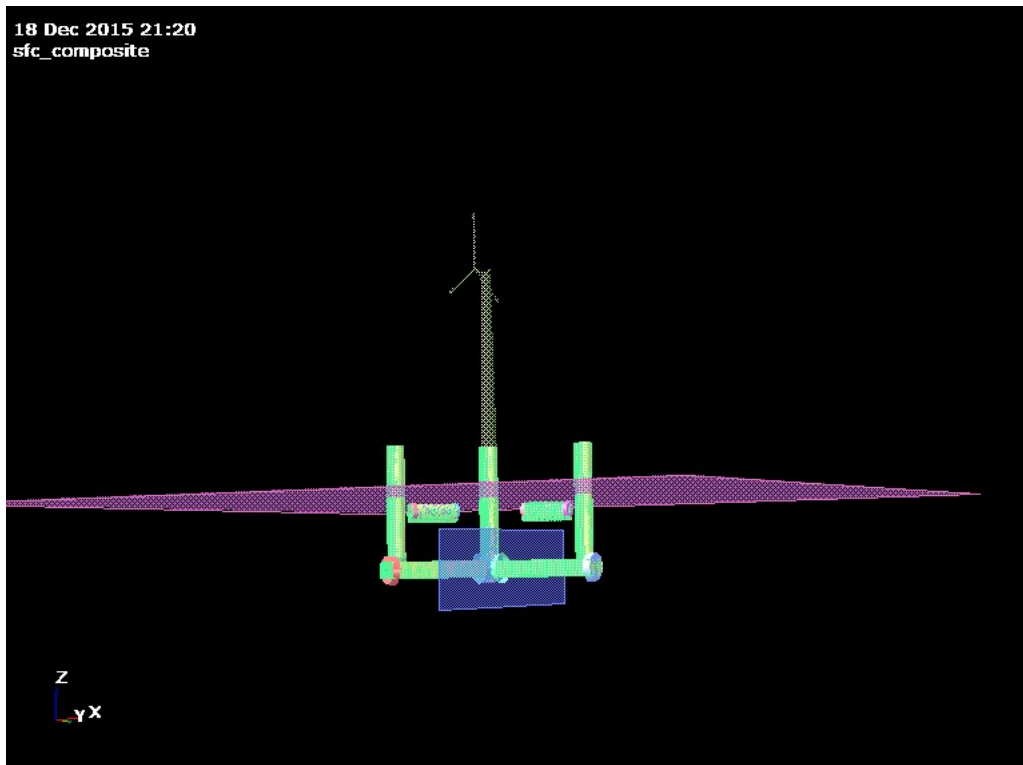
Figure 3.7: The composite model

Table 3.4: My caption

Variables		Scale factor
Linear dimensions (length, height, width, wave height etc.)	λ	50
Mass, force	λ^3	125000
Time, velocity	$\lambda^{.5}$	7.07
Moment	λ^4	6250000
Angular motion, acceleration	1	1

However, the test was performed in the Hydrodynamics and Ocean Engineering Tank in Ecole Central Nantes (ECN), France.

Chapter 4

Results & Discussions

This chapter encompasses the global frequency domain hydrodynamic analysis of the SFC in HydroD. The platform is subjected to regular wave. The comparison of motion RAOs obtained form the numerical analysis in HydroD with the experimental results are discussed. Moreover, the sectional load at the position(3.25m,0m,-27m) is investigated and discussed. The location of the cross-section is illustrated in the previous chapter. Moreover, the structural and load model are also discussed in the previous chapter.

4.1   Stability Analysis in HydroD

The stability analysis represents one of the most important aspects of design of the platform which reflect its ability to carry its own weight and to sustain the heeling moment. Generally, hydrostatic analysis cover several draughts, but here the particulars are investigated only for draft of 30 m. Actually, the whole platform is ballasted in a way so that this draught can be achieved. In the following table 4.1, a comparison between this numerical model result and another numerical model from (Michailides et al., 2014) result are presented. Both of the stability analysis are performed in HydroD. In the paper, regarding the inclining moment a threshold related to the heeling moment is considered as 74 MN-m. This is equal to the maximum induced heeling moment due to the turbine steady force at rated wind speed. Whereas, here a heeling moment of 82.76 MN-m is applied which is also calculated from the maximum thrust force at rated wind speed. Heeling moment= Thrust force at rated speed × distance between the tower top and COB_z = 746 × 110.76 = 82755 KN-m.

Almost all of the parameters are quite close except the 1st intercept. Maybe this is due to

the difference between the applied heeling moment. So, this could affect the stability of the numerical model used here in this thesis topic.

Table 4.1: Comparison of stability analysis results

Parameters	Numerical	$Numerical_{Constantine}$
Ballast mass (tonnes)	8720	8820
1st Intercept(deg)	8.04	7.87
Metacentric height(m)	4.50	4.52
Displacement (tonnes) [Including WECs]	11710	11738
COB_z (m)	-20.76	-20.74
COG_z (m)	-18.02	-18.02
Applied heeling moment (KN)	82755	74000

It is to be noted that, there is a difference in mass of the whole platform in HydroD stability analysis from the Genie model. In Genie, the platform weight is 11526 tons without the mooring system and the reason behind the increase of 100 tons is not found. It is supposed to be 11526 tonnes in HydroD analysis as well as the mass model is taken from Genie without any change in mass. One probable reason could be the mesh size. However, the difference is less than 1%, so this numerical model is taken for further analysis.

4.2   Hydrodynamic analysis in frequency domain

4.2.1   Verification of Rigid body motion RAOs with experimental result

The developed numerical model is verified against the experimental result. In this section the RAO of rigid body motions for 3 degrees of freedoms heave, surge and pitch are compared with the experimental results for regular wave in aligned condition. The rigid body motions are evaluated from HydroD in frequency domain. In the following figure 4.1 and 4.2 the comparisons are illustrated. The comparison are done within wave frequency ranges from 4-18 sec (mentioned in wave period). That is why excitation due to the resonance are not observed here as the natural frequency of the platform are quite far outside this range of wave periods. Moreover, the numerical model is modeled in full scale whereas the experimental model is in model scale. But, the results from the experimental model is scaled up using Froude scaling as given in the previous chapter. While comparing it is to be kept in mind that there are differences between the numerical model and experimental model which has been

(a) Heave RAOs   (b) Surge RAOs
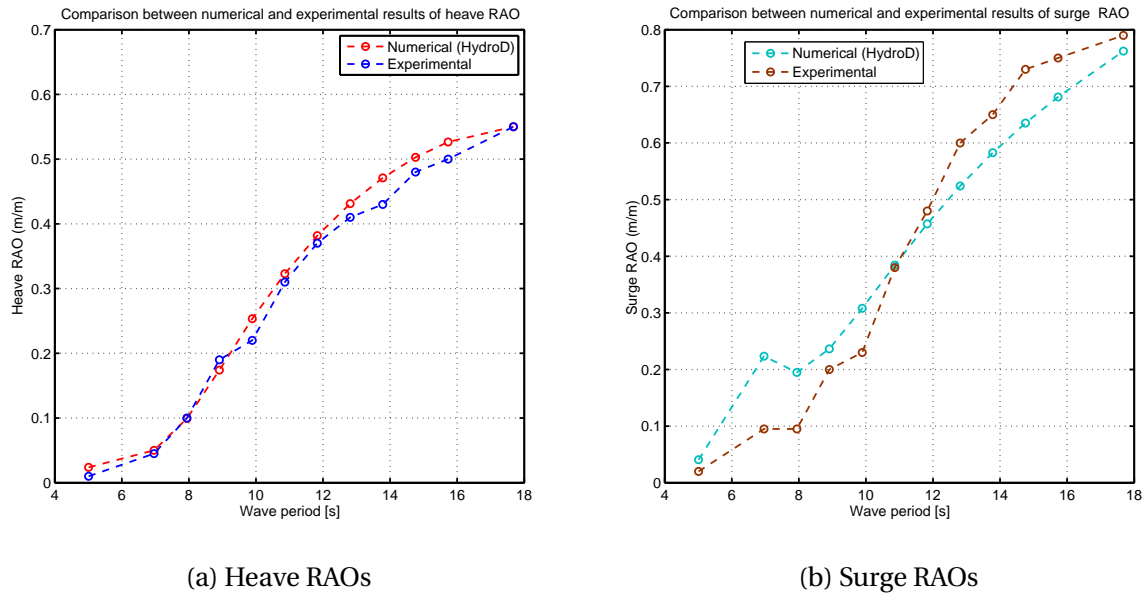
Figure 4.1: Heave & surge RAOs comparison between numerical and experimental results

discussed in the previous chapter. In figure 4.1a the comparison between 1st order heave RAOs which is computed in frequency domain and the experimental heave RAOs for the SFC are performed. It seems that heave transfer functions obtained from the numerical analysis are in good agreement with the experimental results. There are some discrepencies within wave period of 13-16 seconds but not that significant. It seems that absence of mooring line in the numerical model does not have any significant effect on heave RAOs as it is supposed to be. Moreover, only the 1st order potential force has been considered in the numerical model with Morison's drag. But, as the wave amplitude (1m) is less compared to the body dimension, it is expected to have insignificant non-linear effect.

In figure 4.1b, the surge RAOs are compared similarly. It seems that there are some discrepancies between the results obtained numerically and experimentally. There could be a chance that the added mass coefficient for surge is not approximated accurately as it is supposed to be. Because in the wave frequency region the main contribution comes from the inertia loads. Because in this region the effect of damping is very less. Moreover, the body mass matrix of both model agrees quite well. Hence, only term left is the evaluation of added mass coefficient. It may be concluded that this could be the reason of the discrepancy. Moreover, the effect due to the mooring lines becomes significant in the very low frequency region. In practical, within the wave frequency range up to 18 sec the effect can be neglected. Because, in large wave period the response becomes quasi-static and then the

contribution from the mooring stiffness becomes important. So, the absence of mooring in numerical model may not be the significant reason of the discrepancy. It is to be noted that in experimental model, the WECs are in operational condition, whereas the WECs are fixed in the numerical model in HydroD. So, in experimental results close to the resonance of the rotation of WECs which is around 15 seconds the values could be a bit greater than the numerical model. In figure **??** the comparison of pitch motion RAOs are plotted. It seems that
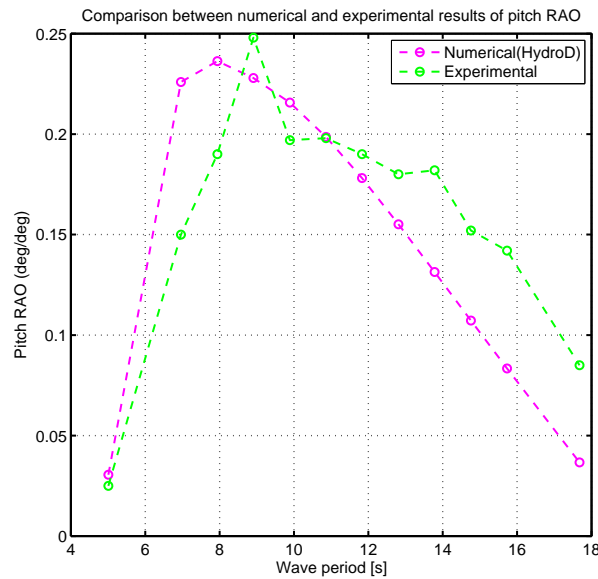
Figure 4.2: Pitch RAOs comparison between numerical and experimental results

there are some discrepancies between numerical and experimental results. This is true that there is some effect on the pitch restoring coefficient due to the mooring stiffness. Since, the numerical model doesn't have the mooring line, so there is a possibility of difference in pitch restoring loads between numerical and experimental models. But, the significant contribution comes from the inertia loads within the range wich is observed here. So, there could be some possibility that the pitch added mass coefficient or the pitch excitation moment is not evaluated accurately. The mesh size of the panel model is taken 1m which is expected to be sufficient. Maybe, decrease of the mesh size could have given more close results.

Overall, this is quite strange that for both surge and pitch RAOs the values around 7-8 seconds are quite different than the values from the experiment. The discrepancy close to the WEC rotation period may contribute to the discrepancy around 13-17 seconds for surge and pitch motions specially.

4.2.2 Case study of Rigid body motion RAOs for different wave directions

In this section, some case studies for rigid body motion RAOs are demonstrated for two wave directions (0^0 and 120^0) in regular waves without wind in HydroD. It is to be noted that the hydrodynamic analysis is performed in frequency domain for a range of frequencies (0.2 to 2 rad/sec). Only first order potential force is considered along with viscous drag forces to calculate the wave loads on the members of the structure. Viscous drag forces are calculated using the Morison's equation. This means that low-frequency forces effect are not considered. It is worth to mention that, the platform's motion is mostly controlled by the loads applied by waves and also body inertia mechanism. Detail is described in the previous chapter. Moreover, mooring line tensions are not considered in this part and that is why there is no coupling effect as well. Aerodynamic loads are not taken to be considered as well in this section.
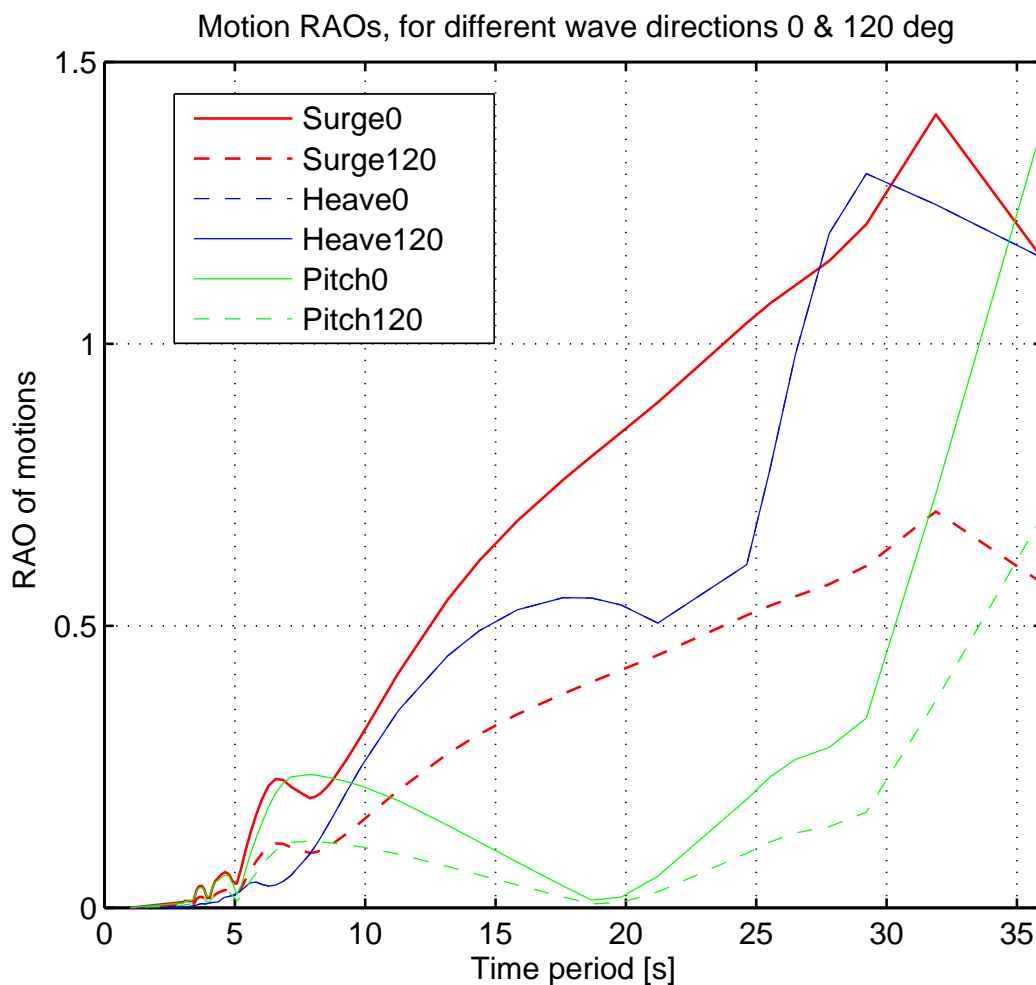
Figure 4.3: Comparison of RAO of surge, heave and pitch

In the above figure 4.3, it is clearly observed that the heave RAO is not affected by the wave direction compared to other motions. For short waves(small time periods) all of the motion RAOs are quite close as the platform is insignificantly disturbed by the waves. There are some cancellation and amplification observed in the figure 4.3. The cancellation jus before the eigen period of pitch motion occurs at 19 sec. Whereas the cancellation of heave is not captured properly due to the lack of data in the range of (20-25 sec). Generally, the cancellation in the wave frequency range occurs just before the eigen period of the body for corresponding motions.

In chapter 3 of (Faltinsen, 1993) a simple theoretical expression is given for evaluating the highest cancellation period for heave motion. The expression is as follows

$$\omega = \frac{\omega_n}{(1 - |z_m|(\omega_n)^2/g)^{0.5}} \tag{4.1}$$

The cancellation period is around 23.5 secs as calculated from the expression. It is to be noted that the expression is derived for an undamped equation of motion. But, the difference is not very large as found from the plot. Similar cancellation is occurred for the pitch motion as well.

The eigen period of heave and pitch are found to be 26.7 & 34.5 seconds respectively. This is to be noted that, as the mass of the platform is overestimated by 100 tonnes this also affects the value of C_{55} as well (The theory is described in the theory part). So there could be a little difference in the eigen period for pitch and roll physically. However, in the plot, the resonance is observed around the region close to the eigen period. The reduction of the application of motions at resonance period depends on the viscous drag coefficients. Maybe the motion RAOs can vary at the resonance period depending on the viscous drag. Because in this region the effect of damping gets important. For long periods the platform is following a quasi-static behaviour as it is supposed to be which is not shown in the plot as the wave frequency range is of interest.

In this wave frequency range the maximum value of pitch RAO is around 0.25 degree, whereas the maximum for surge and heave are around 0.9 m and 0.55 m respectively.

In figure 4.4, the sway and roll RAOs are plotted together. Obviously, for aligned wave condition these values are really insignificant. But, for 120^0 wave direction these motions get dominant like surge and pitch get dominant in 0^0. As the platform is symmetric with
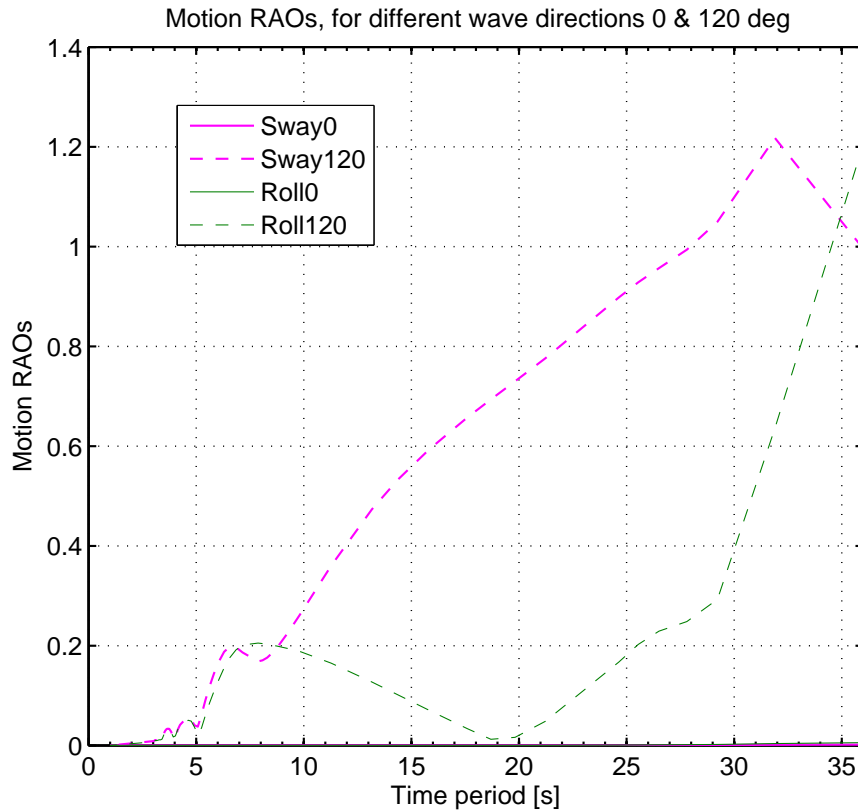
Figure 4.4: Comparison of RAO of surge, heave and pitch

respect to the YZ-plane, the pattern of the sway and roll RAOs are quite similar to the pattern of surge and pitch motion RAOs.

4.2.3 Excitation force RAO

In this section the excitation force RAO plots are presented for two wave directions (0^0&120^0) . The abscissa is in time period (s) and the ordinate is in force (KN). There is significant correlation between sectional force at the examined cross-section and the excitation loads on the platform. This is the reason for presenting the results here so that the behaviour of the sectional loads can be understood more clearly. Another important thing to be noted that the excitation forces are denoted with 'EX, EY and EZ' and the excitation moments are denoted with 'EMX, EMY and EMZ' with respect to X, Y and Z axis respectively.

In figure 4.5 and 4.7 the excitation force RAOs and excitation moment RAOs on the platform due to the wave forces are presented respectively. It is clearly seen from the figure that EX (excitation force in global X-direction) and EY (excitation force in global Y-direction) are dominating for 0^0 and 120^0 respectively. The maximum value has occurred around wave
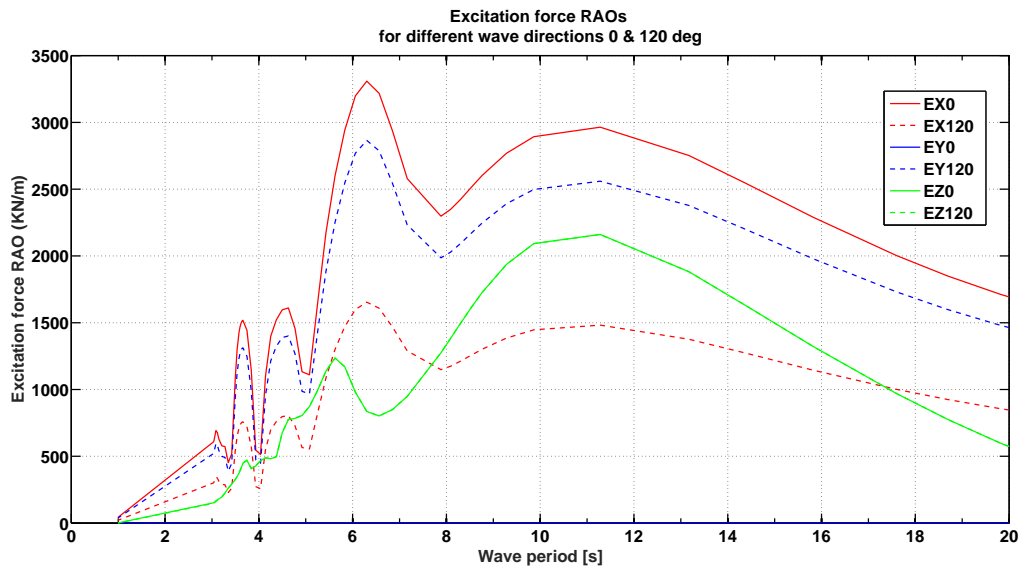
Figure 4.5: Comparison of RAO of excitation forces

period of 6.3 sec while the two peaks of a wave are under the leftmost side columns 2 and rightmost side column 1. Using the expression ($\lambda = 1.56 \times T^2$, the wave length is found to be around 62 m, which is the distance between one end to the other end of the platform as shown in figure 4.4. The abrupt changes in the range of (3-6 seconds) are also due to this type of reason but for other wave lengths. It can be observed that the maximum values of RAO are for EX0 and EY120. After a cancellation around (wave period, T=8 sec) there is another peak but less than the previous one in magnitude. Then the values continue to decrease with the increase of wavelength as the sea is becoming more flattened.

Table 4.2: Excitation load peak analysis

Peaks occurances of EX and EY at different time periods		
Time Period (s)	Wave length (m)	Number of complete wave
3.65	20.7	3
4.63	33.5	2
6.30	61.9	1

For excitation moment there are less abrupt changes compared to the excitation forces. The maximum values or the peaks occur around (T= 9 sec). This implies the wavelength is around 126 m. So, there is one-half wave along the platform from one end to another end. So, when the peak is at the leftmost end and the trough is under the rightmost end, it is causing the highest excitation moment for EMX120(excitation moment around global X-axis) and EMY0(excitation moment around global Y-axis) as shown in figure 4.7.

In conclusion, the excitation force has got its highest and 2nd highest peak around wave
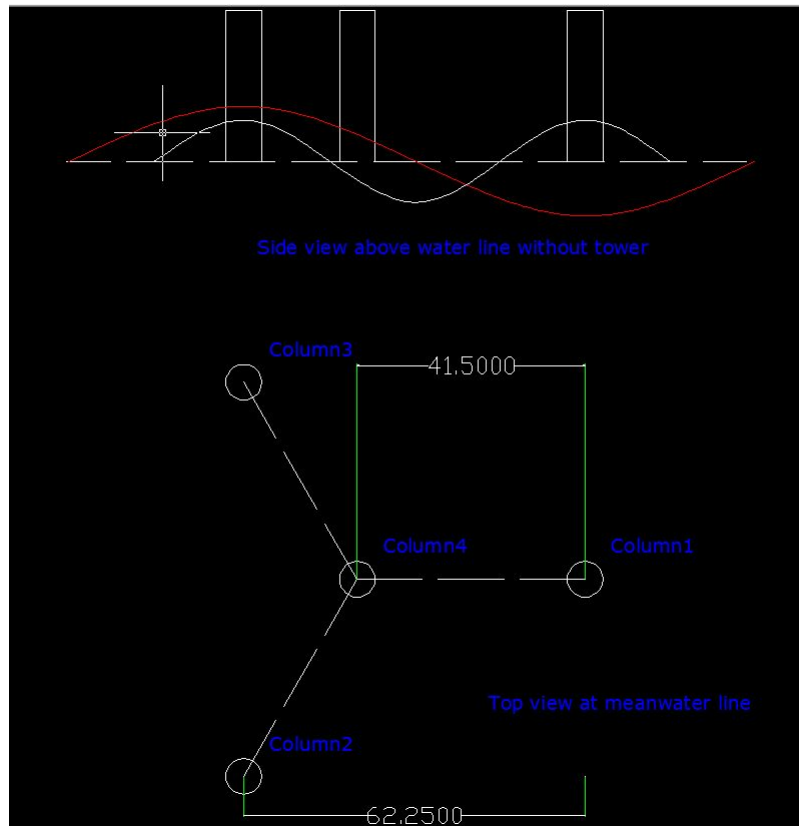
Figure 4.6: Top view at mean water line
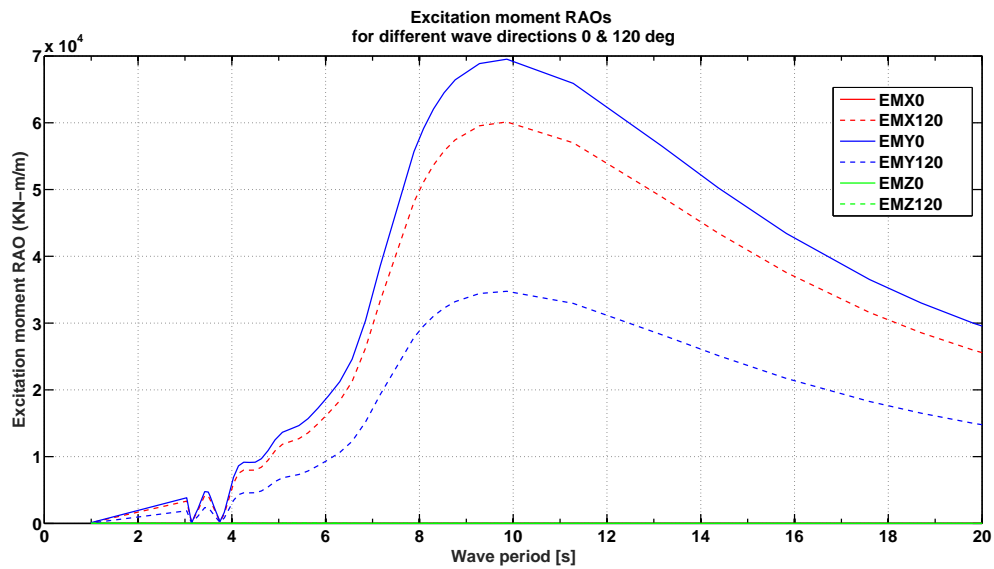
Figure 4.7: Comparison of RAO of excitation moments

period of 6.3 ($\omega = 1 rad/s$) and 8 (0.785 rad/sec) seconds respectively. The excitation moment reaches its maximum around wave period of 9 (0.69 rad/s) seconds. The excitation moment around Z-axis (EMZ) is negligible compared to other excitation moments as it is supposed to be.

4.2.4 Sectional force RAOs in dynamic equilibrium

In this section the sectional loads in all degrees of freedoms are presented at the particular cross section which is located at a distance of 3.3 m from the origin as shown in figure 3.1b as this can be a crucial location in terms of fatigue or load. Moreover, the experiment has been performed to investigate the cross-sectional loads at this same location. But due to some problems with the calibration factor the experimental results could not be post processed in due time. So, it has not become possible to present the comparison between numerical and experimental results. As, the motion RAOs agreed well it is expected that these values would have been in good agreement if compared. Here, the sectional forces are denoted as *FX, FY and FZ* and sectional moments are termed as *MX, MY and MZ* with respect to X, Y and Z axis respectively.
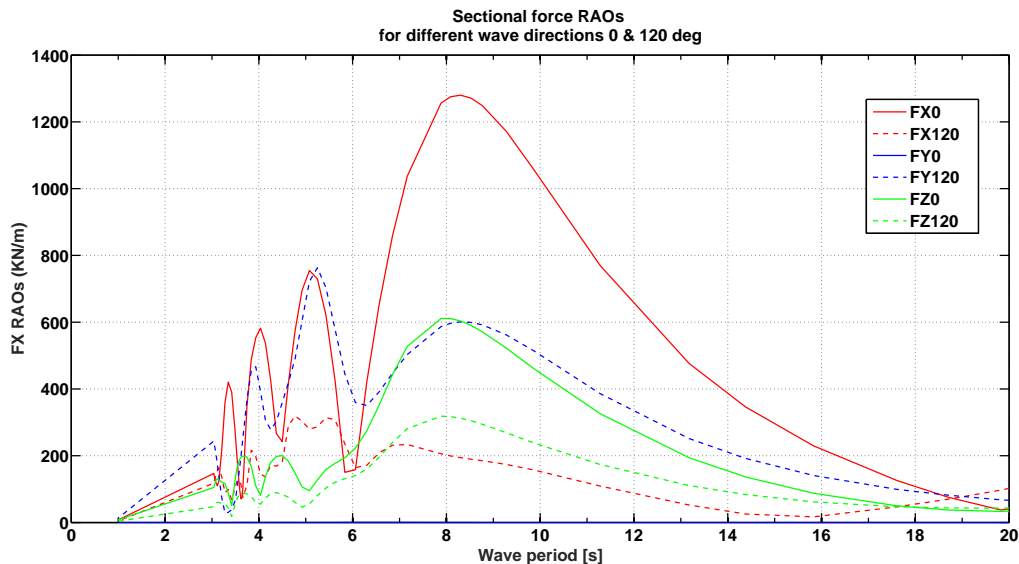
Figure 4.8: Comparison of RAO of sectional forces

In figure 4.8 the sectional force is illustrated where wave periods are plotted in X-axis and the sectional forces are plotted in Y-axis. In figure 4.9 the sectional moments are plotted in Y-axis and the wave periods are plotted along X-axis.

In aligned condition, the contribution from the sway splitting force (FY), the roll moment (MX) and the yaw moment (MZ) at the cross-section are not significant. Contrary to this, these loads play significant role for wave direction of 120^0. In short wave period region (3-6 sec) there are some fluctuations specially for the sectional forces. It's interesting that the amplification and the cancellation for the sectional forces are occurred in out of phase with the excitation forces which is shown in figure 4.5. Elaborately speaking, for instance, FX
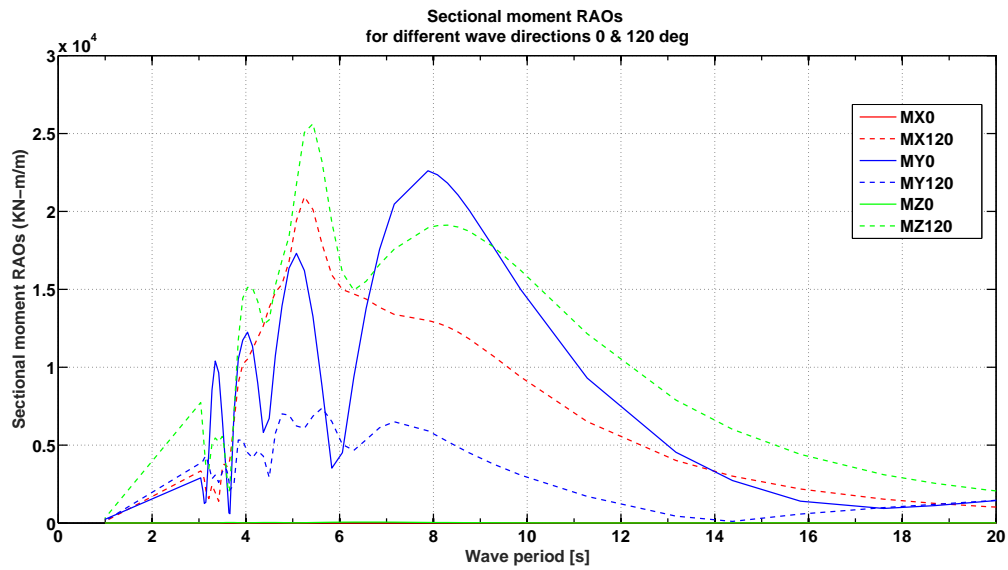
Figure 4.9: Comparison of RAO of sectional moments

gets its amplification around 3.3, 4 , 5 and 8 seconds in wave frequency region whereas the EX get its cancellation around those time period. This may imply that the inertia loads are dominating in short time wave period region. Since, the sectional loads are the integration of $\vec{F}$- **M** $\vec{a}$ over the part of the structure which is on the positive side of the cut or cross-section. $\vec{F}$ is the excitation load vector over the whole platform, **M** includes This is hard to explain accurately and clearly without the data of the phase difference between the excitation forces and inertia loads.

For, sectional moments in figure 4.9 there are some abrupt changes in the range of wave period (T=2-6 sec) as observed in the plot of sectional forces in figure 4.8. It can be observed from both figure of sectional loads (force and moment) that there is a close correlation between MY0 and FX0 and similarly for MX120 and FY120. However, the sectional moments at the cut follows the trend of excitation moment on the whole platform within a range of wave period (6-20 sec). But the peak or maximum value of sectional moments are found to be at 8 sec. The maximum value for pitch and roll RAOs are also found in 8 sec in the wave frequency range. So, it seems that it can be a reason for the excitation since in this region the system is inertia dominated. So, there may be a possibility of increasing inertia load at that wave period.

As a whole, sectional force RAO in X-direction (FX) is dominating in aligned condition and FY is dominating in the other direction of wave. The maximum sectional force RAO is found as 1200 KN/m for FX. From figure 4.9, it is observed that in aligned condition (0^0)

sectional moment around X-axis (MY) is dominating while for (120^0) MX and MZ are dominating.

4.3 Sectional loads in static equilibrium

As earlier mentioned the wind force is given as a thrust of 746 KN at rated speed by user specified option and changed into heeling moment by multiplying with the height from nacelle to COB.

Table 4.3: Mean sectional loads in static equilibrium

FX (KN)	FY (KN)	FZ (KN)	MX (KN-m)	MY (KN-m)	MZ (KN-m)
-1.46E+04	0	1.32E+03	0.027	-4.53E+04	0

As the integration along the positive side is specified , that is why the static buoyancy force is giving positive vertical shear force and a negative vertical bending moment. This applies vice-versa if integration is specified over negative side.

The Fy is really negligible. Hydrostatic pressure from both sides cancels each other on the right of the cut both for pontoon and column. This is the same reason why Mx is also quite negligible compared to My and Mz. Sectional force in x-direction is almost 10 times than in Z-direction. And, this is because the hydrostatic pressure on the side plate of the pontoon is balanced by the cut section so produces larger sectional force in that direction.

4.4 Comments

- The wave can be presented as linear wave if the wave amplitude is small relative to the wave length and the body dimension. So, nonlinear effect is really insignificant in the present case of study. The difference in results due to non-linearity may not be very significant.

- Single Gauss quadrature node is used while performing the analysis which could give less accurate numerical results in high-frequency range.(Wu et al., 1997). Because, for short wavelength maybe single node at each panel can give some discrepancy in results. Although, this is not a great issue for moderately larger wave periods.

- The excitation close to the eigen period in heave or pitch motion may not necessarily contribute to the maximum value of sectional loads at that cross-section in SFC.

- It is important to be noted that the sectional loads are calculated considering the still water line.

- It is observed that in wave frequency range with wave periods till 20 seconds the bulk of the total resistance to the wave excitation loads is from the inertia force.

- Although the mooring effect is not considered in the present study, it may not have any significant effect within the wave frequency range. But, this may have significant effect in low-frequency range (above 18 seconds).

- The sectional loads due to the hydrostatic pressure loads on the panel model are mentioned separately. So for further investigation of local analysis it is to be kept in mind while taking the global sectional load RAO result.

- The multibody wave interaction effect (when an arbitrary number of bodies are close) are not considered in this present hydrodynamic analysis. Hence, the effect in hydrodynamic forces are not included in the force RAOs and the interaction effects are not included in the retardation function as well. But, in the experiment the effect is prevailing so that could cause some changes in the result. Because in reality, the WECs are rotating whereas in the numerical model those WECs are fixed to the body.

Chapter 5

Numerical modeling for Time Domain analysis in SRA

This chapter is covering the step-by-step description of numerical modelling of the SFC and how it has become compatible for performing the global hydrodynamic analysis. It is not possible to make a model by preserving 100% correspondence with the reality. That's why assumptions are made to create the numerical model as much as close to the real model. Then the numerical results are compared to the experimental result for further improvement. Sometimes the results are checked with the real model if possible. Thus day by day, numerical analysis are becoming more and more robust and accurate.

At first an small introduction about coupled SIMO-RIFLEX-Aerodyn(SRA) is given. Then the import of *sys-prefix.dat*(input for SIMO) from the *G1.SIF*(output of HydroD) is discussed. Then some important files such as *prefix-inpmod.imp, prefix-dynmod.imp, etc.* which are modified to some extent are described. The detail of the description of files and necesary data can be found in SIMO and RIFLEX user manual.

5.1   Capabilities and advantages of SRA

'SIMO is a computer program for simulation of motions and station-keeping behaviour of a complex system of floating vessels and suspended loads.'(SIMO user manual) 'RIFLEX is a computer program for analysis of flexible risers and other slender structures, such as mooring lines, pipelines, conventional steel risers etc.' (RIFLEX theory manual)

This SRA(SIMO-RIFLEX-Aerodyn) is a robust tool which is intended to solve aerody-

namic, structural dynamics and hydrodynamic problems simultaneously in a coupled analysis. For aerodynamics it uses BEM (Blade element momentum theory) or GDW (Generalized dynamic wake theory), including tower shadow and dynamic stall. These are not disussed in detail here. Hydrodynamics cover Morison, first and second order potential theory, ringing etc. Structural dynamics considers the slender beam element theory (geometrical non-linearity is accounted as well). There are two options for defining the wave condition i.e built in and user defined wave spectra for genearting irregular wave series. TurbSim is used to generate the wind time series. 3-hours simulation is possible at best but depends on the model type.

There are several advantages of this robust tool. Some of these are mentioned here. For instance, this tool provides sophisticated hydrodynamics, state-of-the-art aerodynamics etc. Moreover, different types of foundations are possible to model including additional elements (i.e. WECs). the computational time is also quite reasonable.

There are some limitations as well and these are under process for solution and modifiation. For instance, due to the limitation of the matrix solver of RIFLEX, part of the hydrodynamic interaction effects cannot be included in the current model. This imples that the cross terms of a body caused by other bodies' motion are not included. It is going to be included in a future version of the RIFLEX. It is difficult to obtain accurate results for the shaft loads and torsional blade loads. But, here these are not investigated so these are not discussed in detail.

5.2 Units and coordinate system

All of the input data are to be given in a consistent set of SI units which are given in the following table 5.1.

Table 5.1: Units and physical constants

	Property	Notation	Example
Basic units	Length	L	m
	Time	T	s
	Mass	M	Mg=tonne
Derived units	Force	F=ML/T^{2}	$Mg\,m/s^2$
	Pressure	P=F/L^{2}	KN/m^2
	Velocity	V=L/T	m/s
	Acceleration	A=V/T	m/s^2

The program applies several right handed Cartesian coordinate systems with taking rotations positive in counter-clockwise direction. The following figure 5.1 illustrates the different coordinate system. In figure 5.1a the global earth fixed coordinate system is illustrated which

(a) Global coordinate system   (b) Local coordinate system
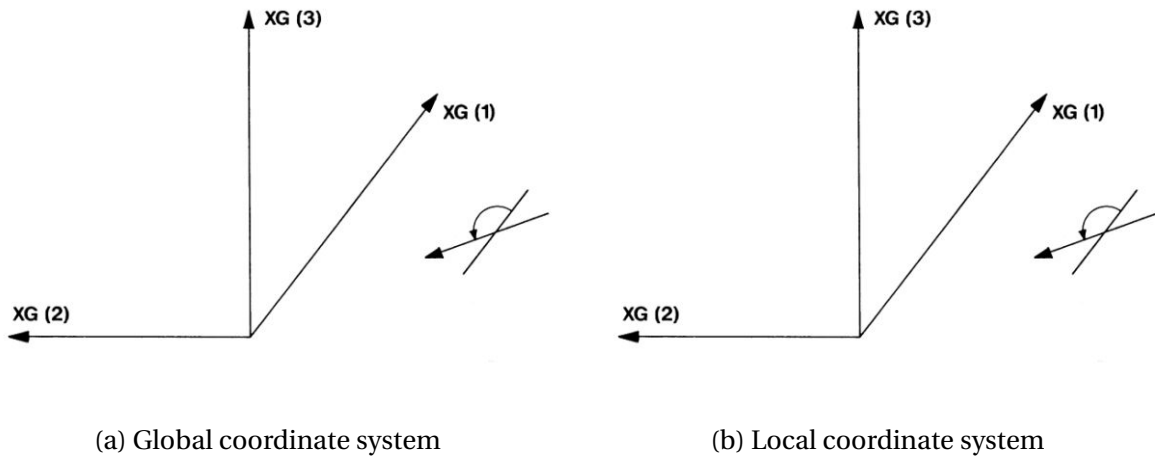
Figure 5.1: Coordinate system

is convenient to specify the location of all local elements with respect to this system. The xy-plane coincides with the calm water and z-axis is pointing at upward direction. In figure 5.1b, the local(body fixed) [XB] and body related [XR] coordinate systems are demonstrated. The first one [XB] follows body motions and is used to specify coordinates of positioning elements & coupling elements. The second one [XR] follows the body horizontal motion of the floating vessels. Most coefficients (transfer functions) are referred to the [XR] coordinate system.

5.3 Simulation outline

The following figure 5.2 of the flowchart is illustrating the simulation outline quite clearly. This is the sequence what it follows while doing the coupled simulation in SIMO-RIFLEX-Aerodyne. Almost all of the necessay input files are taken from the reference files given as example for avoiding unexpected error. Some are kept unchanged (i.e. AirfoilLibrary.dat, ControlInput.txt, NRELControl-fixpitch.jar etc.) which are not broadly dealt here. Rest of the other input files (regarding the modeling in SIMO and RIFLEX) are changed and modified as per requirement and discussed later. Mainly the 'prefix.res' and 'prefix.lis' files are used to check whether there is any error or not. Moreover these are also checked whether these are

writing the given input properly or not. The results of the responses are provided as output in several *B-files* (specially the global displacements)and the guidance is written in X.m (matlab file) file. The force responses are stored in ASCII files for elements & nodes. The information about this file is given in key.dat file.
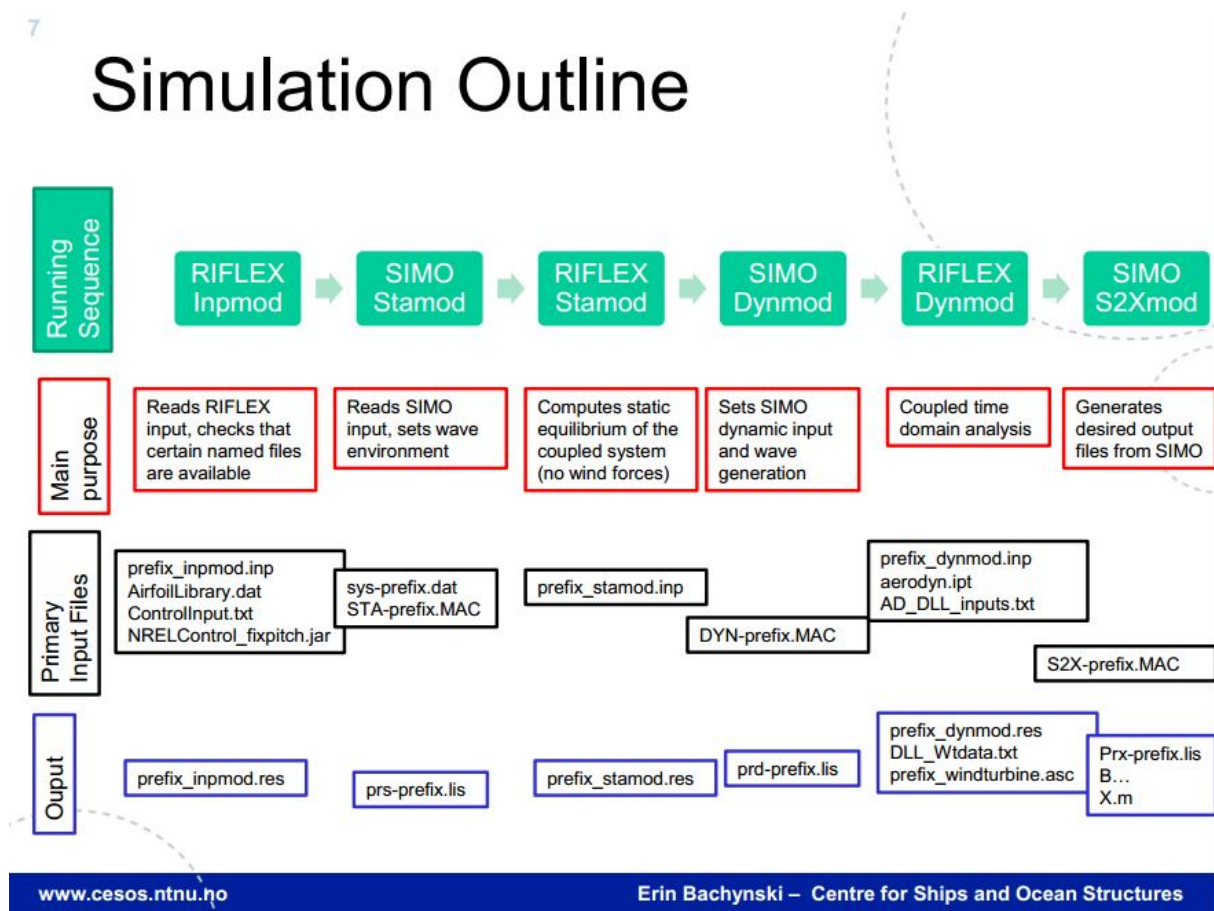
Figure 5.2: Simulation Outline

5.4   Import of Hydrodynamic calculation data

This is the first step which is performed in the beginning of making the numerical model. The hydrodynamic coefficients, retardation functions, excitation force RAOs or motion RAOs are imported from a hydrodynamic software. Here, HydroD(WADAM) output is used to make it compatible for SIMO formats. In the updated version, GUI(Graphical User Interface) of SIMO has an option for importing the G1.SIF(Sesam interface file) , the process has been completed as shown in the figure 5.3. Simply by setting the initial condition and after running the static and dynamic analysis, the *sys-sima.dat* file is generated which mainly

includes the body mass matrix, the hydrodynamic coefficients such as added mass infinity, stiffness matrix, linear damping matrix, force transfer function, retardation function etc. According to the requirement of analysis necessary modifications are performed which are discussed later.
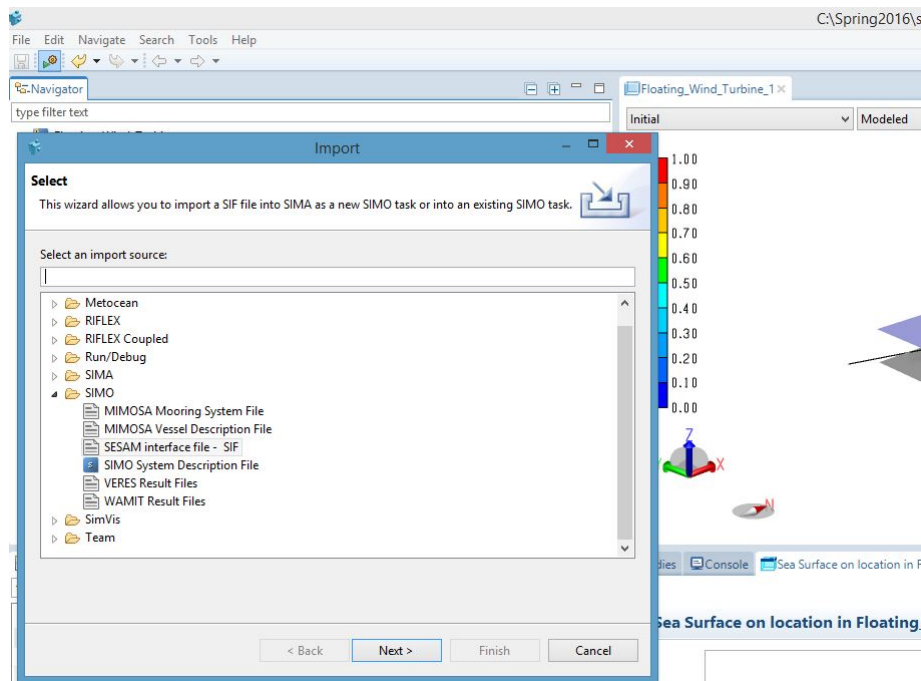
Figure 5.3: Import of G1.SIF file into SIMO

5.5 Structural & external load model

In the following figure 5.4 a short and consize description of the structural and external load model is demonstrated. This has been followed while numerically modeling the SFC in SRA. The floater (hull), hub and nacelle body data are given as input in 'sys-prefix.dat' (SIMO). Wheras, the body data of slender elements such as tower, blades (rotor) and mooring lines are given as input in 'prefix-inpmod.inp' file(RIFLEX).

5.6 Simo input files

5.6.1 Modification in sys-prefix.dat file

The *sys-prefix.dat* file possess all the rigid body data, hydrodynamic coefficients, force RAOs, environmental condition, specified force(if required) etc. Here, the basic steps are written as

Structural Model

Blades: Beam elements, cross-sections with 2 symmetry planes

Tower: beam elements, axisymmetric cross-sections

Hull including WECs: One single rigid body
Hub & Nacelle: Concentrated Mass

Hull : master-slave connection to tower base and fairleads

Mooring lines: beam elements, constant axisymmetric cross-sections

Anchors: Fixed in translation and rotation

External Load Model

Blades: Turbulent wind, BEM or GDW sectional forces, including tower shadow effect

Hub & Nacelle : No wind loads

Tower: Drag forces due to turbulent wind (in rotor region), or mean wind (below lowest passing point)

Hull : Hydrodynamic forces (1st oredr potential and Morison), No current

Mooring lines: Hydrodynamic forces (Morison's equation, wave kinematics at initial position

Figure 5.4: Structural and external load model of the SFC defined in SRA

follows:

- The body mass matrix of the whole platform including the floater, tower, blades, hub and nacelle is automatically imported into this file from the SIF file. But this file is generally accounted for the rigid bodies information only in terms of body mass matrix for this floating wind turbine case. So, the body mass matrix is updated with respect to the body fixed coordinate system. The body mass matrix of these rigid bodies are given in the table.

- Buoyancy compensating force: Typically, SIMO assumes the floating body is neutrally buoyant(excluding the RIFLEX elements). But, in realitythe floater has more displacement than total weight for supporting the wind turbine and the mooring lines. So, if the system is kept as it is, then it would yield into an unphysical situation. There are several ways to make the system physical. Amongst those, one approach is described here.

Table 5.2: Drag coefficient parameters used in SIMO

	C2X	C2Y	C2Z
Column	0	1.66	1.66
Pontoon	0	5.228	9.686

1. The gravity force of all the rigid bodies(floater, hub and nacelle) are included.

2. The gravity force of the RIFLEX elemnts(tower, blades, mooring lines etc.) are already included as nodal force.

3. To achieve the equilibrium the total buoyancy force is included as a specified force in upward direction (global z-direction) at the center of buoyancy.

4. One important thing is to be kept in mind that the restoring matrix has to be updated as well. The details are described in the theory part. The updated restoring matrix are given here in the following table.

An example of the specified force for this situation is included in the appendix.

- **Slender element force** Slender elements are used to include Morison drag on various elements. For the present model all 4 columns and three pontoons are given as slender elements to include the viscous drag. It is important to mention that the specific volume (cross sectional area) is set to zero. Besides, the gravity or buoyancy are not included as well to avoid over estimation. Only, quadratic trnsverse drag coefficients in y (C2Y) and z (C2Z) directions are included. It is also important to mention that, here these are in local axis coordinate system. The notation of the drag coefficient is (FT^2/L^3). The value used here is given below for both pontoon and the columns.

  For instance, $C2y = 0.5\rho C_d D = 0.5 \times 1.025 \times 0.5 \times 6.5 = 1.66$.

- **Environmental condition** is included in this file. There are many options for the choice of wave spectrua (such as JONSWAP with 2 & 3 parameters, PM, with or without swell etc.). So, user has the option to chhose as per requirement. As in the present case, for site 14 JONSWAP is a reasonable choice, so it has been chosen for global dynamic analyses.(Li et al., 2013).

5.6.2 Additional input files in SIMO

Sta-prefix.mac, dyn-prefix.mac, s2x-prefix.mac etc. are the additional input files for specifying other input parameters. For instance, in dyn-prefix.mac the stepping of simulation length, random seeds number, definition of required outputs etc. are specified. However, the detail of these files can be found in SIMO user manual.

5.7 RIFLEX input files

There are three RIFLEX input files such as prefix-inpmod.inp, prefix-stamod.inp and prefix-dynmod.inp. A short overview of inpmod.inp file is given here. The necessary data of RIFLEX elements (i.e slender elements like tower, mooring lines, blades etc.) which are required for Finite Element Model are given as input in this file. Mainly, this file comprises of information about supernodes (fixed and free), rigid connections between nodes (master-slave relationship), lines, cross-sections, flex joints, floater force model etc. as per requirement. The following figure (a 2D representation) illustrates the definition of RIFLEX elements for the SFC. But for convenience and clarity the 3rd blade and the 3rd mooring line is not illustrated in the figure. There are 20 super nodes which are presented by green circle. Among those 3 nodes (anch-1, anch-2 and anch-3) are fixed and 17 nodes are free. There are 12 lines which are presented by black dotted lines. Every line is connected between two super nodes. Every line can have several segments. For instance, the tower has 10 segments of equal length of 7.76 m. Some rigid connections are shown by elipses for clarification. The detail description is also given for all rigid connections in this figure 5.5 The floater is specified by a dummy line referred as 'Semi-dummy'. The slave nodes follow the movemnet of the master nodes. It is to be norted that, while the rotor is to be parked, 'tower-up' has to rigidly connected to 'sh-sn1', which stops the rotation of the rotors.

5.7.1 Mooring configuration

The SFC includes three catenary mooring lines. Each of the side columns is attached to a mooring line. These mooring lines provide the horizontal stiffness. Mass is uniformly distributed for each of the mooring line. The cross-section is simplified as solid circle. Only the axial stiffness is considered here and the bending & torsional stiffness are set to zero. The design parameters are provided in table 5.3. The positions of fairleads and anchors are de-
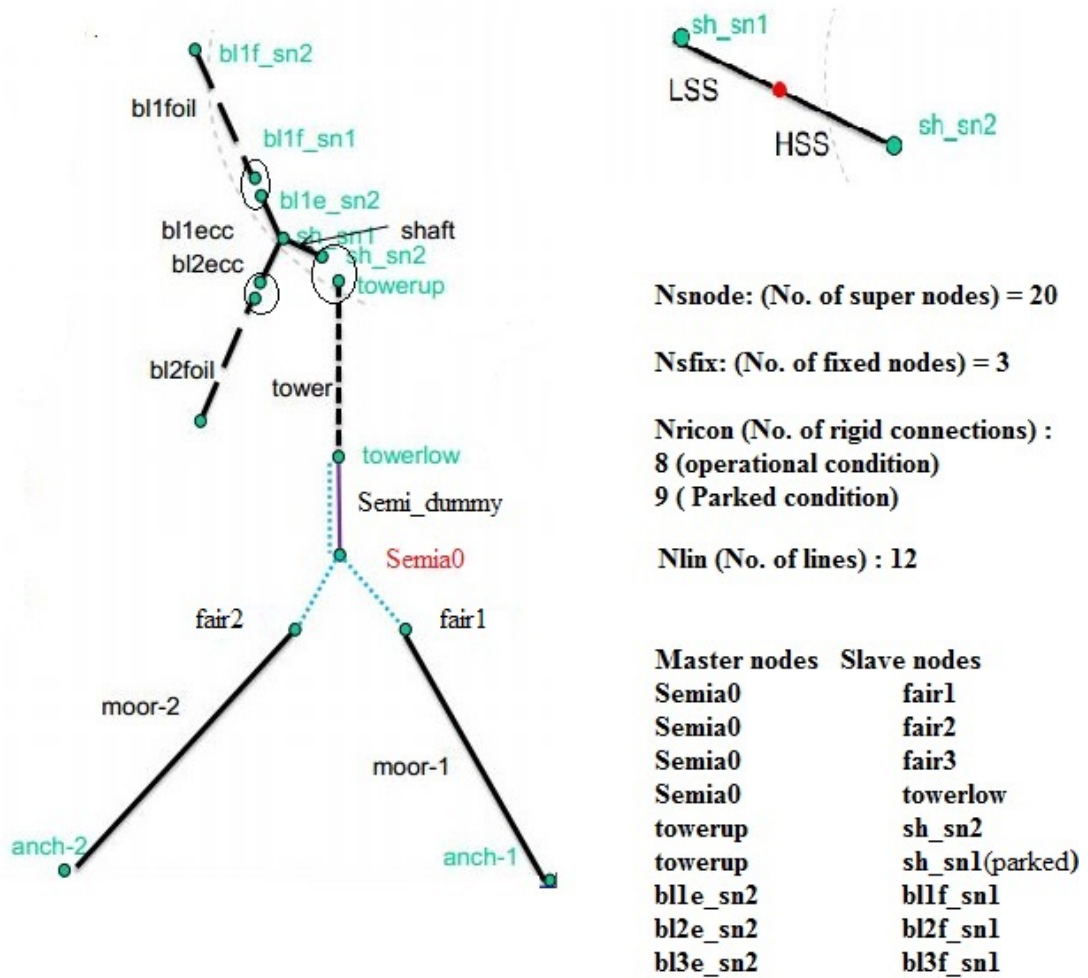
Figure 5.5: Definition of RIFLEX elements in *inpmod*

scribed in table 5.4. It is to be noted that, for increasing the pretension at fairleads, clump weights are used. This is to avoid the slacking in extreme environmental conditions.

Table 5.3: Design Parameter of a single mooring line

Mass per unit length (in air)[tonne/m]	0.115
Unstretched mooring line length [m]	873.10
Diameter of the mooring line crosssection [m]	0.137
Density of the material [$tonne/m^3$]	7.85
Clump weight in water [tonne]	15
Distance from the attached point of the clump to the fairlead [m]	240
Elastic stiffness(EA)[KN]	2.00E+05

Table 5.4: Arrrangement of the mooring line anchors and fairleads, the positions are referred to the global corodinate described in the figure

Fairlead	x(m)	y(m)	z(m)
1	44.25	0	-18
2	-22.125	38.321	-18
3	-22.125	-38.321	-18
Anchor	x(m)	y(m)	z(m)
1	884.362	0	-200
2	-442.181	765.880	-200
3	-442.181	-765.880	-200

5.8   Full field wind files generated using TurbSim

'Turbsim is a stochastic, full field, turbulent wind simulator. It uses a statistical model to numerically simulate time series of three component wind speed vectors at points in a 2D vertical rectangular grid which is fixed in space'. The output can be used into any AeroDyn-based codes as input. In the following figure an example is illustrated how the FF (full field) wind is implemented in AeroDyn.
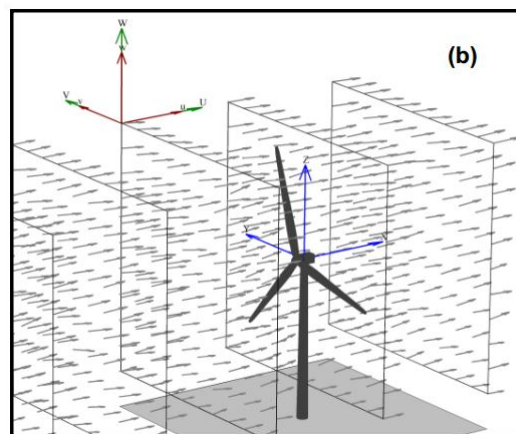
Figure 5.6: example of TurbSim grids as implemented in AeroDyn

A reference input file is modified as per requirements. Then running the simulation in TurbSim generates two files i.e 'prefix.wnd' and 'prefix.sum'. Aerodyne can read these output files and can be used in SRA coupled analysis. Some important parameters which are modified is given in the following table 5.5. More detail description can be found in (Jonkman, 2009). The grid height and width are to be specified according to the rotor diameter. As the rotor diameter is 126 m, so the specified parameter in the table is sufficient. Because, the grid height and width are to be greater than the rotor diameter. The power law can be written as follows:

Table 5.5: Some important input parameters for input file

Vertical grid-point matrix dimension	32
Horizontal grid-point matrix dimension	32
Time step	.05 s
Simulation length	4100 s
Hub height	90 m
Grid (height ×width)	160 × 160
Turbulence model	IECKAI (Kaimal)
IEC turbulence type	NTM
IEC turbulence characteristics	C
U_{ref} (Mean wind speed)	As per requirement
Wind profile type	PL (power law)

$$u(z) = u_{hub}\Big(\frac{z}{hubheight}\Big)^{Pl.Exp}$$

(5.1)

Pl.exp is by default 0.14. Here, to be safe, U_{ref}/u_z is given as the mean wind speed at hub-height. So, the height above mean water line, z is also defined as 90 m (the hub height). So actually u(z) becomes equal to the u(hub).

Chapter 6

Results & Discussions of TD analysis

In this present section the fully coupled numerical analysis of motion responses are performed using SRA (SIMO-RIFLEX-Aerodyn) in time domain. Comparisons between experimental results are made with numerical results to some extent. Then some case studies are given for survival and functional environmental conditions. Additionally, the response analysis of tower base bending moment is also given.

6.1   Calm Water Analysis

As a first step, the calm water analysis has been performed to check the equilibrium position of the SFC platform as well as to verify the correct draft. The necessary input files for performing this task are mentioned in the previous chapter. In the *sys-sima.dat* file environmental condition is defined by dummy parameters so that a calm water analysis can be generated. For instance, an irregular sea state of significant wave height($H_s = 0.01m$) and the peak period ($T_p = 100sec$) is specified. As, the peak period is too long and the significant wave height is too small this can be regarded as calm water. Similarly, the current and wind environmental data are also given as dummy parameters. Here, the *dummy* term implies that, the data are provided in the input files but not to be accounted as the parameters are negligible. Another important step is to set the platform free in RIFLEX [*inpmod* file].

During the analysis it is found that the change in the number of load steps and the number of maximum iterations which can be specified in *'stamod.inp'* file affects the equilibrium position in static analysis. Hence, a sensitivity analysis is performed, in which four cases are illustrated with different number of load steps and iteration numbers to obtain the con-

83

vergence in equilibrium position. The purpose is to check the equilibrium position of the platform. Since, the gravity and buoyancy force are specified in sys.dat file so the platform will obtain the equilibrium with time.

(a) loadstep 250

(b) loadstep500
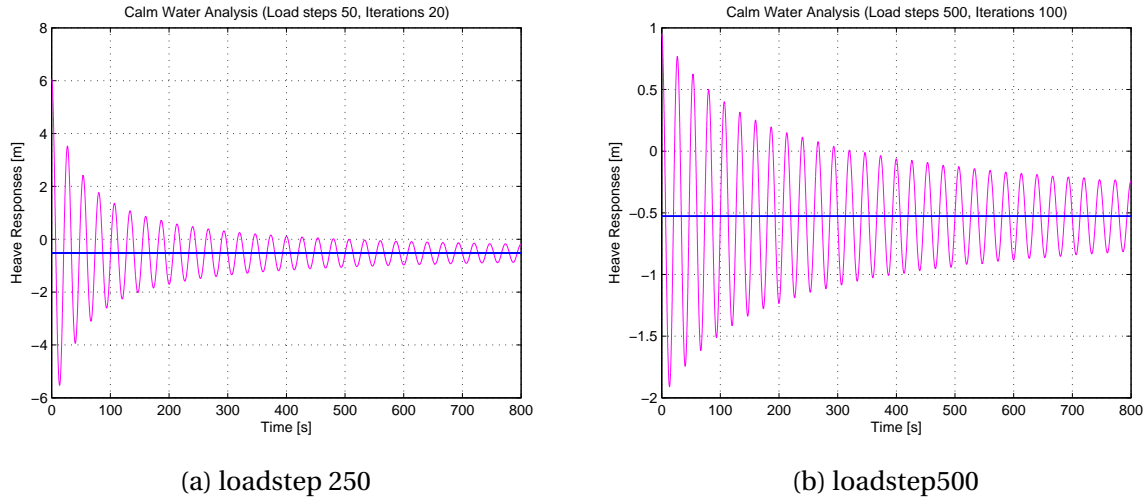
Figure 6.1: Convergence of equilibrium position in calm water analysis

In figure 6.1, it is clearly observed that the heave response oscillation is exponentially decaying with the increase of time and is oscillating with its damped period. But, the damping gets low with the progress of time which will be investigated in decay test. In figure 6.1, it is clearly shown that the mean position is around -0.5 m. And with the increase of load-steps and number of iterations, the static result has also become minimized at the start. To minimize the difference of the equilibrium position and the zero position the platform is de-ballasted with 60 tons (20 tons of water is deballasted from every side columns) in the mass model in Genie. Then again the sys-sima.dat file is updated according to the new mass matrix of the floater to obtain the mean position close to zero. Some cases with different load steps and iteration numbers are illustrated as follows.

From figure 6.3, it is clearly observed that for load steps 750 and 1000 the obtained equilibrium position is quite close to zero.

6.2   Decay Test

The decay test is performed to investigate the natural period of the platform in 3 degrees of freedom (heave, pitch and surge). The reason behind performing a decay test is the limitation in coupled SIMO-RIFLEX. Because, the eigen period analysis can not be performed in

(a) loadstep 250

(b) loadstep500
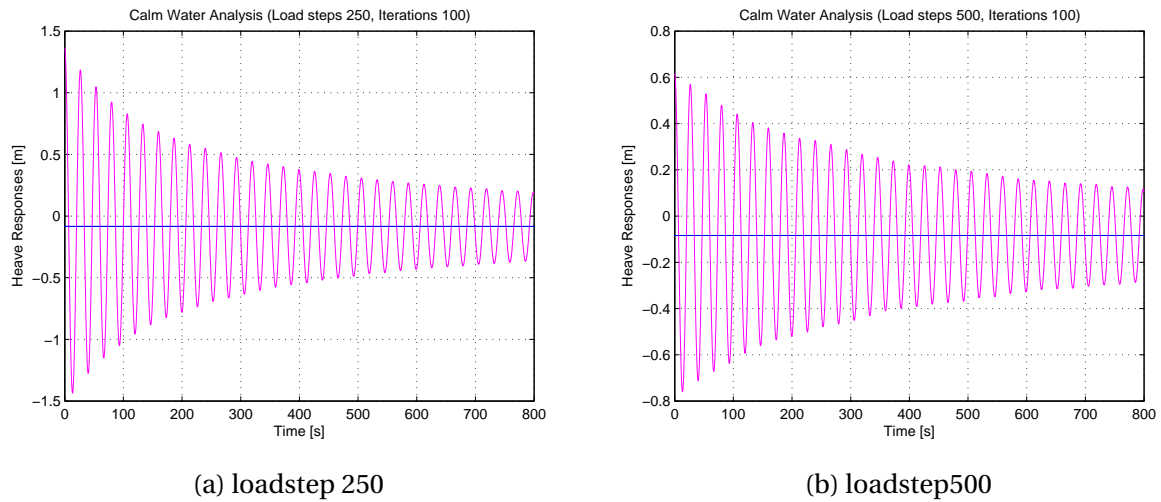
Figure 6.2: Convergence of calm water analysis

(a) loadstep 750

(b) loadstep 1000
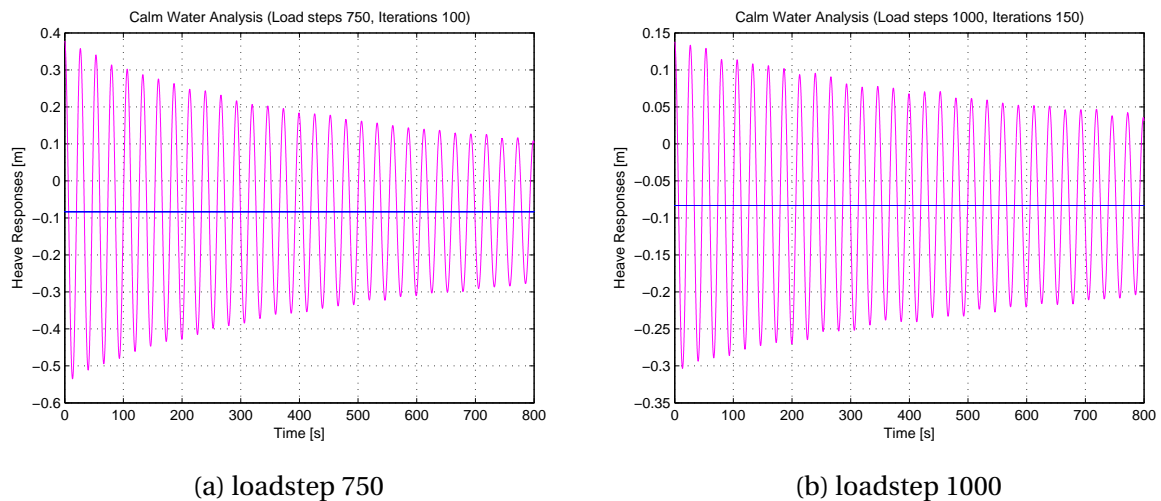
Figure 6.3: Convergence of calm water analysis

the coupled analysis. However, further analysis are performed for aligned wave and wind direction and this direction will not affect other degrees of freedom (i.e. roll, sway and yaw) significantly. So, only heave, surge and pitch decay test have been performed here. But, it is to be noted that for misaligned environmental condition maybe other degrees of freedom can get important. It is performed by simply applying loads (force or moment) at the center of buoyancy of the platform as per requirement. For instance, during heave decay test a required amount of force (i.e 3500-4000 KN) is applied in z- direction and in case of a pitch decay test the moment is applied w.r.t y-direction for a certain length of time. The whole simulation length of time can be divided into three segments i.e. the first segment is the RAMP load, the second segment is the constant load and the third segment represents while

the load is released. The reason behind this to apply the load gradually so that less transient is occurred and the platform can take the load gradually with less disturbance. After releasing the load the platform starts to oscillate with its own damped period and follows an exponential decay. The difference between the damped period and natural period is quite insignificant. It is important to be noted that, during performing the decay test in SIMO-RIFLEX-Aerodyne, the loads are applied only in one degree of freedom. So, the attention is paid to investigate only in one degree of freedom at a time. Other degrees of freedom are uncoupled with the examined one. To check whether other degrees of freedom are affected much or not, the amplitudes of other motions are investigated as well. It is found that, the disturbance in other degrees of freedom are quite insignificant(0.1-0.5%) compared to the examined degree of freedom. So, the uncoupling is ensured and it is important to evaluate the eigen period accurately. For that reason, during applying the load, attention is also paid to set the amount of load. Because, too small load for short length of time may not be sufficient to excite the platform and give sufficient number of complete oscillations. Consequently, it may give less accurate result.

Table 6.1: Simulation parameters for decay test

	Force/moment applied	Simulation lentgth
Surge	500 KN	1500 s
Heave	4000 KN	800 s
Pitch	40000 KN-m	800 s
Point of application	COB(0 m,0 m,-20.76 m)	
Simulation time step(RIFLEX)	0.005 s	
Wave/body response time step(SIMO)	0.1 s	
Turbine status	Parked, blades feathered	
Wave conditions	Hs=0.001 m, Tp=10 s	
Wind condition	No wind applied	

To evaluate the natural time period of the platform, first, the damping period is calculated by taking the average of time of several complete oscillations (for instance, trough to trough). Then using the expression given in chapter 2, ($\omega_d = \omega_0 \sqrt{1-\zeta^2}$) the natural period of the platform is measured for different motions. Even though, the difference between the damped time period and the natural time period is very low. Because, damped time period is not very much affected by the damping.

Calculation of linear and quadratic damping coefficients are performed using the procedure provided by (Hoff, 2001). This postprocessor was provided by *Erin bachinsky*. This is

why the detail theory is not discussed here.

Table 6.2: Eigen period of the platform in heave , surge and pitch direction from decay test

Degrees of freedom	Surge	Heave	pitch
T_{exp} (sec)	111.86	26.59	34.79
T_{num} (sec)	111.94	26.65	30.60

During performing this task, the simulation length is chosen based on the assumption of the time period. As the time period of surge is quite large compared to other motions, the simulation length for this case is chosen as 1200 seconds after releasing the load. For other cases, 500 seconds of simulation length is considered after releasing the load (in total 800 seconds).
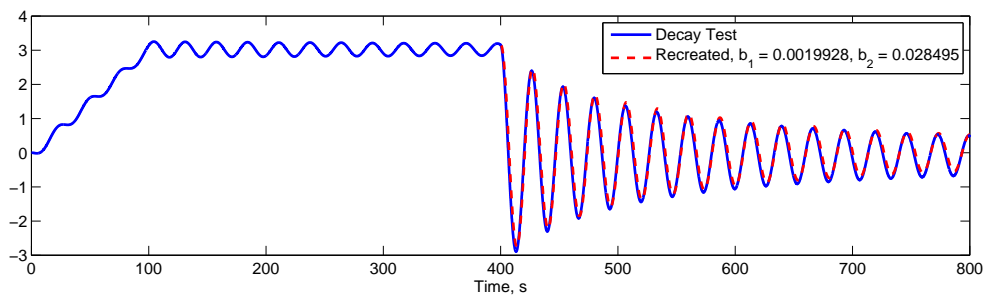
Figure 6.4: Decay test in heave motion
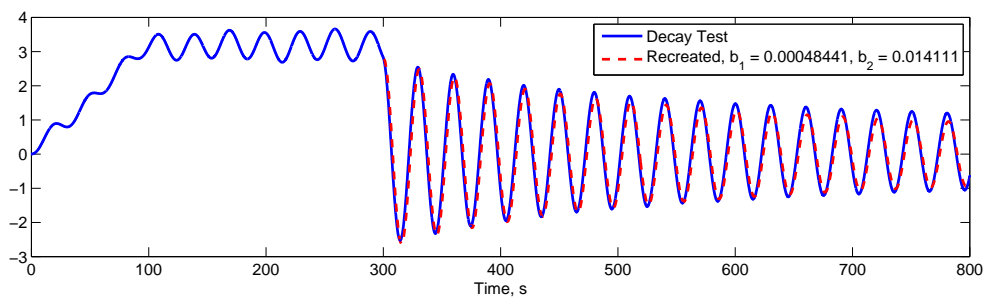
Figure 6.5: Decay test in pitch motion

In the above figure, it is observed that for pitch decay test, the oscillation gets flattened. Maybe, it is supposed to decay more quickly if it is compared with the experimental results published by (Michailides et al., 2016). Even, the decay of heave motion is also showing very slow decay like pitch decay test. That is why the linear damping coefficient which is obtained in HydroD is investigated again to check the reason of very low linear damping coefficient 'b1'.
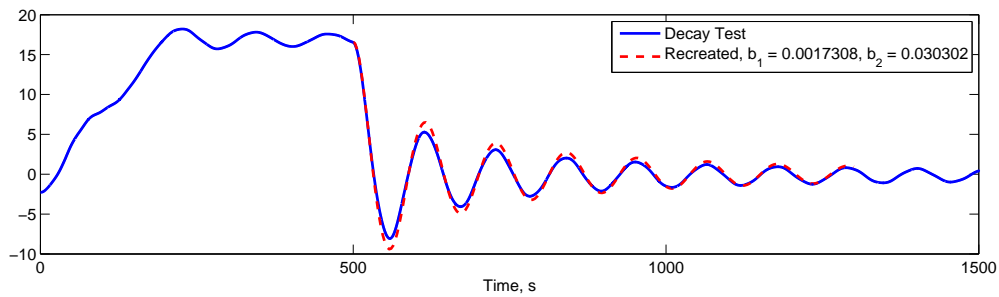
Figure 6.6: Decay test in surge motion
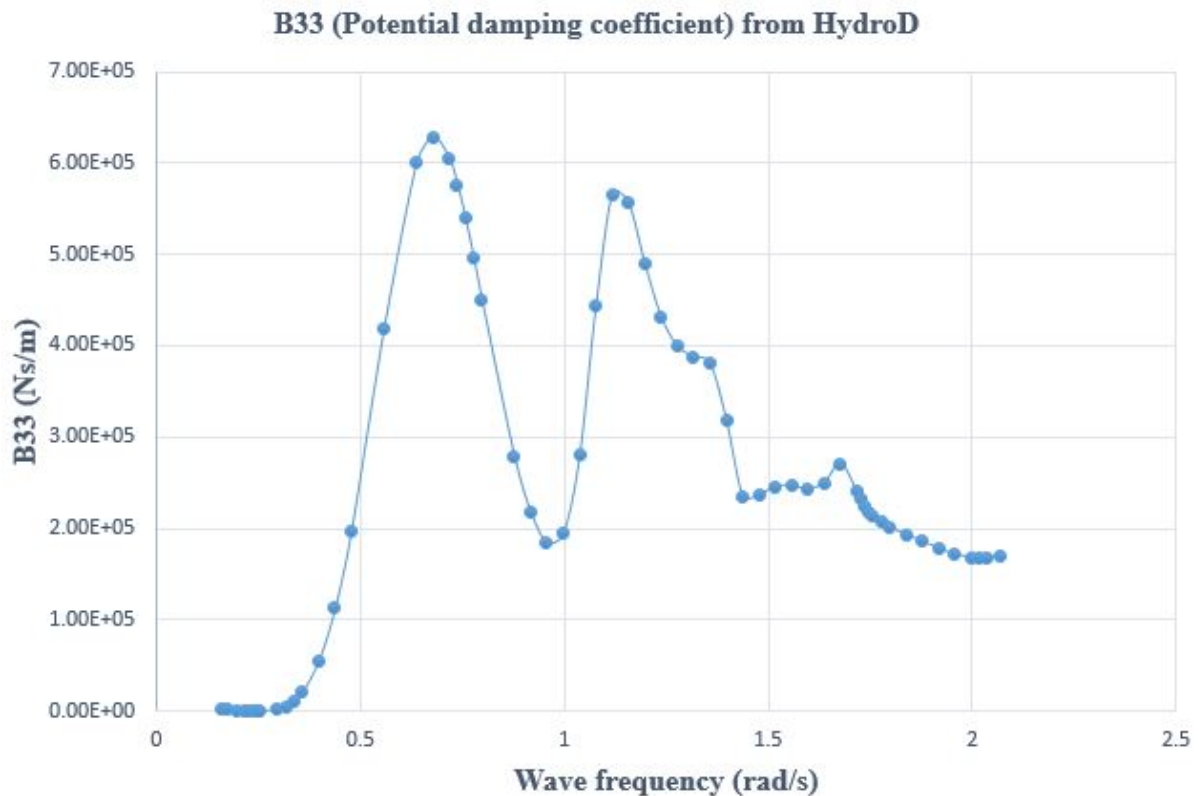
Figure 6.7: Potential damping coefficient, B33 from HydroD

In figure 6.7 & 6.8, it is observed that the value of uncoupled linear damping coefficients B33 and B55 at close to the natural frequency of heave and pitch are very low compared to the highest value. It is less than .001% compared to the highest value for both cases, hence that could be the reason for slow decay and low value of 'b1'. Because, in SIMO-RIFLEX coupled analysis, the input of all hydrodynamic coefficients are taken from the output of HydroD analysis.

The viscous drag is modelled similarly as modelled for CSC platform (Luan et al., 2014a). Moreover, the drag coefficients are checked and discussed in the previous chapter. Only, the viscous damping is not considered for three WECs as some problems were encountered
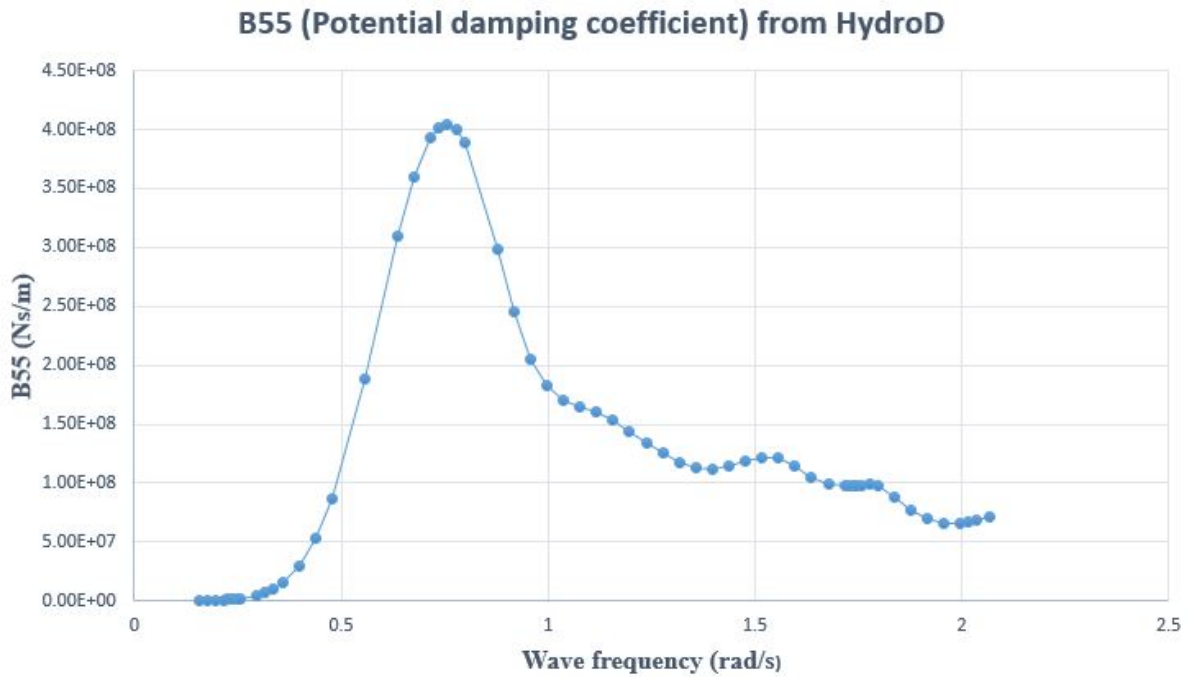
Figure 6.8: Potential damping coefficient, B55 from HydroD

during including those as slender element. But, this may contribute to the difference in result as viscous damping is important around the natural time period. Contradictorily, the volume of the WECs are not very large compared to the volume of the whole platform (only .15% approximately). So, the situation here is quite same with the experimental case. As, in the experimental case, the potential and viscous damping are considered along with the damping due to the mooring system. Even though the decay is very slow here. In conclusion, it can be said that, the low value of linear damping coefficient at natural frequency maybe the reason for this slow decay.

6.3   Environmental conditions

The choice of sites for deploying combined wind and wave energy farm requires the knowledge of the energy resource of wind and wave. Simultaneously, for designing the platform in ultimate limit state it is also important to know 50-year wind and wave conditions.(Li et al., 2013).

The long-term variation in wind and wave is generally presented in terms of mean wind speed (U_w), significant wave height (H_s) and peak period (T_p). The common practice is to assume the process stationary with a 1-hour duration excluding the transient part which may

vary from 500-1000 seconds. Performing a full long term analysis is impractical as it requires long computational time specially for complex response problem. For convenience, contour surface method is generally applied to investigate the long-term extremes while the platform is exposed to a short-term extreme sea state. From 50 year contour surfaces several sea states are selected by extrapolation from a long term joint distribution. The design sea state is the one which causes the largest response. It is also important to keep in mind, the most critical conditions may vary based on the concept of the platform characteristics. (For instance, the natural period of heave for TLP and semisubmersible are totally different. So, the condition which can be very critical for semisubmersible may not be the same critical for TLP.)

It is important to mention that, the short term wind condition is defined in terms of wind speed profile, TI(turbulence intensity factor) and wind spectrum. Similarly, the short term wave condition is described by wave spectrum. In the moderate and extreme sea states along with North Sea sites, the JONSWAP spectrum is regarded to be reasonable and selected to estimate the extreme response. For all cases, the peakedness factor is taken as 3.3 .

However, from the EU project-MARINA Platform 5 offshore sites are finally chosen out of 18 sites for further investigation and prediction of long term environmental conditions. Among those, site 3(Buoy Cabo Sillerio, Atlantic) and site 14 (Norway 5, North Sea) are selected where the analyses of floating concept will be carried out. Site 14 has a water depth of 200 meters. Based on the investigation in **??**, two different conditions, one with maximum H_s and other with for maximum U_{ref} for each site considering the 50-year maximum return value are considered in **??**. These are also selected here to investigate the motion responses of this simplified numerical model of SFC. All of the cases are performed for $\beta = 0^0$, aligned wave direction. The examined extreme environmental conditions are tabulated below.

Table 6.3: Extreme environmental conditions

Extreme conditions	H_s(m)	T_p (sec)	U_{ref} (m/sec)	TI
EEC1	8.8	14.8	-	-
EEC2	11.5	15.7	-	-
EEC3	13.5	15.0	-	-
EEC4	15.3	15.5	-	-
EECW1	8.8	14.8	27.9	.998
EECW2	11.5	15.7	33.3	.100
EECW3	13.5	15.0	24.3	.102
EECW4	15.3	15.5	31.4	.101

In above table 6.3, the wind speed refers to the wind speed at reference height of 10 m

from the mean water level. During the generation of wind profile in *Turbsim*, the wind speed at hub height is derived based on the power law. A short description is given in the previous chapter.

This is also important to investigate the motion and other responses for functional or operational condition. This would be of interest to investigate the response while the turbine is in operation and the coupled effect of aerodynamic loads and hydrodynamic loads are important as well. That is why several operational environmental conditions are chosen from (Michailides et al., 2016). These are tabulated below.

Table 6.4: Operational environmental conditions

Operational conditions	H_s(m)	T_p (sec)	U_{ref} at 10 m (m/s)	U_w at 90 m (m/s)	TI
OECW1	3.0	9.0	5.88	8.0	0.129
OECW2	3.0	7.0	9.35	12.7	0.129
OECW3	3.0	12	9.35	12.7	0.129
OECW4	5.0	7.0	13.23	18.0	0.117

6.4   Sensitivity analysis for the selection of seed number

There are two ways to generate irregular wave time series for performing the simulation. The first one is to use the same time series which is obtained from the experimental analysis. This is to ascertain the accuracy of the results. The second procedure is to generate wave time series for random seeds. In this case, the second procedure is chosen for further investigation. That is why, a sensitivity analysis is performed for one environmental case to investigate the required number of seeds for further analysis to achieve accuracy. The variation of the statistical results of the responses are measured and then the average are taken. The environmental condition $EECW4_n$ is chosen, where n= 1-10 refers the seeds number for the same short term wind and wave condition. So, for aligned wave direction 10 one-hour (3600 sec) simulations are investigated in this present study. It is to be mentioned that for each case the first 500 seconds are not considered which implies the overall simulation length is 4100 seconds. Because, in the beginning there may be some transient effect which is safe to truncate from the simulation length to assure the accuracy of the results. The environmental condition is written in the following table 6.5.

Here, the effect of the wind and wave seed number is demonstrated for surge, heave and

Table 6.5: Environmental condition for sensitivity analysis

$EC_{i,n}$	H_s (m)	T_p (sec)	U_{ref} (m/sec)
$EC_{1,n}$	15.3	15.5	31.4

pitch motion responses. It has been found that 10 different wave and wind seed numbers are quite sufficient for the investigation of the dynamic response of the combined concept (SFC) since the variation is not very significant.
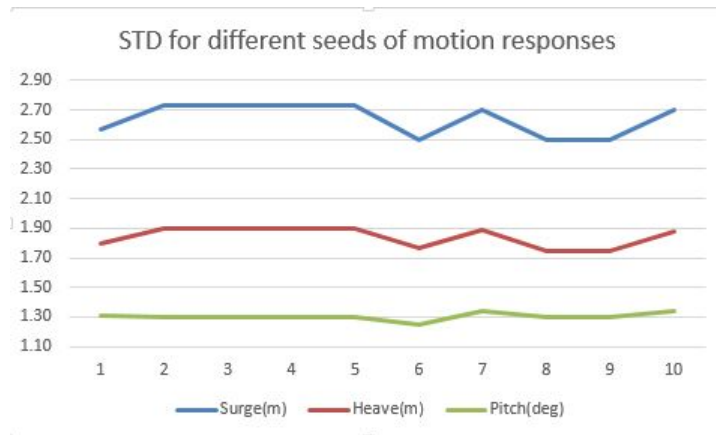
Figure 6.9: Variation of STD values for random seeds
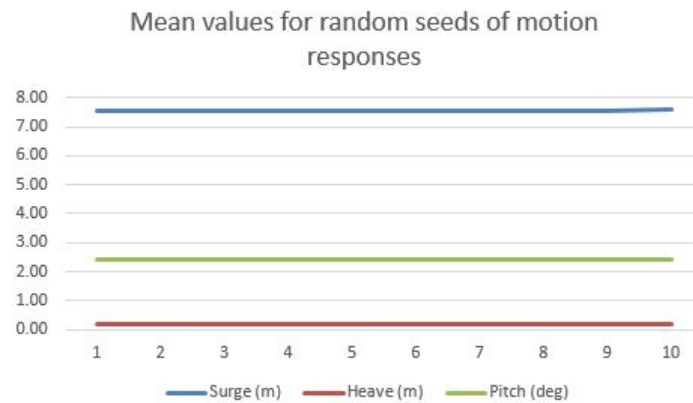
Figure 6.10: Variation of mean values for random seeds

6.5 Verification of response spectra

In this section, the verification has been performed for surge, heave and pitch response spectra for two survival environmental conditions EEC1 and EEC4 (both without wind loading). The response RAO for the mentioned motions are taken from HydroD analysis using 'postresponse'. To obtain accurate results the RAOs are collected by performing 7 analysis in Hy-
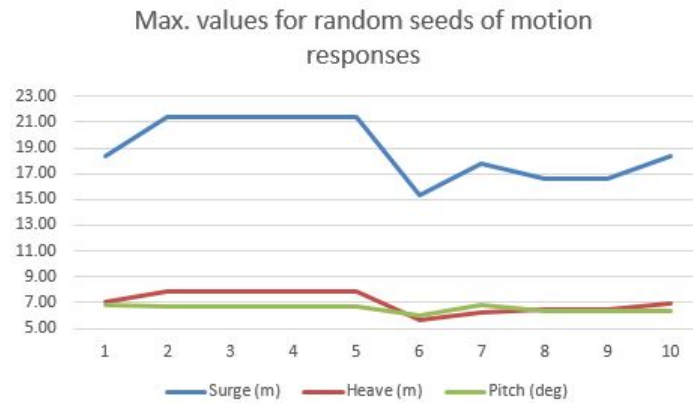
Figure 6.11: Variation of maximum values for random seeds

droD. Each time, 60 steps of frequency are defined. Consequently, the RAOs are collected for a frequency range of (0.2 - 2.25 rad/sec). The reason is the limitation of HydroD for specifying the frequency range as maximum of 60 steps can be given as input. However, the response RAOs are collected for almost 350 steps of frequency step by step. Then simply from the product of the square of RAOs and the wave spectrum, the response spectra are evaluated and plotted using Matlab postprocessor. The JONSWAP wave spectra are presented in the following figure for 4 survival environmental conditions in figure 6.12.
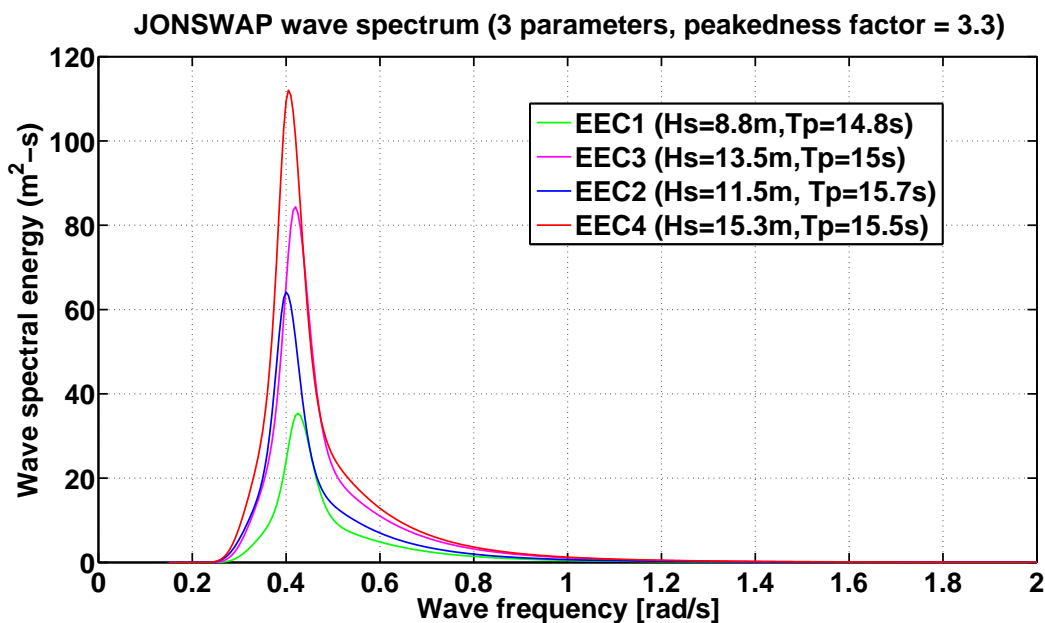
Figure 6.12: JONSWAP wave spectra for survival conditions with peakedness factor 3.3

In figure 6.13, the surge and heave response spectra are plotted from Matlab and fully coupled SRA (SIMO-RIFLEX-Aerodyn) analysis. The patterns are in good agreement for both environmental conditions. Moreover, the location of peaks are also at same position. In

some cases, the response spectra from SRA analysis is less peaky. It is because of the smoothing factor is chosen in 'dat2spec' (Brodtkorb et al., 2000) while the spectra are obtained from the time series using FFT. It is to be noted that, in surge response spectra(SRA) there are some excitations close to the natural period of the platform in surge direction which create the first small peak. There is very less energy at that region in the wave spectrum, but due to the 2nd order force from viscous drag, maybe some excitation is possible close to the eigen period of the platform in surge motion. The largest peak occurs close to the peak frequency of corresponding wave spectrum as it is observed in figure 6.12.
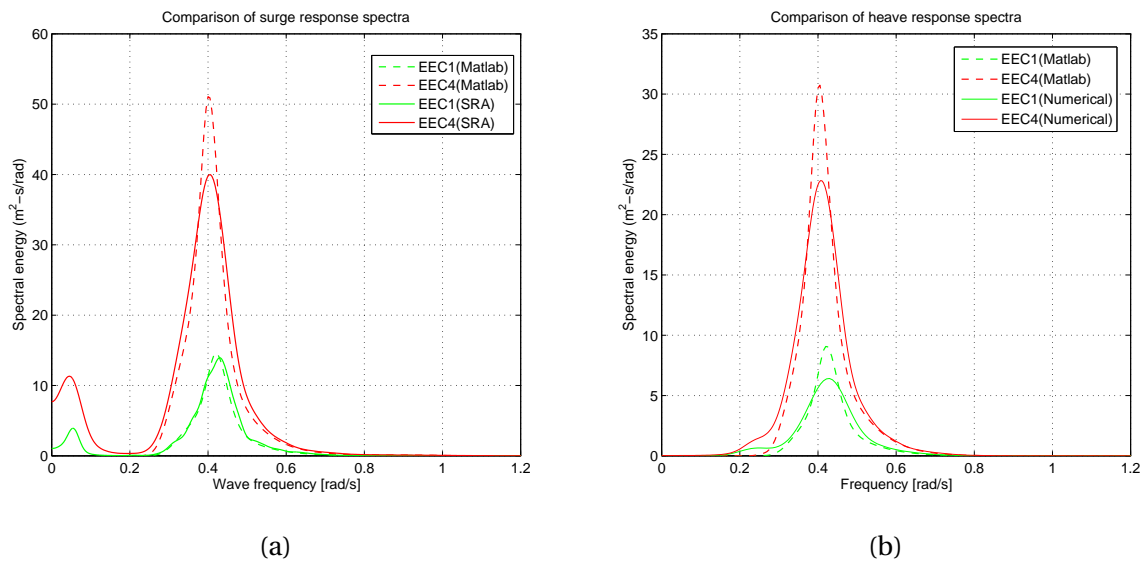
Figure 6.13: Comparison of surge and heave response spectra

For pitch response spectra the 2nd peak is following the same trend for both results and is around the peak frequency. But there is some discrepancy at the first peak. Although the 1st peak is occurred due to the resonance excitation around the eigen frequency (0.2 rad/s) of the platform in pitch. But from HydroD results the values of RAOs are very low there. Moreover, the wave spectra also do not have significant amount of energy close to that region (0-0.15 rad/s). However, in this region, the shape of the spectra found by SRA seem not to be in very good agreement with the spectra found by Matlab. So, this is of question that how SRA interprets the response around that region.
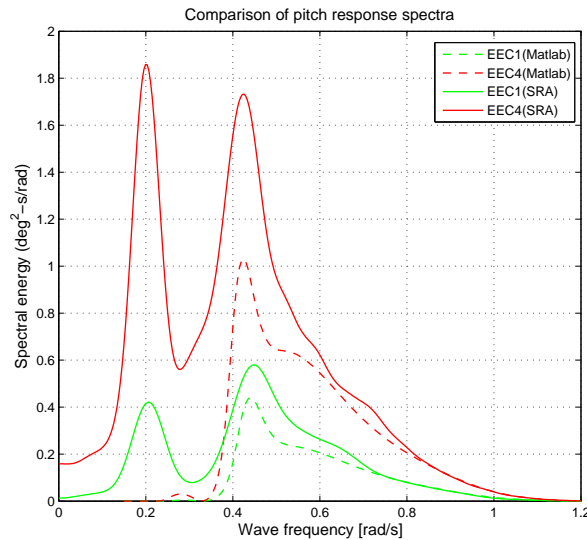
Figure 6.14: Comparison of pitch response spectra

6.6 Comparison between numerical analysis and experimental analysis

In this section, the extreme environmental conditions with wind loading are chosen for comparison between numerical and experimental results. Specially the statistical standard deviations of motion responses are compared here for aligned wave and wind condition. The data of spectra were not available for the experimental results. Hence, comparison of spectral analysis could not be performed here. The description of the environmental conditions is given earlier. This is also mentioned earlier that the Uw refers to the wind speed at 10 m above the mean water line.

In table 6.6, the comparisons are made. The standard deviation for heave and surge agrees quite well with the experimental results for EECW1. The reason of discrepency could be several. First of all, the numerical model is modeled as simplified model which only takes into account the 1st order potential force with Morison drag. Moreover, the water depth is also different for both cases although it may not affect the results much. But the STD of mooring line tension is also larger than the STD of the mooring line tension of the experimental results. Probably, that could affect the discrepency of the surge motioon response. Besides the mooring line tension can also affect the pitch response but not to that extent. The large STD values of pitch response in numerical results could aslo occur due to the lower linear damping coefficients as discussed in decay test. So, that could also be the reason of

Table 6.6: Comparison of STD of motion responses between numerical & experimental results

	EECW1 (Hs=8.8m,Tp=14.8s, Uw=27.9m/s)		EECW2(Hs=11.5m,Tp=15.7s, Uw=33.3m/s)	
	Numerical	Experimental	Numerical	Experimental
Surge (m)	1.505	1.525	1.947	2.190
Heave (m)	0.978	0.880	1.373	1.200
Pitch(deg)	0.887	0.486	0.794	0.587
	EECW3(Hs=13.5m,Tp=15.0s, Uw=33.3m/s)		EECW4(Hs=15.3m,Tp=15.5s, Uw=31.4m/s)	
	Numerical	Experimental	Numerical	Experimental
Surge (m)	2.346	2.480	2.639	3.050
Heave (m)	1.600	1.380	1.841	1.470
Pitch(deg)	1.321	0.712	1.303	0.840

higher excitation around the eigen frequency which can ultimately increase the standard deviation pitch as well. Somewhat the relative differences are in the range of 5-10 % . As, the numerical model is modeled as simplified model it can be acceptable for further investigation.

6.7 Irregular wave analysis for survival and functional conditions

In this section, several case studies are performed for global response analysis of the platform subjected to some specified extreme and functional environmental conditions. Here, this section is divided into two parts i.e. survival and functional conditions for convenience. The simulation parameters are almost same as mentioned in the following table 6.7. The main difference is that, for survival or extreme conditions the rotor is kept parked and feathered. Contradictorily, the rotor is operational for functional environmental conditions. The explanation of these conditions is already described in the previous chapter. All of the statistical results are taken from the average result of 10 random seeds.

6.7.1 Survival Condition

In total 8 extreme conditions are investigated (4 with wind loading and 4 without wind loading). In this section, the global responses in heave, surge and pitch motions are investigated

Table 6.7: Simulation parameters for survival & functional environmental condition

Simulation length (s)	4100
Transient length (s)	500
Simulation time step (RIFLEX) [s]	0.005
Wave/body response time step (SIMO) [s]	0.1
Turbine condition (Extreme cases)	Parked and feathered
Turbine condition (Functional cases)	Operational

for both extreme conditions. The wind and wave are aligned with the platform which implies the direction is 0 degree. That's why other degrees of freedom responses are very insignificant and not presented. In table 6.8 & 6.9 the one hour statistical standard deviation and the mean values of the structural responses are presented respectively. Values for different seeds are presented in the appendix and here only the average is taken. It is to be noted that, the environmental conditions are already described in the earlier section.

Table 6.8: Standard deviation values of motion response for survival conditions

Structural response	EEC1	EECW1	EEC2	EECW2	EEC3	EECW3	EEC4	EECW4
Surge (m)	1.323	1.505	1.874	1.947	2.098	2.346	2.554	2.639
Heave (m)	0.982	0.978	1.375	1.373	1.550	1.600	1.859	1.841
Pitch (deg)	0.431	0.887	0.573	0.794	0.699	1.321	0.810	1.303

Table 6.9: Mean values of motion response for survival conditions

Structural response	EEC1	EECW1	EEC2	EECW2	EEC3	EECW3	EEC4	EECW4
Surge (m)	1.789	5.739	1.953	4.901	2.127	8.183	2.300	7.551
Heave (m)	0.053	0.137	0.056	0.121	0.061	0.203	0.063	0.183
Pitch (deg)	0.140	1.808	0.174	1.474	0.200	2.675	0.234	2.413

From table 6.8 it is observed that the variation in heave response for cases with and without wind are not very significant for same condition. But, in surge and pitch response, the variation is quite significant. That implies, the wind loading contribution in surge and pitch are more dominant than in heave. But, overall in extreme environmental conditions the wave conditions are dominating. This is explained in more detail later with the illustration of the response spectra. In table 6.9 similar kind of behaviour is noticed for the mean values as well. As a whole, the maximum standard deviation values are found for EECW4(Hs=15.3m, Tp=15.5 s, U_{ref}=31.4 m/s). This case is taken with highest significant wave height.

In figure 6.15b the heave response spectra are plotted for extreme environmental conditions. This can show a bit peaky pattern but this depends on the smoothing factor what is

(a)   (b)
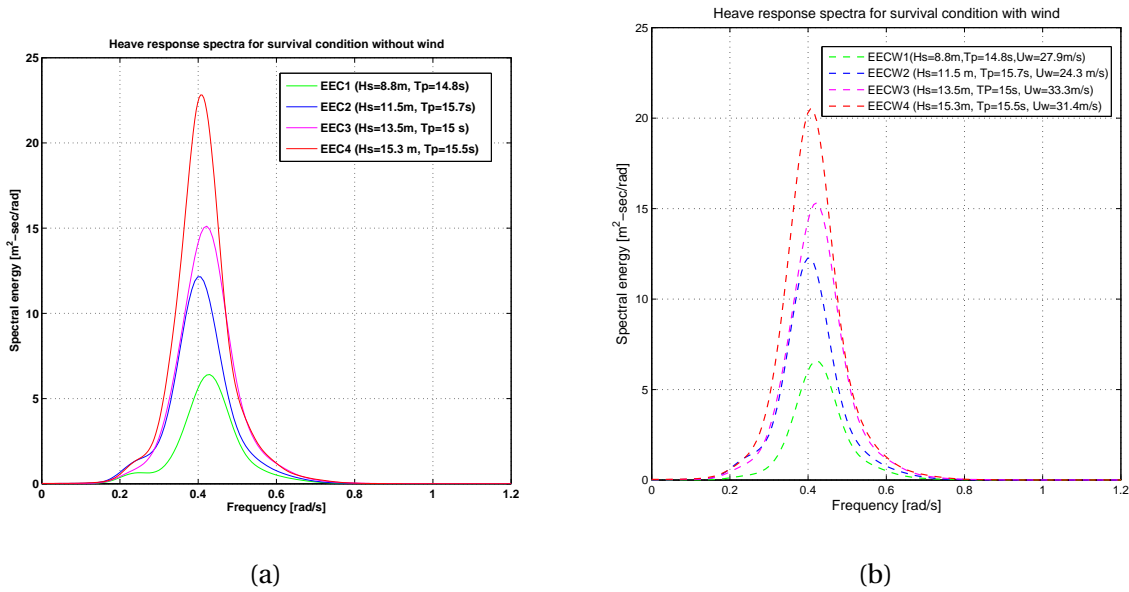
Figure 6.15: Heave response spectra for survival conditions

used to capture the peak properly. But the overall energy under the curve will be approximately same whether the spectrum is peaky(too detailed) or too smoothed. The peak is seemed to occur close to the peak frequency of the wave for every case. It is noted that the excitation around the eigen frequency is not as significant as around the peak frequency. This is also noticed from the figure that due to the presence of wind the heave response spectra are not affected significantly. Both spectra are almost same. In extreme conditions, wave condition is dominant.

(a)   (b)
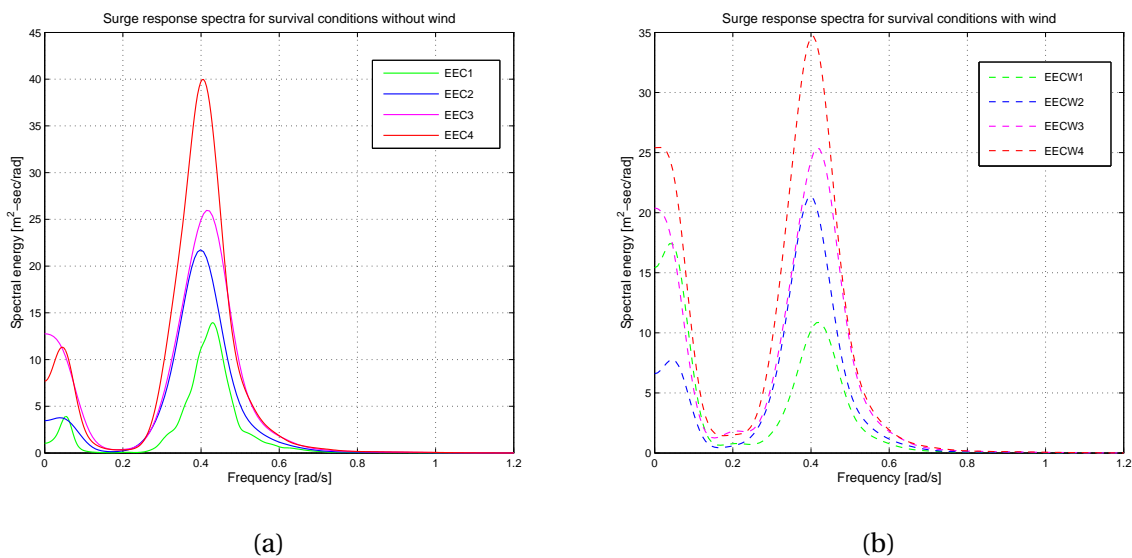
Figure 6.16: Surge response spectra for survival conditions

In figure 6.16a the surge response spectra are plotted for extreme conditions without wind loading. In figure 6.16b surge response spectra are plotted for extreme environmental conditions with wind loading. Here, it is observed that the surge response spectra shows some energy around the eigen frequency of the platform in surge. That totally comes from the stiffness due to the mooring line. It is close to around 112 seconds (0.06 rad/sec). Even though this is very small compared to the second peak which is excited around the peak frequency of respective sea states. The reason of increase of STD of surge response for EECW cases can be observed from figure 6.16b. Due to the wind loading the first peaks get more increased around the very low frequency range.

(a)   (b)
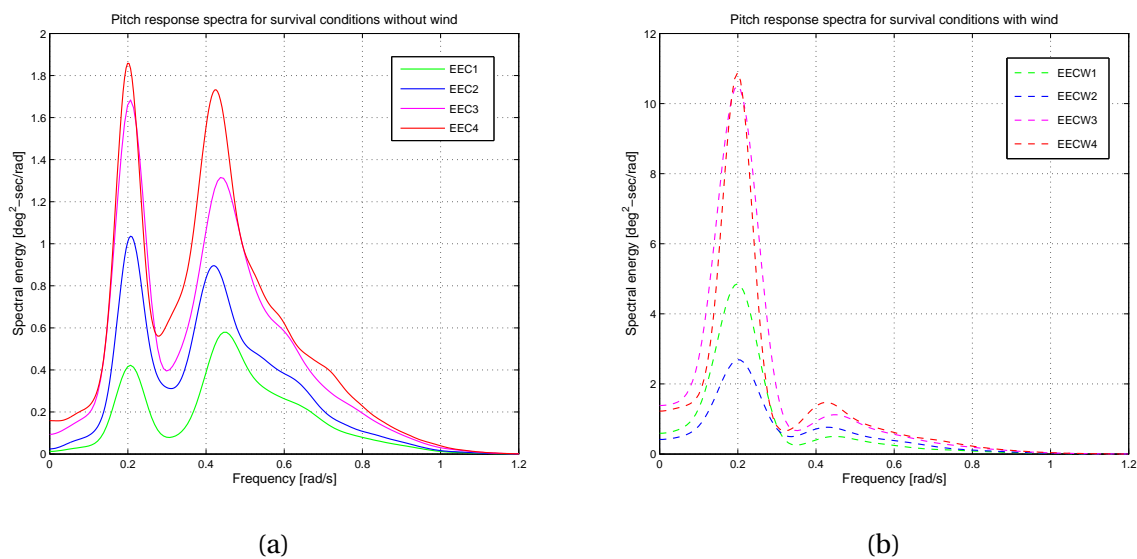
Figure 6.17: Pitch response spectra for survival conditions

In figure 6.17, the pitch response spectra are plotted for extreme conditions with and without wind loading. There are two prominent peaks are noticed on the plot. The first peak occurs around the eigen frequency for pitch (approx 0.21 rad/s) and the second peak occurs at the peak frequency of respective sea states. The second peak is found to be in same position for every sea state as the T_p is quite close for every sea state. In this case, still the wave condition is dominating the response behaviour of the platform in pitch direction like other degrees of freedoms. In figure 6.17b, it seems that, the first peak gets quite dominant compared to the second peak. Here, the excitation around the eigen frequency gets quite large with wind loading. It seems that, the majority contribution is coming from this region. Here, it seems taht the wave condition is no longer as dominant as in the left plot 6.17a.

6.7.2 Functional Condition

In this section, the responses are investigated for the operational environmental condition. The description of the environment is given in the environmental conditions section. Heave response is not very significant for functional environmental conditions. Hence, only surge and pitch statistical response values along with the spectra plot are presented here. Three wind speed is taken i.e. 8 m/s, 12.7 m/s and 18 m/s (U_w,at tower top).This is to be mentioned that, now the rotor is in operational condition. So, additionally there will be aerodynamic damping as well.

Table 6.10: Standard deviation & mean values for surge & pitch response in operational environmental conditions

	STD			
	OECW1	OECW2	OECW3	OECW4
Surge (m)	1.93	1.98	2.10	0.80
Pitch (deg)	2.30	2.26	2.25	1.32
	Mean			
	OECW1	OECW2	OECW3	OECW4
Surge (m)	9.50	9.54	9.54	7.31
Pitch (deg)	4.72	4.73	4.75	3.46

In table 6.10, the standard deviation and the mean values are presented for surge and pitch response in functional environmental conditions. The standard deviation of surge and pitch are quite close for the first 3 conditions as there is no big difference in wind speeds. Here, the wind condition is the dominating one compared to the wave condition. The STD is quite low for the fourth condition which is an above rated condition and quite far away from the rated wind speed (approximately 11.4 m/s). From the thrust curve of the 5 MW NREL WT, it can be found that the thrust is gets decreased after the rated wind speed. For getting constant power, the blade angle is pitched in a way so that thrust becomes low for above rated wind speed. This is the reason why the valus of STD for both surge and pitch response get decreased for OECW4(Hs=5 m, Tp= 9 s, Uw = 18 m/s).

In figure 6.18a and 6.18b the surge and pitch response spectra are plotted respectively for the operational environmetal conditions. Here, it is observed that the majority of the contribution in the spectral energy is coming from the low frequency range where the wind loading is dominant. The peak has occured around the eigen frequency. The second peak is so insignificant that it is hardly seen in the plot, but there is a very small peak around the peak frequency of the wave spectrum.
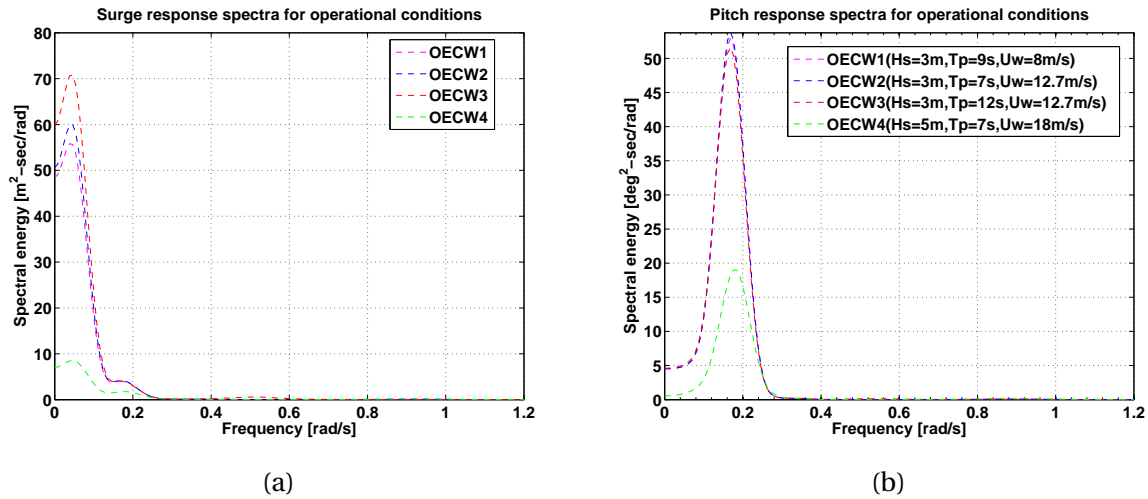
Figure 6.18: Surge & pitch response spectra for operational conditions

6.8 Tower base bending moment

In this section a spectral analysis of tower base bending moment is performed. Moreover the statistical response results are presented as well for both extreme and operational conditions to investigate more detail knowledge about the tower base bending moment. The investigation of tower base bending moment is crucial and important as this location is prone to fatigue. The tower base is located at 10 m above from the mean water line. The tower base bending moment is investigated with respect to the local y and z axis. The local coordinate system is illustrated in the previous chapter. The tower base bending moment around the local y-axis is termed as fore-aft bending moment (BMY) and the one around the z-axis is denoted as side-side bending moment (BMZ). The same simulation parameters are used as described in the previous section. The statistical results are presented in the following table 6.11 and 6.12. The following figure shows the illustration of the tower base bending moment notations.

Table 6.11: Standard deviation of tower base bending moments for extreme conditions

	EEC1	EECW1	EEC2	EECW2	EEC3	EECW3	EEC4	EECW4
BMY(KN-m)	13249.1	15021.7	16617.1	23137.0	17118.1	20646.2	23203.2	24396.9
BMZ(KN-m)	14.4	4126.7	19.2	5783.8	23.93	3340.1	28.2	5185.9

From the statistical results, it is observed that for BMY there is less difference in STD for conditions with and without wind loading. As the blade is parked in extreme condition there is almost no aerodynamic damping. Besides, in extreme condition the wave is the
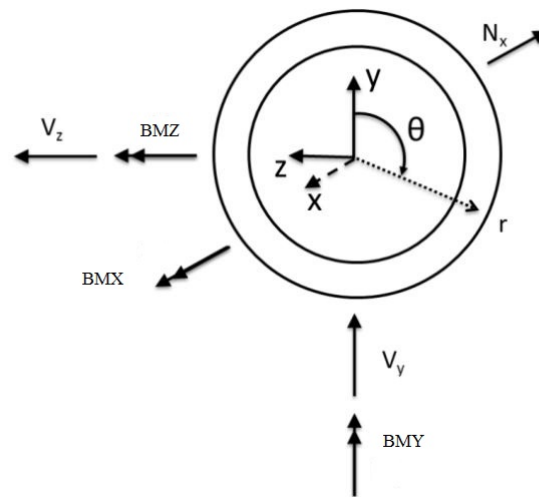
Figure 6.19: Tower base bending moment w.r.t local axis seen from top

Table 6.12: Mean values of tower base bending moments for extreme conditions

	EEC1	EECW1	EEC2	EECW2	EEC3	EECW3	EEC4	EECW4
BMY(KN-m)	368.1	25968.2	608.1	38653.7	757.18	20665.7	964.1	34442.1
BMZ(KN-m)	0.4	-3595.6	0.6	-5997.9	0.99	-2669.3	1.3	-5138.0

dominant criterion. But for 2nd and 3rd condition the difference is almost 15%. Since in extreme condition the blades are parked and feathered so very less thrust may be faced by the rotor. maybe, the hub will face increasing wind thrust due to the increasing wind speed at tower top. So, it is quite reasonable to get the difference as the thrust force due to wind loading contributes a major part to the fore-aft tower base bending moment. The length of the arm for the moment is almost 80 m [Moment = Thrust force × arm]. This can roughly give an estimate for the static mean value.So, maybe this thrust is contributing to the high mean values of BMY as obtained in 6.12 for EECW cases. However, the condition with the maximum significant wave height(Hs) is playing the crucial role which gives the largest STD for BMY. The side-side bending moment is totally insignificant without wind loading and it may be reasonable. But, the standard deviations and the mean values of BMZ are getting significant for EECW (with wind) cases. Even though the blades are parked and feathered, due to the wind loading the blades may get some lifting which can create torque in side-side directions as well. Probably, due to this effect the BMZ are getting significant in this case.

In figure 6.20a and 6.20b the spectra of BMY are plotted for extreme conditions without and with wind loading respectively. The spectral analysis has been performed using WAFO (Brodtkorb et al. (2000)) toolbox in Matlab. The 'dat2spec' and 'pot spec' functions are used

(a) Without wind loading

(b) With wind loading
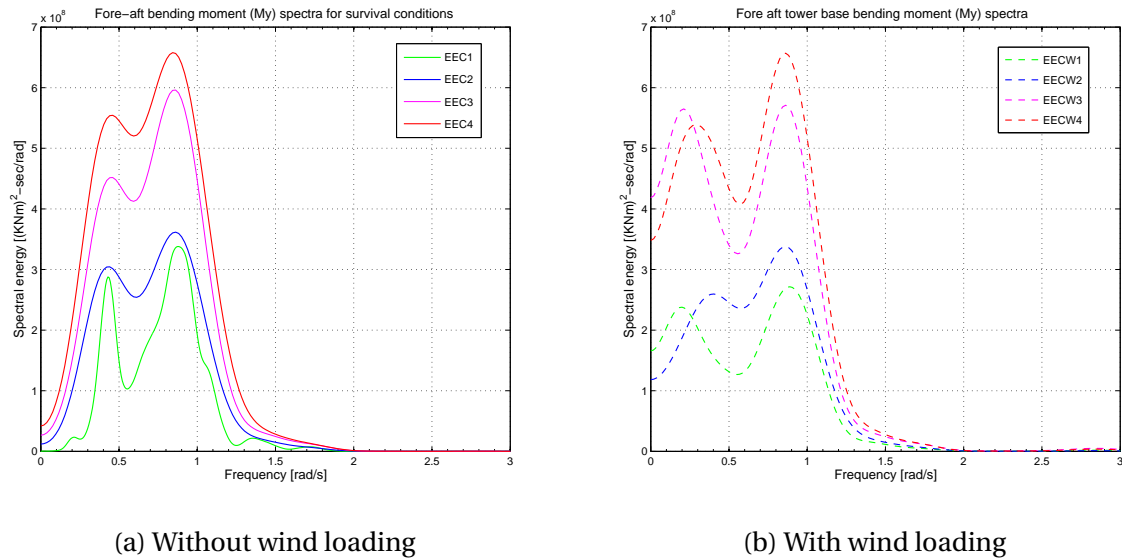
Figure 6.20: Tower base bending moment(BMY) spectra for extreme conditions

with default parameters except the smoothing factor. The detail can be found in the documentation of WAFO toolbox. The first peak is occurred around the peak frequency of respective environmental conditions for all of the cases. For EEC1 condition, a peak around the pitch eigen frequency is observed in the plot. But for other condition with increasing Hs, this peak gets merged and it seems that the excitation which is occurred around the peak frequency gets significantly dominant. However, the second peak (highest) is around 0.85 rad/s (7.4 sec). It is of query about this 2nd prominent excitation which is also contributing a significant portion of spectral energy. But, it can be noted that there was some excitation cose to this frequency in surge and pitch motion RAOs plot which is described in chapter 4. As, the tower base bending moment RAOs which is induced from platform motion directly relates with the surge and pitch RAOs of acceleration. Simultaneously the acceleration RAOs are related to the motion RAOs. So, this could be a reason. As, the RAO of tower base bending moment is not available right now it can't be taken as firmly but there maybe a probability.

In figure 6.20b, the spectra are showing quite a similar trend with the wind loading but the first peak gets bit shifted towards low frequency region. Specially for EECW1 and EECW3, the first peak is a bit more shifted. Since the wind loading has a very low frequency so it excites the platform in low frequency region. The spectral energy has also get increased around low frequency region compared to the environmental conditions without wind. Overall, the responses are dominated by the wave loads in extreme environmental conditions.

In figure 6.21a and 6.21b the spectra of BMZ are plotted for operational environmen-

(a) Without wind loading   (b) With wind loading
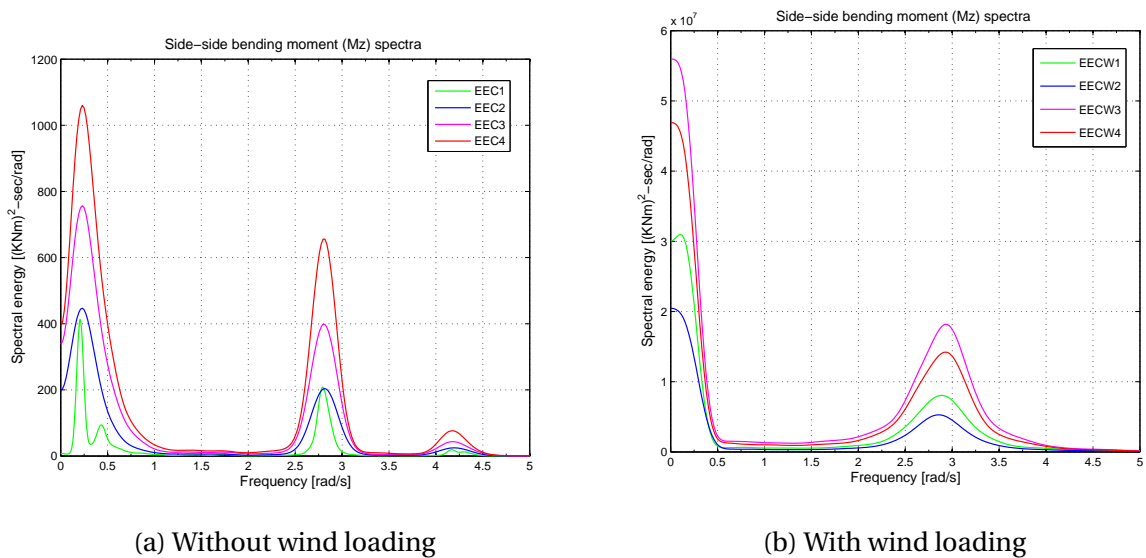
Figure 6.21: Tower base bending moment (BMZ) spectra for extreme conditions

tal conditions without and with wind loading respectively. Here, it is observed that the BMZ spectral energy for EEC environmental conditions are negligible compared to the EECW conditons. The first peak is found around the roll eigen frequency (approximately 0.2 rad/sec) of the platform. The second peak is around 2.8 rad/sec for both environmental conditions. But, it is also true that here, the wave load is the dominant criterion. There could be a chance that that this is due to the eigen frequency of the 1st global side-side tower bending mode. Because similar type of phenomena is observed in figure 6.20b where a small paek which is hard to observe because the first peak is so large that the other small peaks can't be observed properly. Generally, the natural frequency of first global fore-aft and side-side tower bending mode are quite close.

In table 6.13 the statistical results are presented for the tower base bending moment (both BMY and BMZ) in operational environmental conditions. The standard deviation and the mean values are considered. From the mean value for operational environmental condition with wind loading, it is observed that the mean values are quite large. This is because at rated wind speed the thrust is the largest. The wind speeds for first 3 cases are close to the rated wind speed (approximately 11.4 m/s). The thrust force is almost 600-700 KN which can easily give a moment of 50000-60000 KN-m while the distance between the tower base and tower top is almost 80 m. This is a rough estimate of static value. So the mean values seems reasonable.

For operational condition the rotor is now operational, this implies it is not parked any-

Table 6.13: Statistical results of BMY & BMZ for operational conditions

	STD			
	OECW1	OECW2	OECW3	OECW4
MY(KN-m)	28776	28473	26036	26505
MZ(KN-m)	2457	2426	2391	3496
	Mean			
	OECW1	OECW2	OECW3	OECW4
MY(KN-m)	73794	73858	74096	53666
MZ(KN-m)	7357	7357	7360	8983

more. So, there will be some excitation around 1P and 3P frequencies. Generally the constant rotational speed of the rotor (at rated wind speed) is termed as 1st rotational frequency (1P). In the following figure 6.22 the rotational speed of rotor is shown. The second excitation frequency is the rotor blade passing frequency which is equal to $N_b \times P$, where N_b is the number of blades. As this is a 3-blade rotor, so the second excitation frequency will be 3P.
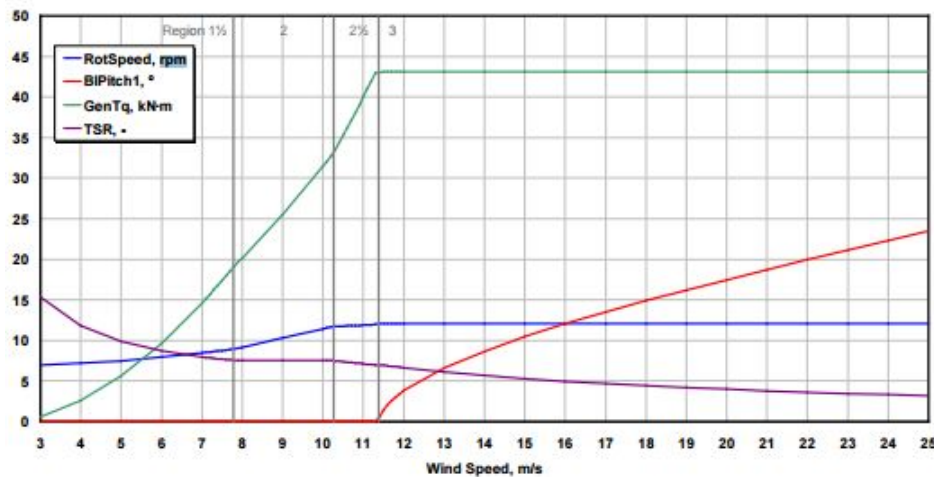
Figure 6.22: Steady-state response as a function of wind speed for NREL 5MW WT.(Jonkman et al., 2009)

Here, it is to be kept in mind that due to the smoothing of the spectra maybe some peaks are not observed clearly. In figure 6.23a the BMY spectra are plotted for operational conditions. Here, it is clearly observed that the majority of the contribution of spectral energy is coming from the low frequency region due to the wind. Here, wind loads are dominating since significant spectral energy is around the low frequency region. The second peak is around the 1P frequency of the blade (0.9-1 rad/s). But the peak around 3P frequency (approximately 3 rad/s) is very small and hence is not observed very well.

In figure 6.23b the BMZ spectra are plotted for functional environmental conditions. This
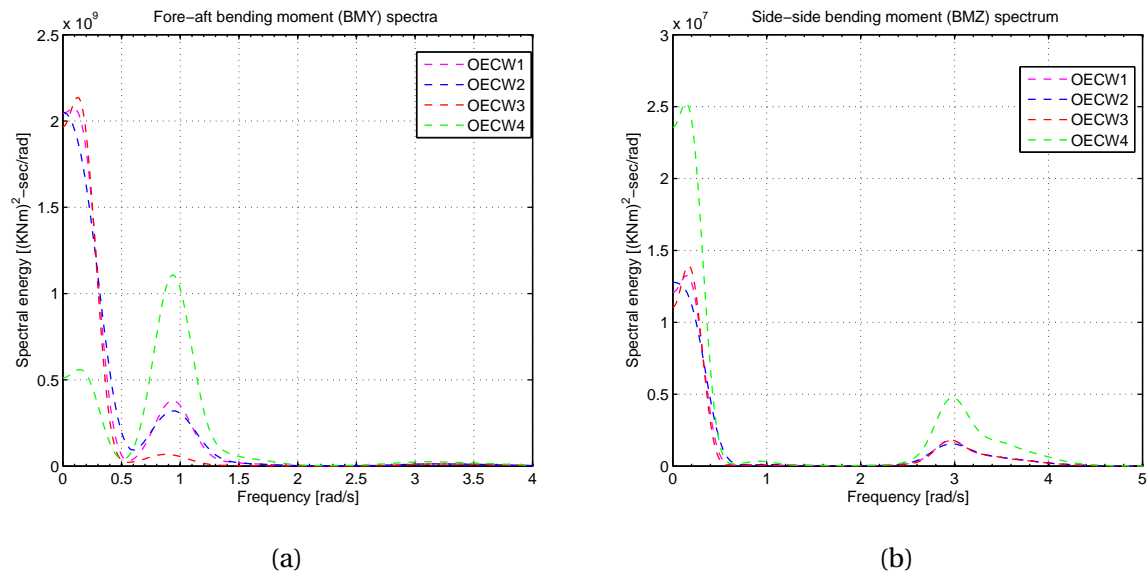
Figure 6.23: Tower base bending moment(BMY & BMZ) spectra for operational conditions

is the side-side bending moment spectra. All of the conditions are in aligned condition, so less spectral energy is expected for BMZ as it is. The contribution is mainly coming from the tilting in roll direction due to the aerodynamic lift of the blades. Similar type of patterns are observed for this case as well. Here, the 3P excitation can be observed clearly.

Chapter 7

Summary and Recommendations for Further Work

7.1 Conclusion

This section highlights some key findings from the result and discussion parts. The results and discussions are subdivided into two parts. One part contains the result of frequency domain analysis performed in HydroD. Another part contains the results of time domain analysis performed in fully coupled SIMO-RIFLEX-Aerodyn(SRA).

The frequency domain analysis which is performed in HydroD was a very important step. There were some errors in the numerical model in Genie from the previous work carried out in the project. So, the redesign of the model has been done so that the parameters of the numerical models become as close as possible compared to the experimental model. However, for comparison of motion responses, only heave, surge and pitch motions have been considered since the analysis is performed in the aligned condition.

The comparisons are made considering only the wave condition. It has been found that the absence of mooring line does not have a significant effect in the wave frequency range. But, the WECs are modelled as rigidly connected to the pontoon in the numerical model. So, close to the natural period of the rotational WEC, it is found that there are quite significant discrepancies for surge and pitch motion RAOs. Because, close to this region, it has been found that the experimental results are larger than the numerical results. So, probably due to the absence of excitation in the numerical model the RAOs close to this region gets lower. But, the heave RAOs did not get affected a lot due to the inability of rotation of the WECs in

the numerical model.

During the investigation of sectional loads at the specific position, it is found that the maximum values of internal loads occur just out of phase of the excitation loads. Elaborately speaking, sectional loads get amplified where the excitation loads get cancellation effect. This can imply, despite having low excitation load at certain wave period, the sectional loads get amplified due to the domination of inertia loads.

In fully coupled time domain numerical analysis of SFC, the response behaviour of the SFC is observed both for survivability and functional environmental conditions. A sensitivity analysis for choosing the number of seeds have been performed first. It is found that one-hour simulation with 10 seeds for each environmental conditions provides satisfactory results. During the verification of response spectra obtained in SRA with the response spectra processed with the help of Matlab, a significant difference between two results is found for pitch response at low-frequency range. Even though close to the eigen frequency of pitch there will be some excitation, but the energy carried by the wave spectra is really insignificant from 0 to 0.2 rad/s. So, the exact reason behind could not be found. Later on, while comparing the numerical results with experimental results regarding the statisical parameter , a large difference is found for pitch response. Probably this could be the reason for the big difference. Whereas, the standard deviation found by Matlab was more close to the STD of experimental results for pitch response.

From the analysis in survival and operational environmental condition, it is found that wave conditions are dominating in extreme environments whereas wind loads get dominant in operational environmental conditions. Moreover, this is also observed the peak of the heave, surge and pitch response spectra occur generally close to the peak frequency of the respective wave spectrum. Another peak also gets found for surge and pitch response close to their respective eigen period. Whereas, in functional environmental condition it is found that the heave motions are insignificant and that is why not given in the result section.

The tower base bending moment are investigated with respect to the local axis. It is found that STD of the fore-aft bending moment is at least 10 times larger than the side-side bending moment for extreme conditions with the wind. However, the side-side bending moment is negligible for the cases without wind loading. The mean value of the fore-aft bending moment at tower base is almost 3 times larger than extreme environments. In operational environmental condition, the wind loads are dominating and wind thrust felt by the blades

are larger compared to the extreme case. Besides, in extreme environments, the rotor was parked. But there was less difference in STD of fore-aft tower-base bending moment between the extreme and functional environmental conditions.

Appendix A

Acronyms

ALS Accident Limit State

BMY Tower base bending moment wrt local Y axis

BMZ Tower base bending moment wrt local Z axis

DLL Dynamic link library

EMX Excitaion moment RAO in X-direction

EMY Excitaion moment RAO in Y-direction

EMZ Excitaion moment RAO in Z-direction

EX Excitaion force RAO in X-direction

EY Excitaion force RAO in Y-direction

EZ Excitaion force RAO in Z-direction

FD Frequency domain

FX Sectional force RAO in X-direction

FY Sectional force RAO in Y-direction

FZ Sectional force RAO in Z-direction

FOWT Floating Offshore Wind Turbine

FLS Fatigue Limit State

FFT Fast Fourier Transform

HAWT Horizontal Axis Wind Turbine

IEC International Energy Comission

ML2 Mooring line tension of line 2

MW Megawatt

MX Sectional moment RAO in X-direction

MY Sectional moment RAO in Y-direction

MZ Sectional moment RAO in Z-direction

NREL National renewable energy laboratory

NTM Normal Turbulence Model

RAO Response amplitude operator

SRA SIMO-RIFLEX-Aerodyn

SFC Semi-submersible Flap type Concept

SIF SESAM interface file

TD Time domain

TI Turbulence intensity

WT Wind Turbine

A.1 List of symbols

U_w Mean wind speed at tower top

U_{ref} Mean wind speed at 10 m above from the mean water line

$H_s \, or \, Hs$ Significant wave height

$T_p \, or \, Tp$ Peak period

$T_n \, or \, Tn$ Eigen period

ρ Density

ζ_a Wave amplitude

ϕ Velocity potential

λ Wave length

D Diameter

C_D Drag coefficient

$T_n \, or \, Tn$ Eigen period

ρ Density

ζ_a Wave amplitude

ϕ Velocity potential

λ Wave length

D Diameter

C_D Drag coefficient

Appendix B

Additional Information

B.1 Results for different seeds for all cases

Some results are given in this section for extreme environmental conditions with wind for random seeds.

Table B.1: Statistical motion results for different seeds for EECW1

EECW1	Seed 1	Seed 2	Seed 3	Seed 4	Seed 5	Seed 6	Seed 7	Seed 8	Seed 9	Seed 10
STD										
Surge(m)	1.54	1.58	1.53	1.50	1.49	1.57	1.47	1.49	1.48	1.54
Heave(m)	1.00	1.03	1.00	0.99	0.96	1.00	0.96	0.95	0.97	1.00
Pitch(deg)	0.91	0.87	0.87	0.87	0.93	0.87	0.87	0.89	0.89	0.88
Max										
Surge(m)	11.15	11.53	11.62	12.10	10.80	11.08	10.81	11.77	10.94	11.36
Heave(m)	4.12	4.12	3.83	3.66	3.80	3.88	3.47	3.89	3.83	4.51
Pitch(deg)	4.66	4.55	4.27	4.15	5.09	4.34	4.62	4.36	4.71	4.37
Mean										
Surge(m)	5.73	5.76	5.74	5.73	5.73	5.74	5.75	5.74	5.73	5.74
Heave(m)	0.14	0.14	0.14	0.14	0.14	0.14	0.14	0.14	0.14	0.14
Pitch(deg)	1.81	1.81	1.81	1.81	1.81	1.81	1.81	1.81	1.81	1.81

Table B.2: Statistical results of BMY_{tower}, BMZ_{tower} & ML2 for different seeds for EECW1

EECW2	Seed 1	Seed 2	Seed 3	Seed 4	Seed 5	Seed 6	Seed 7	Seed 8	Seed 9	Seed 10
					ML2 (KN)					
STD	91.6	93.4	91.3	88.7	86.6	93.7	86.6	87.9	87.9	91.1
Max	1563.8	1582.3	1541.0	1474.0	1532.0	1566.3	1492.2	1551.9	1551.9	1660.5
Mean	1165.9	1165.1	1165.4	1166.0	1165.5	1165.8	1165.6	1165.9	1165.9	1166.0
					BMY_{tower} (KN-m)					
STD	15284.0	15104.7	15001.3	14711.4	15518.0	14940.7	14969.1	14837.4	14837.4	15012.6
Max	81435.8	85581.9	84748.6	80476.7	99457.6	75181.2	78741.4	82202.3	82202.3	86654.9
Mean	25988.7	25977.7	25977.5	25967.4	25961.0	25982.9	25948.3	25955.7	25955.7	25967.5
					BMZ_{tower} (KN-m)					
STD	4127.7	4148.2	4120.4	4110.0	4136.3	4140.4	4112.9	4130.1	4130.1	4111.1
Max	11229.9	11615.6	11458.3	10686.2	11177.7	11083.4	11594.5	11457.1	11457.1	10780.5
Mean	-3614.1	-3609.9	-3603.6	-3590.6	-3591.3	-3585.4	-3580.2	-3598.0	-3598.0	-3585.2

Table B.3: Statistical motion results for different seeds for EECW2

EECW2	Seed 1	Seed 2	Seed 3	Seed 4	Seed 5	Seed 6	Seed 7	Seed 8	Seed 9	Seed 10
					STD					
Surge(m)	1.91	1.97	1.98	1.93	1.96	1.94	1.97	2.01	1.80	1.95
Heave(m)	1.36	1.39	1.39	1.37	1.41	1.40	1.40	1.43	1.26	1.37
Pitch(deg)	0.79	0.82	0.79	0.79	0.82	0.83	0.79	0.82	0.79	0.79
					Max					
Surge(m)	11.87	12.50	12.61	11.01	12.47	11.56	13.81	12.60	11.48	11.43
Heave(m)	4.84	5.30	5.50	3.97	5.67	4.52	5.53	5.18	4.50	4.79
Pitch(deg)	4.16	4.15	3.98	4.09	4.40	4.22	3.98	4.18	4.31	4.20
					Mean					
Surge(m)	4.93	4.92	4.92	4.91	4.94	4.94	4.92	4.92	4.87	4.90
Heave(m)	0.12	0.12	0.12	0.12	0.12	0.12	0.12	0.12	0.12	0.12
Pitch(deg)	1.48	1.48	1.47	1.47	1.48	1.47	1.48	1.48	1.47	1.47

Table B.4: Statistical results of BMY_{tower}, BMZ_{tower} & ML2 for different seeds for EECW2

EECW2	Seed 1	Seed 2	Seed 3	Seed 4	Seed 5	Seed 6	Seed 7	Seed 8	Seed 9	Seed 10
					ML2(KN)					
STD	133.5	137.6	139.1	132.0	140.3	139.5	137.6	137.6	119.6	133.7
Max	1760.7	1856.1	1925.0	1684.9	1869.8	1790.5	1771.8	1771.8	1661.1	1758.4
Mean	1191.2	1191.1	1191.7	1192.1	1190.9	1191.1	1191.3	1191.3	1193.1	1191.8
					BMY_{tower} (KN-m)					
STD	17081.3	16851.8	17209.8	16939.4	17369.0	17257.3	17202.6	17202.6	16837.4	17229.9
Max	83565.4	88673.6	76659.6	77032.4	86405.5	92612.8	83558.7	83558.7	84912.9	84943.2
Mean	20685.4	20698.9	20650.2	20651.9	20691.3	20672.9	20671.4	20671.4	20608.8	20654.5
					BMZ_{tower} (KN-m)					
STD	3346.9	3343.7	3335.1	3314.9	3315.5	3356.8	3339.5	3339.5	3379.3	3329.9
Max	10366.4	9429.0	9388.9	9705.7	9739.1	9224.0	10199.6	10199.6	9446.3	9233.9
Mean	-2672.7	-2682.9	-2659.3	-2667.7	-2680.5	-2671.5	-2665.4	-2665.4	-2662.1	-2665.5

Table B.5: Statistical motion results for different seeds for EECW3

EECW3	Seed 1	Seed 2	Seed 3	Seed 4	Seed 5	Seed 6	Seed 7	Seed 8	Seed 9	Seed 10
					STD					
Surge(m)	2.32	2.19	2.19	2.37	2.29	2.43	2.31	2.33	2.28	2.35
Heave(m)	1.58	1.48	1.47	1.63	1.55	1.65	1.54	1.57	1.55	1.60
Pitch(deg)	1.40	1.36	1.37	1.39	1.37	1.37	1.35	1.30	1.37	1.32
					Max					
Surge(m)	15.87	15.32	16.47	17.37	17.57	16.77	16.09	16.46	16.97	15.63
Heave(m)	5.90	5.07	4.56	6.62	6.50	6.00	5.27	6.09	5.48	5.39
Pitch(deg)	6.71	6.53	6.64	7.28	6.63	7.11	6.81	6.70	6.53	6.49
					Mean					
Surge(m)	8.21	8.18	8.13	8.24	8.17	8.22	8.15	8.17	8.18	8.18
Heave(m)	0.20	0.20	0.19	0.20	0.20	0.20	0.20	0.20	0.20	0.20
Pitch(deg)	2.68	2.66	2.66	2.68	2.67	2.67	2.67	2.67	2.67	2.67

Table B.6: Statistical results of BMY_{tower}, BMZ_{tower} & ML2 for different seeds for EECW3

EECW3	Seed 1	Seed 2	Seed 3	Seed 4	Seed 5	Seed 6	Seed 7	Seed 8	Seed 9	Seed 10
					ML2 (KN)					
STD	150.8	135.9	132.9	152.8	145.3	156.6	143.2	146.7	144.0	149.3
Max	1714.5	1675.9	1606.1	1769.0	1962.8	1820.3	1650.7	1749.1	1680.1	1666.7
Mean	1091.4	1092.7	1094.2	1091.3	1092.3	1091.2	1093.0	1093.3	1091.9	1091.9
					BMY_{tower} (KN-m)					
STD	23191.5	22358.0	22774.6	23309.1	23226.9	23559.5	22598.4	22308.8	23145.4	23137.0
MAx	129402.8	107397.8	132261.3	129711.8	130345.6	136137.6	121489.6	117457.1	120962.8	128603.8
Mean	38598.8	38548.9	38495.1	38644.9	38614.3	38584.5	38588.0	38593.9	38574.9	38653.7
					BMZ_{tower} (KN-m)					
STD	5824.9	5825.8	5837.5	5780.8	5780.5	5869.5	5775.7	5837.6	5849.8	5783.8
Max	18315.4	14984.0	15638.2	17458.1	16293.4	14561.4	14885.4	17312.6	16833.2	13819.3
Mean	-5976.0	-5974.8	-5980.0	-6009.6	-6013.5	-6006.8	-6004.7	-6006.2	-5993.3	-5997.9

Table B.7: Statistical motion results for different seeds for EECW4

EECW4	Seed 1	Seed 2	Seed 3	Seed 4	Seed 5	Seed 6	Seed 7	Seed 8	Seed 9	Seed 10
					STD					
Surge(m)	2.57	2.73	2.73	2.73	2.73	2.50	2.70	2.50	2.50	2.70
Heave(m)	1.79	1.89	1.89	1.89	1.89	1.76	1.89	1.75	1.75	1.88
Pitch(deg)	1.31	1.30	1.30	1.30	1.30	1.25	1.33	1.30	1.30	1.34
					Max					
Surge(m)	18.42	21.39	21.39	21.39	21.39	15.32	17.81	16.64	16.64	18.32
Heave(m)	7.01	7.84	7.84	7.84	7.84	5.64	6.18	6.51	6.51	6.89
Pitch(deg)	6.83	6.66	6.66	6.66	6.66	6.05	6.82	6.30	6.30	6.35
					Mean					
Surge(m)	7.54	7.55	7.55	7.55	7.55	7.56	7.53	7.53	7.53	7.61
Heave(m)	0.18	0.18	0.18	0.18	0.18	0.18	0.18	0.18	0.18	0.18
Pitch(deg)	2.42	2.42	2.42	2.42	2.42	2.41	2.42	2.40	2.40	2.42

Table B.8: Statistical results of BMY_{tower}, BMZ_{tower} & ML2 for different seeds for EECW4

EECW4	Seed 1	Seed 2	Seed 3	Seed 4	Seed 5	Seed 6	Seed 7	Seed 8	Seed 9	Seed 10
					$ML2$ (KN)					
STD	177	189	189	189	189	171	190	169	195	189
Max	1957	2195	2195	2195	2195	1812	1876	2015	1918	2001
Mean	1111	1111	1111	1111	1111	1110	1111	1112	1110	1108
					BMY_{tower} (KN-m)					
STD	24414	24367	24367	24367	24367	23927	24649	23924	24493	25094
Max	149578	142629	142629	142629	142629	120775	121602	120478	128924	134443
Mean	34449	34458	34458	34458	34458	34396	34470	34369	34454	34452
					BMZ_{tower} (KN-m)					
STD	5230	5153	5153	5153	5153	5185	5175	5276	5202	5178
Max	14375	13474	13474	13474	13474	14485	13586	15717	15833	16108
Mean	-5123	-5144	-5144	-5144	-5144	-5120	-5152	-5159	-5123	-5128

Appendix C

Additional theories

C.1 Convolution using Parseval's theorem

Here, for convenience, capital letter is used for frequency domain variable and small lettter is used for time domain variable. For matrix bold letter and for vector $'\rightarrow'$ are used.

For the second term in the equation of motion , it may be said that the Fourier (or Inverse Fourier) transform of product is a convolution of the Fourier transforms. The Perseval's theorem is written as follows:

$$2\pi \int_{-\infty}^{+\infty} F(\omega).\overline{G(\omega)}d\omega = \int_{-\infty}^{+\infty} F(\tau).\overline{G(\tau)}d\tau \tag{C.1}$$

This equation is used here to derive the convolution. Now using the definition of inverse Fourier transform the following equations can be obtained:

$$F(\omega) = \mathscr{F}\Big[f(t)\Big] = 1/2\pi \int_{-\infty}^{+\infty} f(\tau)e^{-i\omega\tau}d\tau \tag{C.2}$$

$$G(\omega) = \mathscr{F}\Big[g(\tau)\Big] = 1/2\pi \int_{-\infty}^{+\infty} g(\tau)e^{-i\omega\tau}d\tau \tag{C.3}$$

The detail theory about Fourirer transform can be found in chapter 4 of (Newland, 2012)).

Now, assuming $F(\omega) = \big(i\omega a_{kj}(\omega) + b_{kj}(\omega)\big)e^{i\omega t}$ and $\overline{G(\omega)} = i\omega X_j(\omega)$, each component of

the second term can be written as follows using the above mentioned theorem:

$$\int_{-\infty}^{+\infty} \left(i\omega a_{kj}(\omega) + b_{kj}(\omega)\right) e^{i\omega t} . i\omega X_j(\omega) d\omega = 1/2\pi \int_{-\infty}^{+\infty} f(\tau).\overline{g(\tau)} d\tau \tag{C.4}$$

So now,

$$f(\tau) = \left[\mathscr{F}(\omega)^{-1}\right] = \int_{-\infty}^{+\infty} \left(i\omega a_{kj}(\omega) + b_{kj}(\omega)\right) e^{i\omega t} e^{i\omega \tau} d\omega \tag{C.5}$$

If we define $\mathbf{k}(\tau) = 1/2\pi \int_{-\infty}^{+\infty} \left(i\omega \mathbf{a}(\omega) + \mathbf{b}(\omega)\right) e^{i\omega \tau} d\omega$ and hence $f(\tau) = 2\pi k_{kj}(t + \tau)$

$$\overline{g(\tau)} = \overline{\mathscr{F}^-\left[G(\omega)\right]} = \overline{\int_{-\infty}^{+\infty} G(\omega) e^{i\omega \tau} d\omega} \tag{C.6}$$

From the proeprty of conjugate of complex variable the above equation can be further modified(i.e conjugate of $e^{ix} is e^{-ix}$ and vice-versa) and by replacing the value of $\overline{G(\omega)}$ the following equation is found

$$\overline{g(\tau)} = \int_{-\infty}^{+\infty} \overline{G(\omega)} e^{-i\omega \tau} d\omega = \int_{-\infty}^{+\infty} i\omega X_j(\omega) e^{-i\omega \tau} d\omega = \dot{x}_j(-\tau) \tag{C.7}$$

So, by replacing the value of $f(\tau)$ and $\overline{g(\tau)}$ the second term component becomes

$$\frac{1}{2\pi} \int_{-\infty}^{+\infty} 2\pi k_{kj}(t + \tau) \dot{x}_j(-\tau) d\tau \tag{C.8}$$

If $-\tau = \acute{\tau}$ and collecting the component in matrix form, it becomes

$$\int_{-\infty}^{+\infty} \mathbf{k}(t - \acute{\tau}) \dot{\tilde{x}}(\acute{\tau}) d\acute{\tau} \tag{C.9}$$

If $\mathbf{K}(\omega) = i\omega \mathbf{a}(\omega) + \mathbf{b}(\omega)$ is defined then there will be the Fourier transform pair and can be written as follows. But it is to be noted that, this pair are not the same Fourier and Inverse Fourier transforms what is mentioned earlier

$$\mathbf{k}(\tau) = \frac{1}{2\pi} \int_{-\infty}^{+\infty} K(\omega) e^{i\omega\tau} \, d\omega = \frac{1}{2\pi} \mathscr{F}^{-1}\left[\mathbf{K}(\omega)\right] \tag{C.10}$$

$$\mathbf{k}(\omega) = \int_{-\infty}^{+\infty} K(\tau) e^{-i\omega\tau} \, d\omega = 2\pi \mathscr{F}\left[\mathbf{K}(\tau)\right] \tag{C.11}$$

Bibliography

Brodtkorb, P. A., Johannesson, P., Lindgren, G., Rychlik, I., Rydén, J., Sjö, E., et al. (2000). Wafo-a matlab toolbox for analysis of random waves and loads. In *The Tenth International Offshore and Polar Engineering Conference*. International Society of Offshore and Polar Engineers.

Chakrabarti, S. (2005). *Handbook of Offshore Engineering (2-volume set)*. Elsevier.

Chakrabarti, S. K. (1987). *Hydrodynamics of offshore structures*. WIT press.

Commission, I. E. et al. (2005). Wind turbine—part 1: Design requirements, iec 61400-1. *International Electrotechnical Commission, Geneva, Switzerland.*

de Bruijn, R., Huijs, F., Bunnik, T., Huijsmans, R., and Gerritsma, M. (2011). Calculation of wave forces and internal loads on a semi-submersible at shallow draft using an ivof method. In *ASME 2011 30th International Conference on Ocean, Offshore and Arctic Engineering*, pages 175–185. American Society of Mechanical Engineers.

Faltinsen, O. (1993). *Sea loads on ships and offshore structures*, volume 1. Cambridge university press.

Gao, Z. (2016). Lecture materials of integrated dynamic analysis of wind turbine.

Gao, Z., Moan, T., Wan, L., and Michailides, C. (2015). *Comparative numerical and experimental study of two combined wind and wave energy concepts*. PhD thesis, Dept. of MArine Technology, NTNU, Centre for Ships and Ocean Structures, Norwegian University of Science and Technology Centre for Autonomous Marine Operations and Systems, Norwegian University of Science and Technology Department of Marine Technology, Norwegian University of Science and Technology Trondheim, Norway.

Gao, Z., Wan, L., Michailides, C., and Moan, T. (2014). Numerical modelling and analysis of combined concepts of floating wind turbines and wave energy converters. In *International Conference in Offshore Renewable Energy, Glasgow, Scotland*, Centre for Ships and Ocean Structures, Centre for Autonomous Marine Operations and Systems and Department of Marine Technology, Norwegian University of Science and Technology.

Hoff, J. (2001). Estimation of linear and quadratic roll damping from free-decay tests. Technical report, Tech. Rep. 601882, NTNU.

Jonkman, B. J. (2009). Turbsim user's guide: Version 1.50.

Jonkman, J., Butterfield, S., Musial, W., and Scott, G. (2009). Definition of a 5-mw reference wind turbine for offshore system development. *National Renewable Energy Laboratory, Golden, CO, Technical Report No. NREL/TP-500-38060.*

Li, L., Gao, Z., and Moan, T. (2013). Joint environmental data at five european offshore sites for design of combined wind and wave energy devices. In *ASME 2013 32nd International Conference on Ocean, Offshore and Arctic Engineering*, pages V008T09A006–V008T09A006. American Society of Mechanical Engineers.

Luan, C., Gao, Z., and Moan, T. (2014a). Conceptual designs of a 5-mw and a 10-mw semi-submersible wind turbine with emphasis on the design procedure. *Journal of Offshore Mechanics and Arctic Engineering (submitted, 2014).*

Luan, C., Michailides, C., Gao, Z., and Moan, T. (2014b). Modeling and analysis of a 5 mw semi-submersible wind turbine combined with three flap-type wave energy converters. In *ASME 2014 33rd International Conference on Ocean, Offshore and Arctic Engineering*, pages V09BT09A028–V09BT09A028. American Society of Mechanical Engineers.

Martínez, I. and Pavn, C. (2011). Deliverable d3. 4: Recommended concepts for further documentation and analysis. *Marine Renewable Integrated Application Platform.*

Michailides, C., Gao, Z., and Moan, T. (2015). Response analysis of the combined wind\ wave energy concept sfc in harsh environmental conditions. In *Renewable Energies Offshore – Guedes Soares (Ed.)*, Centre for Ships and Ocean Structures (CeSOS), Centre for Autonomous Marine Operations and Systems (AMOS) andDepartment of Marine Technology, Norwegian University of Science and Technology (NTNU), Trondheim, Norway.

Michailides, C., Gao, Z., and Moan, T. (2016). A sensitivity study of wave and wind induced rresponse of the combined energy concept sfc based on experimental measurements. CeSOS,AMOS,NTNU.

Michailides, C., Luan, C., Gao, Z., and Moan, T. (2014). Effect of flap type wave energy converters on the response of a semi-submersible wind turbine in operational conditions. In *ASME 2014 33rd International Conference on Ocean, Offshore and Arctic Engineering*, pages V09BT09A014–V09BT09A014. American Society of Mechanical Engineers.

Morison, J., Johnson, J., Schaaf, S., et al. (1950). The force exerted by surface waves on piles. *Journal of Petroleum Technology*, 2(05):149–154.

Murray, J., Wu, S., and Winsor, F. (1993). An investigation into the response of the glomar arctic iii semisubmerssemi with sponsons. Technical report, Institute for Marine Dynamics, National Research Council Canada.

Newland, D. E. (2012). *An introduction to random vibrations, spectral & wavelet analysis.* Courier Corporation.

Newman, J. N. (1977). *Marine hydrodynamics.* MIT press.

Quarton, D. (2005). Wind turbines, part 3: Design requirements for offshore wind turbines. *International Electrotechnical Commission.*

Wu, S., Murray, J., and Virk, G. (1997). The motions and internal forces of a moored semi-submersible in regular waves. *Ocean Engineering*, 24(7):593–603.